NON-INVASIVE MONITORING OF DISEASE PROGRESSION IN DUCHENNE MUSCULAR DYSTROPHY

By

RAVNEET SINGH VOHRA

A DISSERTATION PRESENTED TO THE GRADUATE SCHOOL
OF THE UNIVERSITY OF FLORIDA IN PARTIAL FULFILLMENT
OF THE REQUIREMENTS FOR THE DEGREE OF
DOCTOR OF PHILOSOPHY

UNIVERSITY OF FLORIDA

2012

To my parents, brother and wife

ACKNOWLEDGMENTS

I am grateful to several individuals for their guidance and support in my dissertation work. The greater part of this work was made possible by the guidance of my mentors and by the love and support of my family, friends and colleagues. It is with my heartfelt gratitude that I acknowledge each of them.

First and foremost, I would like to thank my advisor and mentor Dr. Krista Vandenborne, for her constant guidance and support. Also, I am grateful to Dr. Walter for his feedback and thought provoking research questions. I would like to thank Dr. Martin for his help with most of the statistical analysis, constant encouragement and support throughout my doctoral education. I would also like to express my sincere thanks and gratitude to Dr. Shechtman for encouraging me to strive harder towards my goals and aspirations.

A special thanks to all my lab members, without whose help this dissertation would have never been possible. I would like to thank Min, Fan, Arun, and Wendy for teaching me all the necessary skills and techniques in the lab and for also guiding me through the PhD process. I would like to thank Dr. Mathur, Dr. Lott, Dr. Forbes, Dr. Baligand and Dr. Willcocks, for helping me throughout the entire process. I would like to thank Jasjit, Wootaek, Arjun, Abhinandan and Ishu for helping me in completing the final stages of my dissertation. I would also like to thank Dr. Day for her assistance and support. I would also like to thank the staff of the Physical therapy department, especially Ellen Esparolini and Christa Richmond for keeping me up to date with every deadline during my doctoral studies.

Finally, I would like to express my sincere appreciation to my parents for their love and support. Last but not the least; I would like to thank my beloved wife Daman

who has been supporting me through this process. Thank you for all the sacrifices and difficulties that you have patiently endured during this process. This project would never have happened without their unending support.

TABLE OF CONTENTS

page

LIST OF TABLES

LIST OF FIGURES

LIST OF ABBREVIATIONS

BMD	Becker muscular dystrophy
CSA	cross sectional area
C-CSA	contractile cross sectional area
DMD	Duchenne muscular dystrophy
EDL	Extensor digitorum longus muscle
FID	free induction decay
FOV	field of view
GAS	Gastrocnemius muscle
mdx	muscular dystrophy X-linked
MRI	magnetic resonance imaging
NC-CSA	non-contractile cross sectional area
SNR	Signal to noise ratio
SOL	Soleus muscle
T_1	longitudinal relaxation rate
T_2	transverse relaxation rate
TA	Tibilais anterior muscle

Abstract of Dissertation Presented to the Graduate School
of the University of Florida in Partial Fulfillment of the
Requirements for the Degree of Doctor of Philosophy

NON-INVASIVE MONITORING OF DISEASE PROGRESSION IN DUCHENNE MUSCULAR DYSTROPHY

By

Ravneet Singh Vohra

December 2012

Chair: Krista Vandenborne
Major: Rehabilitation Science

Skeletal muscle cytoskeletal proteins not only maintain the structural integrity of the myofiber, but also transmit forces generated by the actomyosin complex. Muscle fibers are protected from outside the cell by a basal lamina and inside by the actin network. This structure is further bolstered by the presence of proteins such as dystrophin, utrophin and various trans-membrane proteins. Absence of any of these proteins can lead to devastating alterations in the muscles that can cause muscular dystrophy.

The muscular dystrophies represent a class of neuromuscular diseases characterized by rapid muscle wasting. Duchenne muscular dystrophy (DMD) is one of the most common forms of muscular dystrophy, affecting 1 in every 3500 newborn males.[1] Absence of the dystrophin protein makes the sarcolemmal membrane more susceptible to muscle contraction induced sarcolemmal injury. Progression of fatty tissue infiltration and muscle atrophy occurs secondary to sarcolemmal injury. DMD patients usually loose ambulation in their mid to late teens. Death usually occurs due to respiratory and cardiac muscle failure. Although, the underlying cause of DMD was discovered in 1980 there is no definite treatment to cure DMD. There is an increasing

interest in developing and administration of different therapeutic agents in order to counteract muscle pathology and more so, muscle wasting in DMD patients. In order to monitor both the disease progression and effects of therapeutic agents different outcome measures used.

Muscle biopsies have been used as the gold standard to diagnose Duchenne muscular dystrophy. However, it becomes almost impractical to use multiple biopsies in order to monitor the disease progression. Apart from being invasive in nature, this technique fails to represent the heterogeneous distribution of the disease. On the other hand, non-invasive techniques, such as magnetic resonance imaging (MRI) have the ability to detect and quantify the tissue pathology in three dimensions. This doctoral dissertation presents results of five studies of non-invasive monitoring of structural changes in skeletal muscles in DMD.

CHAPTER 1
INTRODUCTION

Structure and Organization

Skeletal muscle is composed of several myofibers, which are organized into fascicles. Myofibrils are interconnected with intermediate filament proteins called Desmin. Desmin forms a three-dimensional scaffolding around the Z disks and connects the entire contractile apparatus to a subsarcolemmal cytoskeleton.[2] Myofibers are divided into subunits called sarcomeres, which are arranged in a series and are composed of contractile filaments. These contractile filaments are divided into two types; a) Thick filaments: contain polymers of protein myosin and b) Thin filaments: contain polymers of protein actin. Furthermore, actin is linked to laminin in the extracellular matrix through a protein called dystrophin which is a component of the dystrophin-associated glycoprotein (DAG) complex.[3]

Dystrophin-Glycoprotein Complex

The Dystrophin glycoprotein complex (DGC) is a large complex of membrane-associated proteins that is critical for skeletal muscle fibers integrity. The DGC serves as a link between the extracellular matrix and the subsarcolemmal cytoskeleton. Furthermore, DGC is thought to protect muscle cells from contraction-induced damage.[4] This complex consists of the following proteins: dystrophin, dystroglycans, sarcoglycans, sarcospan (α,β, γ, δ), syntrophins (α1, β1, β2; γ1 and γ2), α-dystrobrevin. Dystrophin binds to cytoskeletal actin and to transmembrane protein β-dystroglycan. The extracellular domain of β-dystroglycan binds to the peripheral membrane protein, α-dystroglycan. α-dystroglycan binds to laminin-2 in the basal lamina. Thus, the DGC

serves as a link between the extracellular matrix and the subsarcolemmal cytoskeleton. Therefore, it is thought to protect muscle cells from contraction-induced damage.[4]

Structure of Dystrophin

The dystrophin gene was one of the first genes that was identified using genomic technology.[5] The gene is located on the human chromosome Xp21 and is one of the largest human genes identified. It is composed of 79 exons spanning more than 2.5 million base pairs, which corresponds to about 1.5% of the entire X-chromosome.[6, 7] The dystrophin gene encodes the protein dystrophin. Full-length dystrophin mRNA is about 14kb and is mainly expressed in skeletal, cardiac and smooth muscles and the brain. Analysis of the amino acid sequence of dystrophin reveals its rod shaped structure. It consists of four domains. a) An amino terminal that binds with actin, b) A rod domain that consists of 24 spectrin-like rod repeats and 4 hinges, c) A cysteine rich domain that interacts with dystroglycan and sarcoglycan complexes, and d) A carboxy terminus that interacts with syntrophins and dystrobrevins.

Four other, shorter isoforms of the dystrophin protein of different molecular mass have also been reported and are 260 kDa, 140 kDa, 116 kDa, 71 kDa. These shorter isoforms lack the actin-binding domain, which suggests that they may have some function, which is altogether different from that of dystrophin.

Dystrophinopathies

Dystrophinopathy is a general term used to describe the disorders that occur due to lack of functional protein dystrophin. The first gene to be cloned was the dystrophin gene that is mutated in both Duchenne Muscular Dystrophy (DMD) and Becker Muscular Dystrophy (BMD). Although both DMD and BMD are caused by mutation in the dystrophin gene, BMD is considered a less severe form of muscular dystrophy.

DMD is the most common form of muscular dystrophy whereas BMD is a less common form.[8] DMD/BMD is a severe X-linked degenerative disorder that occurs with an incidence of 1 in 3500 children and 1 in 30,000 children respectively.[1]

The term DMD is coined after the French neurologist Duchenne de Boulogne, who described the disease approximately 150 years back. He also devised a harpoon like needle and a procedure (muscle biopsy) to study and demonstrate the severity and progressive nature of the disease. Twenty-five years ago, the genetic defect underlying DMD was mapped to chromosome Xp21 in humans.[9, 10] Since the gene is the largest gene identified, the size of the gene itself could account for its relatively high frequency of mutation.[11] The large DMD gene can accommodate production of several dystrophin isoforms. Mutations/deletions in the dystrophin gene prevent the production of dystrophin leading to its absence in muscle fibers.[12] However, in BMD, the nature of mutations is such that synthesis occurs of a truncated and partly functional dystrophin protein.

In DMD patients, various mutations in the DMD gene, such as missense, nonsense, deletion, insertion or duplication have been identified. When the reading frame has been disrupted by a mutation (out of frame), dystrophin is not expressed and this results in a phenotype of DMD. On the contrary, if the reading frame is maintained, a truncated but still functional dystrophin is expressed. This result in a milder form called Becker muscular dystrophy. In a DMD gene, there are two hot spots for mutations: around exons 3-7 and 45-55.

Clinical Features

Boys who have DMD exhibit a progressive loss of muscle function. Although the muscles are affected at birth, the clinical symptoms of proximal muscle weakness

usually manifest between 3 to 5 years of age. The boys usually start walking at about 18 months of age, compared to their siblings. Toe walking is commonly seen in patients with DMD. Initially the appearance of the lower limbs may be normal but, by the age of 3 to 4 years, pseudo-hypertrophy of the calf muscle can be seen. DMD patient has difficulty performing daily activities like, running, jumping and hopping even during early stages of life. As the disease progresses, the affected boys develop a lumbar lordosis and a Trendelenburg gait. They fall more often and have trouble when rising up. When rising up from the floor, children with DMD show a typical sign called “Gower’s sign”. They get into a knee-elbow position, extend their elbows and knees, bring their hands and feet as close as possible and place one hand a time on their knees. They then place their hands on their thighs and move proximally in steps, climbing up their legs. Boys with DMD are at increased risk for certain cognitive concerns. However, unlike their muscle weakness, which is progressive in nature, their cognitive skills do not deteriorate over time. Furthermore, muscle biopsy of patients with DMD demonstrates necrotic or degenerating muscle fibers, which are often observed in clusters. These necrotic fibers are surrounded by macropahages. Small immature fibers with central nuclei are observed which reflects muscle regeneration. This regenerative capacity later on gets exhausted and muscle fibers are gradually replaced by connective and adipose tissue.

Unlike DMD, BMD patients show much more heterogenous clinical manifestations. Initially it was reported that the mean age of onset for BMD was 11 years, but this may vary.[13] Patients with BMD stay ambulatory until 20 years of age and mean age at death is around the mid-40s.[13] With the improvement in diagnostic

techniques, it has become well known that a number of patients can remain ambulatory until 40 years or beyond and they can survive up to 60 years of age. Clinically, hypertrophy of the calf muscle is a characteristic feature of juvenile BMD patients.[14] Calf muscle hypertrophy tends to vanish with aging. There is symmetrical weakness of muscles of the pelvic girdle and thighs. Moreover, it is well known that cardiac function is afflicted in the patients with BMD. Patients with BMD have normal developmental milestones and can carry out strenuous exercises.

Pathophysiology

DMD is characterized by progressive muscle fibers degeneration and replacement by fibro-fatty tissue. The degenerative process becomes more evident with time. During late teenage years, there is a predominance of fibro-fatty tissue with only small amounts of muscle tissue left. Furthermore, the ability of muscle fibers to endure eccentric contraction appears to be reduced in DMD.[4,15] The absence of dystrophin could compromise the muscle membrane integrity particularly after sustained contractions. Membrane fragility results in the accumulation of cytoplasmic proteins that are normally not present in muscle fibers, such as albumin and immunoglobulins. Furthermore, muscle biopsies from DMD patients reveal that there is an increased amount of intracellular levels of calcium and hypercontracted muscle fibers.[16] Increase in intracellular levels of calcium for prolonged periods of time activates proteases, especially calpains. Consequently, there is additional damage to the muscle membrane, escalating calcium entry. Additionally, it has been documented that CD4+ cells promote the pathology of the dystrophic muscle.[17] Therefore, depletion of these cells or macrophages significantly reduces the pathology in dystrophic muscle. In order to void the inflammatory effects, corticosteroids, like prednisolone and deflazacort, have

been used. These drugs slow down the disease progression, prolong ambulation, and forestall development of scoliosis.[18,19] In addition, decreased production of nitric oxide (NO) has been shown to escalate the pathophysiology in DMD.[20] In skeletal muscles, nNOS is bound to the DGC complex through a protein called α-syntrophin.[21] Absence of dystrophin leads to disruption of DGC complex. The DGC complex is responsible for recruitment of neuronal nitric oxide synthase (nNOS) to the sarcolemma to produce a signaling molecule called nitric oxide (NO).[22,23] Therefore, absence of dystrophin leads to removal of nNOS from the sarcolemma, which in turn attenuates NO production. Attenuation of NO production leads to functional ischemia due to impaired vascular relaxation in DMD.[24-26] In order to study potential therapeutic agents various animal models have been developed in laboratories. Since many experimental studies in dystrophy use animal models in the laboratory setting, a thorough explanation of different animal models is warranted.

Animal Models of Muscular Dystrophies

With more understanding of underlying genetic causes of various diseases it has become easier to develop knockout animal models. These knockout animal models have been helpful in providing insights about the pathophysiology of various diseases. The genetic models to study muscular dystrophy cover a wide range of species.

The dystrophin gene is highly conserved among various species. Homologues of DMD have been identified in both vertebrates and invertebrates. There is a mounting pressure for different therapies to be developed, including gene and drug therapies to treat DMD. In order to study potential therapies several animal models of muscular dystrophy have been used in laboratory settings. Caenorhabiditis elegans (C. elegans) is the first multicellular organisms in which the genome has been sequenced

completely.[27] It was discovered that approximately 65% of human disease genes have their counter parts in C. elegans.[28] C. elegans move by contraction of longitudinal striated muscles which express a dystrophin homologue called *dys1*.[29] This model has an advantage over other models in that they are readily available and can be grown in laboratory settings. This makes them ideal for genetic and pharmacological studies. The second model is the Drosophilla melanogaster or the fruitfly. This model is one of the most commonly used animal models to study neuromuscular development and function. Drosophilla muscle cells share many molecular, cellular and physiological features of vertebrate muscles. About 75% of all known human diseases have fly homologues.[30] Furthermore, the drosophila model of dystrophinopathies has been helpful in providing new insights into the function of the dystrophin-dystroglycan complex. Insights gained from drosophila genetic system could therefore be applied to vertebrate systems. The third model to study DMD is the murine model, the mdx mouse. This model is one of the most commonly used animal models for Duchenne muscular dystrophy. Loss of dystrophin occurs as result of a point mutation in exon 23 of the dystrophin gene.[31] Although, the *mdx* mouse has proved to be a valuable model for understanding the underlying mechanisms responsible for muscular dystrophy it has been criticized, since the model presents a mild phenotype with the mice living nearly a normal life span. Progression of the disease is thus much milder as compared to humans.[32] This has been attributed to the presence of 1) a dystrophin homologue, Utrophin, 2) better calcium homeostasis and 3) presence of revertant fibers. Subsequent to the discovery of the *mdx* mouse a number of other mutant mice have been created. *mdx*2^{cv}, *mdx*3^{cv}, *mdx*4^{cv} and *mdx*5^{cv} were produced

following administration of a mutagen to C57BL6 mice.[33] Later on it was discovered that *mdx*2^{cv} and *mdx*3^{cv} resulted from mutation in intron 42 and 65 respectively.[34,35] On the other hand *mdx*4^{cv} and *mdx*5^{cv} resulted from mutation in exon 53 and 10 respectively. Furthermore, in order to look at the efficacies of therapeutic strategies laboratories have been interested in a more severe model of DMD. As a result, mice lacking both dystrophin and utrophin (utrn-/-/*mdx*) were genetically engineered. These mice show more similar progression to Duchenne muscular dystrophy. For example they have a reduced life span (between 4 and 20 weeks), suffer from severe muscle weakness with joint contractures, growth retardation, kyphosis, and show signs of cardiomyopathy. This model suggests that both dystrophin and utrophin play complementary roles. Finally, the canine model, includes the golden retriever (GRMD), Rottweiler, German shorthaired pointe, [36] Labrador retriever, Cocker spaniel, and Tibetian spaniel. These models have been studied both at a clinical and molecular level. The Golden retriever is the most commonly studied canine model of muscular dystrophy. Several studies have defined clinical signs of GRMD [37,38] suggesting that the pathogenesis of GRMD is similar to DMD. There is a high mortality rate in GRMD dogs due to selective muscle degeneration. Surviving dogs show signs of muscle degeneration followed by muscle regeneration and an inflammatory response.[39] GRMD dogs develop a stiff gait and atrophy of trunk and temporalis muscles occur. Affected dogs display hyperextension of carpal joints and flexion at tibio-tarsal joints. Furthermore, because of phyrangeal muscle involvement they show signs of excessive drooling.

Limitations of canine models: Although the GRMD model provides valuable insight about the pathology of muscular dystrophy, for practical reasons like availability and high cost of maintenance it is unlikely to replace the *mdx* model. However, dogs can be used as a translational model between human subjects and the murine model. They can be used to assess the feasibility of applying technologies to human subjects that have been validated in mouse model.

Approaches to Treatment of Muscular Dystrophy

In 1987, the underlying genetic defect causing DMD was identified. However, the specific mechanism of myofibre damage is still not clearly defined [40] and there is still no effective treatment for DMD. Therapeutic approaches for DMD fall into two primary categories gene therapy and pharmacological therapy.

Restoration of dystrophin: The fundamental cause of pathology is the absence of dystrophin. Therefore, the bulk of therapeutic approaches are aimed at restoration of a functional version of dystrophin protein. Various experimental approaches that have been undertaken to achieve this goal include gene repair,[41,42] modification of splicing, [43,44] and gene transfer.[45,46] Stop mutations account for about 5% to 15 % of all DMD cases. These mutations occur when deletion of substitution of individual DNA bases leads to the formation of premature stop codon. Such signals terminate the translation of protein, which is then rapidly degraded. Administration of aminoglycoside antibiotic gentamicin leads to read-through of the stop mutation in the *mdx* mouse and production of sufficient amount of dystrophin protein.[47] A similar study was performed on the DMD patients.[48] Although there was no clear clinical benefit, the DMD patients demonstrated reduced levels of serum creatine kinase. Treatment of the patients harboring nonsense mutation with gentamycin promotes production of dystrophin gene,

however, the lack of potency and the need for intravenous and intramuscular gentamycin have limited the clinical usefulness of this approach.[49] On the other hand, Ataluren, a small molecule appears to read through at much lower doses and has less toxic side effects than gentamycin.[50]

Muscle growth: Increasing the muscle mass is yet another aspect that have gained enormous focus from scientists around the world. Myostatin is a member of transforming growth factor-β (TGF-β) superfamily. It is a critical autocrine/paracrine inhibitor of skeletal muscle growth.[51] The deletion of myostatin in mice induces an extensive growth of skeletal muscle mass. This increase has been attributed both to hypertrophy and hyperplasia.[51,52] The double-muscling phenotype of a few cattle and sheep breeds is caused by mutations in their myostatin genes.[53,54] Therefore, the most important function of myostatin is the regulation of skeletal muscle growth. Furthermore, myostatin appears to initiate signaling by directly binding to its serine/threonine kinase receptor.[55,56] Downstream of the receptors, Smads are first demonstrated to be mediators of signals for myostatin.[55,56]

Anti-inflammatory strategies: The ultimate treatment of DMD includes repairing the defective gene through various therapeutic agents. Considering the large size of dystrophin protein it is a daunting task to introduce dystrophin protein through various vectors. Furthermore, gene therapy may be able to target individual or group of muscles however to treat DMD a more systemic approach is required. Pharmacological approaches involving systemic delivery are more likely to enhance muscle function globally and thereby increase patient survival. Corticosteroids are routinely utilized in clinics for DMD, but there are varieties of alternative compounds that are being tested,

either in *mdx* mice or in limited human clinical trials. Currently, Prednisone and deflazacort are the sole available therapies for DMD. An improvement in functional muscle strength and a sustained slowing of disease progression for up to three years has been observed with oral prednisone[57]. Another study showed that DMD children responded well to an intermittent, low dosage regime of prednisone[58]. Both prednisone and deflazacort are associated with adverse side effects like weight gain. However, these side effects appear to be less severe with Prednisone. Furthermore, different immunosuppressive drugs have demonstrated benefits in animal models, resulting in increasing recognition for treating inflammation in DMD. Various anti-inflammatory drugs like cyclosporine,[59,60] pentoxyfylline,[61,62] Oxatomide have shown to improve muscle strength in animal models. However, a clinical trial with oxatomide in DMD has showed only minor benefits. Another alternative approach that has been undertaken is to reduce muscle necrosis. This approach involves targeting tumor necrotic factor (TNF alpha), a key pro-inflammatory cytokine with neutralizing antibody infliximab.[63] Furthermore the protective effect of TNF alpha blockade has been bolstered by other studies as well.[64] In addition, it has been documented that high levels of reactive oxygen species can damage skeletal muscles.[65]On the other hand antioxidants such as Coenzyme Q10 and green tea extract have been shown to prevent the damage caused by reactive oxygen species.[66,67] Furthermore, absence of dystrophin causes damage to sarcolemmal damage. This leads to increase in calcium ions influx thus initiating a series of cellular events including activation of proteases leading to further muscle damage. Studies have shown that protease inhibitors help in reducing the pathological conditions seen in *mdx* muscle.[68-70]

Although there are many exciting new discoveries in the therapeutic approaches however they are still in experimental stage and most of them have been developed and tested in the *mdx* mouse. Scientist face number of concerns associated with translating the studies from small animals to DMD patients including (1) Muscle size: In order to effectively deliver gene in DMD patients a grid of injections will be required spaced not further than 1-2 cm apart. On the other viral and non-viral vectors have been administered via arterial[71,72] and intravenous route[73,74] (2) Immunological response: Most of the vectors that show promising results in murine models are based on the viruses that commonly infect man. As a consequence humans tend to develop immune response to previous trials on any treatment involving these vectors.[75]

Summary

The muscular dystrophies represent a heterogeneous and devastating group of neuromuscular disorders. DMD is one of the most common of the muscular dystrophies affecting male children. The underlying cause of DMD is absence of the dystrophin protein. Recent discoveries have opened new avenues in both gene and drug cased treatment strategies. The ultimate treatment for DMD lies in the systemic introduction of dystrophin gene in muscles of DMD boys. However, it is difficult to predict when this treatment will be available. In the meantime, focus has been on the novel pharmacological drugs to improve muscle function. However, current drug selections for DMD patients are primarily limited to corticosteroids. Different novel treatments have shown promising results in animal models of DMD and are progressing towards clinical trials.

CHAPTER 2
NON-INVASIVE TECHNIQUES FOR ASSESSMENT OF MUSCLE DYSFUNCTION

Throughout the present work on both boys with DMD and animal models of DMD, emphasis has been laid on characterizing the lower extremity muscles using non-invasive techniques. Traditionally, invasive techniques such as muscle biopsy have been used in order to study skeletal muscle properties as well to study pathological processes in DMD. However, different non-invasive techniques have gained momentum in assessment of muscle dysfunction.

Computed Tomography

CT is a cross sectional technique that uses ionizing radiations. In CT, an X-ray beam is projected through the patient at different orientations and attenuation of X rays is measured using gas-ionizing chambers. Unlike radiography, CT has superior contrast resolution and it can distinguish between bone, tendons and ligaments, muscle, and fluid. Since CT can differentiate between normal and pathological muscle it can be used is assessment of DMD progression. In 1977, Doherty et al. used CT to scan skeletal muscle in DMD patients. Muscle CT scans can be used to assess nature and extent of lesions. Although CT has a clear edge over radiography but the spatial resolution in other modalities give clearer and artifact free images. Besides computed tomography (CT), other techniques such as Ultrasound (US), magnetic resonance imaging (MRI), as well as EMG, are frequently used in the diagnosis of neuromuscular disorders

Ultrasound

Ultrasound has been used in medical practice since the early 1950s. Wild and colleagues[76] discovered the ability of high-frequency ultrasonic waves to visualize living tissues. After they showed its application to visualize the living tissue, use of

ultrasound rapidly expanded leading to its widespread use especially in the field of medicine because of its non-invasiveness nature. In 1980, it was first discovered that affected muscles showed a different appearance on ultrasound compared to healthy muscles. Subsequently, several studies have established high sensitivities and specificities of ultrasound in the detection of neuromuscular disorders[77],[78,79]. Ultrasound uses longitudinal sound waves with the frequency of 2-12 MHz above the range of human hearing. Ultrasound techniques have been vastly improved, resulting in display of muscle tissue with resolutions up to 0.1 mm. Pathological changes, which disrupt normal muscle architecture, will increase the number, and alter the orientation of reflective surfaces within a muscle, leading to an increase in the ultrasound echo. As well as an increase in echo from abnormal muscle, ultrasound may show a reduction in the intensity of the reflection from underlying bone and may be used to measure muscle bulk, atrophy and hypertrophy.[80] DMD patients demonstrate normal muscle thickness with increased muscle echo intensity.[80,81] Further, within the muscle the echo intensity has a homogenous i.e. fine granular distribution and the proximal muscles have the highest echo intensities. Moreover, these echo intensities can become so high that the bone echo is diminished or absent in the later cases. The severity of the ultrasound findings has been reported to relate to age and clinical severity of the disease.[82]

Magnetic Resonance Imaging (MRI)

MRI forms an integral component of present work and is used to monitor the changes occurring in DMD patients as well as *mdx* mouse. Magnetic resonance imaging (MRI) is an imaging technique, used to produce high quality images of the inside of the human body, involving magnetic fields and radiofrequency (RF)

electromagnetic waves. Although, the MR was discovered in 1946 its clinical application was recognized in 1977. Since then, MRI has been considered a useful tool. MRI can produce images with excellent contrast between soft tissues and high spatial resolution in every direction. Furthermore, the radiation has low energy and appears to be safe under normal operating conditions.

Basics of Magnetic Resonance

The key components of any magnet include a static magnetic field, which is sustained by a liquid helium cooled, super-conducting electromagnet. The field strength (B) is measured in the unit Tesla (T), which is equivalent to 10,000 Gauss (G). The field strength of the magnet is the strongest at the convergence of the magnetic field lines i.e. in the middle of the magnet bore. Furthermore, the signal strength is directly related to the field strength. The stronger the B_0 is, greater the signal strength will be. The majority of the work presented in this dissertation was collected at 3.0 T and 4.7T, Electromagnetic gradient coils, which are used for spatial encoding of the signal, and Radio-frequency (RF) coil, which is used to excite and receive the NMR signal

Properties of Atomic Nuclei

The nucleus accommodates most of the elemental mass of the atom and consists of neurons and protons. Nuclei with an odd number of neutrons or protons possess spin-angular momentum. The nuclei of certain elements, such as Hydrogen and Fluorine, have these properties. Every one of these nuclei with an odd number of protons or neutrons can be used for imaging in MR.

Spin. It is the fundamental property of the protons that forms the core of MRI. Two or more particles with spins having contrasting signs can pair up to eliminate the signs of spin. In nuclear magnetic resonance, it is unpaired nuclear spins that are of

importance. When a particle is placed in a magnetic field of strength B, it can absorb a photon, of frequency. This frequency depends on the gyromagnetic ratio, of the particle and is denoted by equation: $\upsilon = \gamma B$ where γ is the gyromagnetic ratio. For hydrogen, γ = 42.58 MHz / T.

Radio Frequency (RF) pulse. RF pulse of a specific frequency is delivered to the patient. Before the RF pulse is transmitted, all the spins are aligned with the axis of external magnetic field B_0. By convention, we apply RF pulse in the X-direction and for this reason the vector ends up along Y- axis (Figure 2-1). When RF pulse is transmitted along the X-axis the protons start to precess about the axis of that magnetic field at frequency ω_o. The protons precess about the axis of B_0. RF pulse also has a magnetic component that is in the direction of X-axis. As soon as RF pulse is switched off, there are two basic phenomenon that occur namely, 1) T_1 relaxation and 2) T_2 relaxation.

Relaxation Times

Longitudinal (T_1) relaxation time: The term relaxation means that the spins are relaxing back to their lowest energy state or back to equilibrium state. Right after the excitation, there is no longitudinal magnetization as it has been tipped into the transverse plane (Figure 2-2). As soon as the RF pulse is turned off, the protons give up all their excess energy and realign themselves with axis of B_0.

T_1 is called longitudinal relaxation time because it refers to the time it takes for the spins to realign along the longitudinal axis. It is also called spin-lattice relaxation time because it refers to the time it takes for a spin to give off excess energy to the surroundings in order to return to their equilibrium state. After the RF pulse is turned off:

The M_{xy} component of the vector decreases and the M_z component recovers along the z axis (Figure 2-2). The recovery of longitudinal magnetization (M_Z) can be given by the formula:

$$M_Z(t) = M_o\ (1 - e^{-t/T1}) \qquad (2\text{-}1)$$

where T_1 is the exponential time constant that is required for longitudinal component to recover to 63% of its equilibrium alignment.

Transverse (T_2) relaxation time: After the protons have been tipped into the transverse plane, the longitudinal magnetization vector recovers and the transverse vector M_{xy} decays. This decay rate is characterized by T_2 relaxation or spin - spin interaction. It includes exchange of energy among neighboring spins and is given by the formula:

$$M_{xy}\,(t) = M_o\ e^{-t/T2} \qquad (2\text{-}2)$$

T_1 recovery and T_2 decay are two independent processes and T_2 decay occurs 5-10 times more rapidly than T_1 recovery. This is because of a phenomenon called dephasing. Dephasing is a phenomenon by which the spins, which are in phase after a 90^o pulse gets out of phase. Two underlying causes are responsible for dephasing (A) Interaction between Individual spins: When two spins are in close proximity to each other, magnetic field of one proton affects the proton next to it. Furthermore, the proton aligned with B_0 creates slightly higher magnetic field for its neighboring proton. On the contrary, the proton that points against B_0 experiences slightly less magnetic field. This interaction is inherent property of every tissue and is measured by T_2. Therefore, the spin – spin interaction is the first cause of dephasing. (B) External magnetic field inhomogeneity: Because of external magnetic field inhomogeneity, each spin is

exposed to slightly different magnetic field and therefore the protons precess at different frequencies. Unlike T_1 and T_2, which are inherent properties of the tissue, TR (the repetition time) and TE (echo time) are under operators control. By apropriate setting of TR and TE we can put more “weight” on T_1 or T_2 (Figure 2-3, 2-4).

TR (the repetition time). The time interval between application of two RF pulses is called TR (Repitition time) (Figure 2-5). After application of a 90^o pulse, the transverse component of the magnetization vector M_{xy} decays much faster than the longitudinal component M_Z. Between the application of two RF pulses the following processes take place: (A) Immediately before a 90^o RF pulse is applied, the magnetization vector points along z axis. (B) Immediately after a 90^o RF pulse, the magnetization vector is tipped in the xy- plane. (C) After time t = TR another 90^o RF pulse is applied. By this time some of the magnetization vector has recovered in z direction. However, most of the magnetization vector is lost in transverse direction. Therefore the magnitude of the magnetization vector along z axis is given by :

$$M_z(TR) = M_o(1 - e^{-TR/T1}) \qquad (2\text{-}3)$$

(A) At time t = TR the magnetization vector (M_z) is less than the original vector M_o. This is because the second RF pulse is applied before complete recovery of the M_z component of the magnetization vector. (B) Again after second TR the longitudnal magnetization vector will be flipped into xy plane. However this time longitudnal magnetization vector will be equal to the preceding vector.

Image Formation

The signal received contains information from the entire part of the body imaged. The fundamental process used to define the location of the sources of MR signal and hence identify the specific body part imaged, is by application of magnetic field

gradients. In a homogeneous magnetic field, water protons resonate at the same frequency, regardless of location. If a second magnetic field is now superimposed upon the main magnetic field, a predictable variation is observed in the magnetic field along a predetermined axis. The resulting magnetic field is highest at one end of the gradient and lowest at the other; between are intermediate values along the axis of the gradient. As a result of application of gradient field, protons at one end of the gradient spin slower and protons at the other end spin faster. Gradients therefore create temporary inhomogeneties in the main magnetic field to obtain spatial information. These signals from the protons can now be measured and used to construct images. Depending on the function, gradients are referred to as the slice-select gradient (G_x), the frequency-encoding gradient (G_y), and the phase encoding gradient (G_z).

The three basic steps in an imaging process are discussed below:

Slice selection. This process involves use of G_x during application of an excitation or refocusing pulse. Application of a gradient causes tipping of protons only in a specific slice. A slice is selected by simultaneous application of a selective RF-pulse and gradient along the z-axis such that alignment of protons in a specific width of tissue is disturbed. At the end of the brief RF pulse, specific spins that are exposed to a specific gradient in a sample are excited. Magnetization vectors representing out-of-phase locations remain undisturbed. Although the signal is obtained from the entire slice, the slice image is not yet seen because of lack of in-plane spatial information about the slice. In order to gather that information the signals are phase and frequency encoded. Further depending on the frequency bandwidth, slice thickness can be established.

Phase encoding. This step involves application of magnetic field gradients and therefore image construction in the y-direction. In order to get spatial information in the y- direction, a gradient is applied in the same direction. The phase encoding gradient is turned on before application of the frequency encoding gradient (G_x). It is usually applied right after the RF pulse or just before the G_x gradient or anywhere in between. Because the gradient brings about a change in the phase of proton spins this process of image construction is termed “phase encoding”.

Frequency encoding. Frequency encoding conventionally defines application of magnetic field gradients and hence image construction in the x-direction. This process occurs after the application of G_y and it is during this cycle that the signal is recorded as a function of time. The different frequencies are summed to form a signal that is detected by the receiver coil.

MRI Applications in Skeletal Muscle

The availability of magnetic resonance imaging (MRI) scanners offers a variety of methodologies to monitor musculoskeletal structure and function. MR is considered one of the best imaging modality to perceive soft tissue abnormalities. It provides three-dimensional high-resolution information, which can be used to measure muscle size i.e muscle cross sectional area as well as muscle volume, monitor muscle damage, and intramuscular fat. In addition, it is used to evaluate the presence or absence of muscle edema, its extent and also potential sites for muscle biopsy.[83,84] T_1-weighted, T_2–weighted and Short Tau Inversion recovery (STIR) are the most common form of imaging technique used for skeletal muscle imaging. T_1–weighted images are used to detect contrast between skeletal muscles and fat, therefore can provide valuable information regarding fatty tissue infiltration in the skeletal muscles. On the other hand,

both STIR and T_2–weighted images are used in detecting edema and are therefore referred to as fluid sensitive sequences.

Skeletal muscle function depends on the morphological properties of the muscle.[85-87] Muscle size measurements include anatomical and physiological cross-sectional area (CSA), muscle thickness and length, and muscle volume. Methods like limb circumference, ultrasonography and dual X-Ray absorptiometry (DEXA) have been used to assess muscle size. These measurements however, do not clearly differentiate between contractile and non-contractile tissue. Consequently, inclusion of non-contractile tissue like intramuscular fat and connective tissue in muscle size measurements tend to overestimate muscle size. MRI can differentiate between contractile and non-contractile tissues within a muscle and can image the entire length of more than one muscle at the same time.[88-90] Numerous studies have used MRI as a standard technique to assess skeletal muscle size following disease processes,[89,91] progression of muscle atrophy following disuse[92] and effects of interventions.[93]

Specifically, in DMD patients T_1-weighted scans are normal during early stages of life.[94] Subsequently, they may show a characteristic pattern of muscle involvement that evolves over time. Furthermore, during the ambulant stages[94,95] children with DMD exhibit abnormal signals in the gluteus maximus and adductor magnus, followed by quadriceps, rectus femoris and biceps femoris, with selective preservation of the sartorius, gracilis, semitendinosus and semimembranosus.[90,96] In the lower leg, peroneals, gastrocnemius and soleus are more severely affected than the other muscle groups.[97] However, use of T_2 and short T_1 inversion recovery imaging will show

edema and/or inflammation in other muscles that are spared from fatty infiltration and have normal signal intensity on T_1-weighted imaging. These findings are of interest because they suggest that an inflammatory component plays a significant role in the early phases of muscle damage, before the muscle is replaced by fat or fibrotic tissue.

The transverse relaxation time constant (T_2) is a quantitative measure of a basic biophysical property that leads to signal contrast on MRI. Furthermore, muscle T_2 relaxation properties are sensitive to muscle contraction and therefore possess widespread applications in studying muscle characteristics. Following the first study by Fleckenstein in 1988, which reported that there is increase in signal intensity of skeletal muscle T_2 after a bout of exercise[98] numerous studies have successfully demonstrated positive correlations between elevated T_2 times following exercise with integrated EMG patterns.[99] Furthermore, exercise induced contrast in muscles has been detected by using T_2 maps.[86] Consequently, if a muscle shows more contrast, it reflects more use of the muscle and vice versa.[99],[100],[86] This phenomenon of muscle T_2 has been used to infer muscle activity and the extent of their contribution. Thus, T_2 changes are sensitive to the activity status of the muscle and therefore hold tremendous potential in identifying muscle activation patterns in both normal and diseased conditions.

Although the exact mechanism for increase in T_2 has not been elucidated, studies indicate that the mechanisms of change in muscle T_2 following rest to work transitions are a consequence of increase in T_2 relaxation times of muscle water [101],[102]. This is probably a result of osmotically driven shifts of water into

intramyocellular spaces secondary to accumulation of end products of muscle metabolism and/or intracellular acidosis.[103],[104],[102]

The increase in T_2 values after normal activity is transient and has been shown to resolve within minutes to a couple of hours.[98],[105] However, persistence of T_2 values for longer periods may indicate muscle damage.[106] This is commonly observed following eccentric exercise protocols.[107] Several studies have reported that eccentric exercise-induced muscle injury is associated with marked elevations in T_2 values in both healthy and patient populations.[86],[103],[108] Elevated T_2 values following strenuous exercises correlate with markers of muscle damage including serum creatine kinase activity, muscle soreness and maximal isometric force.[109],[110] Repeated MRI measurements of skeletal muscle for as long as two to three months following eccentric exercise continue to show elevated T_2 relaxation times; suggesting of a long lasting change in the muscle. Intriguingly, long lasting elevated T_2 relaxation times reflective of muscle damage have also been reported following reloading after hind limb immobilization, spaceflight and disease processes in both humans and animals.[111],[20,112-114] Muscle damage following reloading is attributed to mechanical disruption of muscle fibers and inflammation in muscle.[115] Frimel et al. have shown strong correlations between the elevated T_2 relaxation times and histological markers of muscle damage.[112]

High-resolution MRI has the ability to differentiate between soft tissues within the muscle using distinct MRI techniques. Therefore, MRI has served as a non-invasive measure to quantify and monitor disease progression within the skeletal muscles

conditions.[116],[117,118] Furthermore, because of its non-invasive nature MRI it can be applied repeatedly in the same subject for longitudinal studies.

Furthermore, elevated T_2 values can suggest different pathological processes occurring in muscles including damage,[119],[120],[112] edema,[103],[102] fibrosis and fat,[90,121] investigators are now making attempts to discriminate between these physiological processes utilizing a variety of advanced MR techniques including DIXON imaging, diffusion weighted imaging, magnetization transfer contrast and spectroscopy. Thus, the scope of MR in studying skeletal muscle is on a constant rise.

Summary

Ever since MRI was proposed to scan three-dimensional biological structures in 1972, the use of MRI to monitor changes in biological tissues has grown by leaps and bounds. This chapter reviews the fundamental concepts of MRI and compares different non-invasive techniques. MRI has become the tool of choice because of its non-invasive nature. Furthermore, use of T_1 and T_2 parameters are discussed to monitor physiological changes occurring in skeletal muscles.

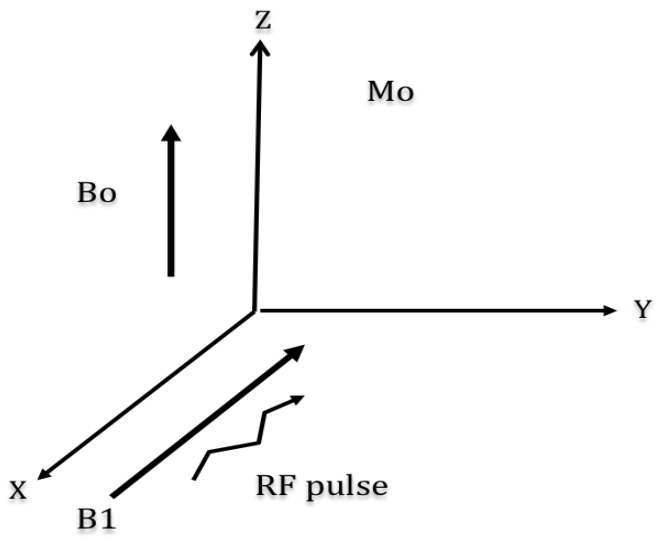

Figure 2-1. Representative three-dimensional figure showing RF pulse application.

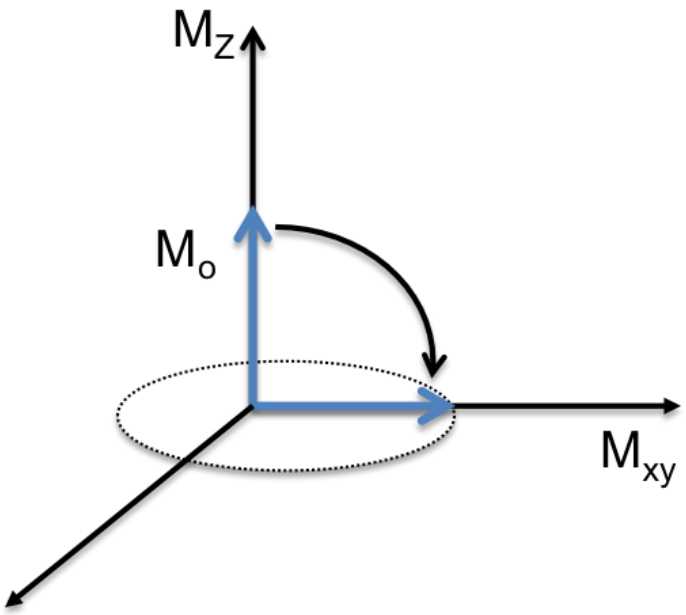

Figure 2-2. Schematic representation of 90 degree RF pulse application and its consequence.

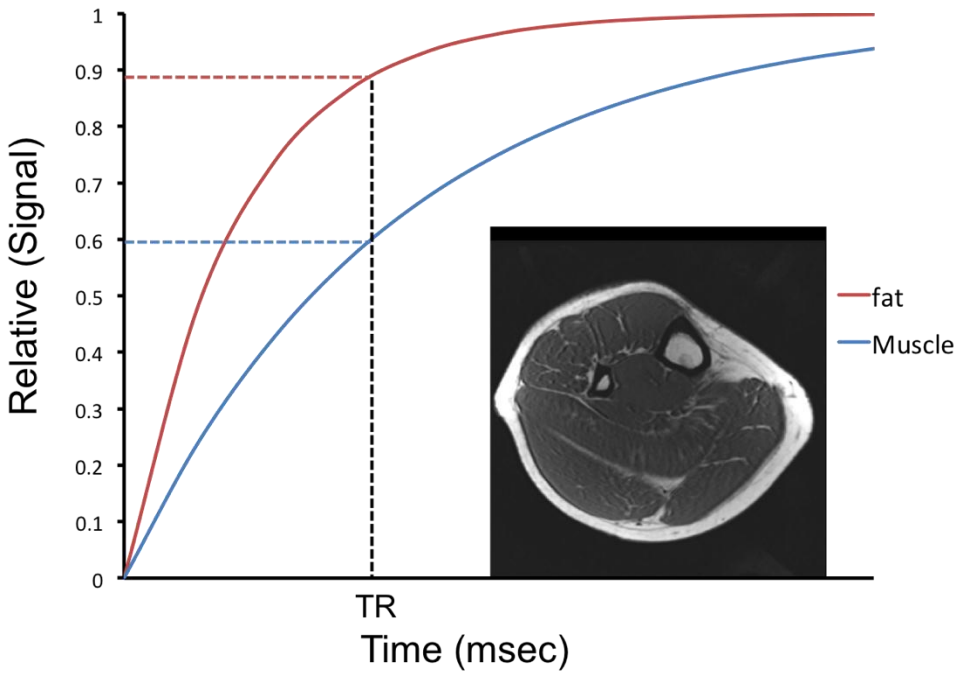

Figure 2-3. Schematic diagram showing T_1 recovery curves of fat and muscle

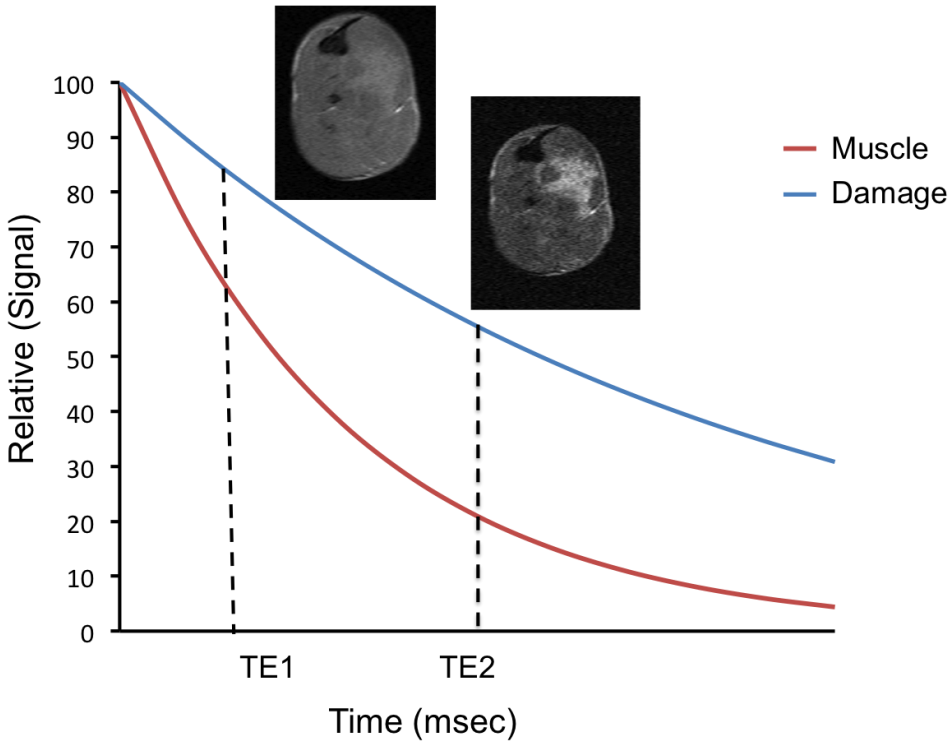

Figure 2-4. Schematic figure showing T_2 decay curve for muscle and damage

Figure 2-5. Time interval between two successive 90-degree RF pulses denoted by TR.

CHAPTER 3
OUTLINE OF EXPERIMENTS

The overall objective of this dissertation was to monitor the pathological variations occurring in the skeletal muscles of DMD patients and the *mdx* mouse, a murine model of DMD. An outline of the aims and hypotheses related to each experiment is given below.

Experiment One

Specific Aims

1. Quantify the CSA and torque production of primary lower- extremity muscles in ambulatory boys with DMD
2. Examine the relationship of age with muscle strength, CSA, and specific torque in boys with DMD and compare these relationships with controls
3. Examine the relationship of lower limb muscle strength with functional ability in boys with DMD.

Hypotheses

1. Boys with DMD have larger CSA of all lower-limb muscles but lower torque production compared with healthy controls.
2. Increase in muscle CSA and torque production with age is lower in boys with DMD compared with controls.
3. Torque production of the lower-extremity muscles is related to performance on functional tasks such as walking and transfers in boys with DMD.

Experiment Two

Specific Aims

1. To assess contractile and non-contractile content in individual muscles of the lower leg in DMD and age matched healthy controls.
2. To evaluate the relationship between the proportion of non-contractile content in leg muscles and functional ability.

Hypotheses

1. The non-contractile content in the lower leg muscles of boys with DMD is higher than in age matched healthy controls.

2. The non-contractile content in leg muscles is positively correlated to functional ability in boys with DMD.

Experiment Three

Specific Aim

To monitor the progression of dystrophic alterations with age in the hindlimb muscles of *mdx* mice using Transverse relaxation (T_2) time constant.

Hypothesis

Transverse relaxation (T_2) can be used to assess pathological changes occurring in the hindlimb muscles of *mdx* mice with age.

Experiment Four

Specific Aims

1. To monitor the response of muscle T_2 over a time course of 48 hours after a single bout of downhill running in *mdx* mice to wild-type (control) mice

2. To compare the effects of horizontal vs. downhill running on muscle damage, assessed by T_2 MRI in *mdx* mice.

3. To compare the effects of downhill running on the lower anterior vs. posterior hindlimb muscles of *mdx* mice.

Hypotheses

1. After a single bout of downhill running muscles of *mdx* mice demonstrate a greater increase in T_2 than control mice.

2. A single bout of downhill running instigates a greater increase in T_2 than horizontal running in mdx mice.

3. The anterior compartment muscles of *mdx* mice display greater increase in T_2 than the posterior compartment after a bout of downhill running.

Experiment Five

Specific Aim

To monitor the response of muscle T_2 on cardiac muscle after a single bout of uphill running in *mdx* mice to wild-type (control) mice.

Hypotheses

1. Myocardium of *mdx* mice is more susceptible to activity-induced muscle injury than wild type mice.
2. T_2 is a sensitive marker of myocardial damage in *mdx* mice.

CHAPTER 4
RELATIONSHIP BETWEEN LOWER-LIMB MUSCLE CROSS-SECTIONAL AREA AND TORQUE PRODUCTION IN BOYS WITH DUCHENNE MUSCULAR DYSTROPHY[1]

Boys with DMD experience profound muscle weakness and functional limitations as early as ages 3 to 5 years of age. The progressive decline in muscle function is first observed in the proximal muscle groups (e.g., shoulder girdle, hips), with the distal muscle groups being affected at a later age. Manual muscle testing (MMT) has been used to look at the age-related changes in strength in DMD children [122,123] and this method has also been used in clinical trials. However, the MMT has been criticized for having limited reliability, accuracy and sensitivity; therefore other muscle testing methods such as dynamometry are preferred for assessing muscle strength.

A hallmark of muscle quality is the amount of force produced per unit of muscle mass.[124] A recent study on boys with DMD showed only low to moderate correlations between regional lean body mass measured using Dual-energy X-ray absorptiometery (DXA) and muscle strength.[125,126] However, the main limitation was that DXA could not be used to quantify the size of the muscle. The cross sectional area (CSA) of individual muscles or muscle groups can be quantified using MRI and this technique has been used repeatedly to examine muscle atrophy after disuse,[87] spinal cord injury,[127] and in other chronic conditions.[128]

[1] Sunita Mathur, Donovan J Lott, Claudia Senesac, Sean A Germain, Ravneet S Vohra, H Lee Sweeney, Glenn A Walter, Krista vandenborne. Age-related differences in lower-limb muscle cross sectional area and torque production in boys with Duchenne muscular dystrophy. Arch Phys Med Rehabil. 2010 Jul;91(7):1051-8 (Used with permission from the American congress of Rehabilitation Medicine).

Specific Aims

The primary objectives of this study are:

1. To quantify the CSA and torque production of primary lower extremity muscles in ambulatory boys with DMD.

2. To examine relationship of age with muscle strength, CSA and specific torque in boys with DMD and compare these relationships with those in healthy age matched controls.

3. To examine the relationship of lower limb muscle strength with functional ability in boys with DMD.

Hypotheses

Our hypotheses are as follows:

1. All lower limb muscles in boys with DMD have larger CSA but lower torque production compared with healthy controls.

2. Torque production of the lower-extremity muscles is related to performance on timed functional tasks in boys with DMD.

Research Design and Methods

Participants

Twenty-two boys with DMD and 10 healthy boys from the general population (controls) aged 5 to 14 years old volunteered to participate in the study. A report confirming the diagnosis of DMD using molecular genetic testing (e.g., polymerase chain reaction amplification) and/or immunohistochemical staining of muscle biopsy was obtained from the subject's pediatric neurologist. All DMD participants were ambulatory and were being treated with corticosteroids (either prednisone or deflazacort). The study was approved by the institutional review board at the University of Florida. Written informed consent was obtained from the participants' parents, and written assent was obtained from each participant. Each subject's height and weight were measured in light clothing with shoes off.

Methods

Isometric muscle strength testing: Isometric peak torque of the KEs, PFs, and DFs of the right leg was measured using a Biodex dynamometer[2]. For KE testing, the knee and hip joints were placed at 90° of flexion. For PFs and DFs, the knee was placed between 0° to 10° of flexion and the ankle was placed in neutral (for PFs) or 30° of plantarflexion (for DFs). The subject was instructed to push or pull as hard as possible for 5 seconds, followed by a 2-minute rest. Five trials were performed for each muscle group, and the highest torque value was used for analysis (peak torque). One subject with DMD was unable to perform the dorsiflexion contraction. This protocol was tested for between-day reliability (2-month interval) by the same tester, in a subset of children with DMD (n=6) and controls (n=10). ICCs were calculated for both groups of subjects. High reliability was found for all 3 muscle groups (KEs: ICC=.89 in DMD and .99 in controls, PFs: ICC=.88 in DMD and .98 in controls, and DFs: ICC=.87 in DMD and .95 in controls P<.001 for all ICCs).

Because the body size of boys between the ages of 5 and 14 years varies considerably, peak torque was normalized to BSA. BSA is widely used as a biometric unit to normalize physiologic parameters. Hence for each of the functional muscle groups, torque normalized to BSA (ie, normalized torque; units=$N*m/m^2$) was reported. BSA (m^2) was calculated using the equation developed by Gehan and George[129] and modified by Mosteller.[130]

[2] Biodex Medical Systems, 20 Ramsay Rd, Shirley, NY 11967-4704.

Muscle CSA: MRI was performed on either a 1.5T (Signa)[3] or 3.0T (Achieva)[4] whole-body scanner. Subjects were placed in a supine position with their lower leg positioned in either a lower-extremity quadrature coil (1.5T) or an 8-channel sensitivity encoding, receive-only extremity coil (3.0T) for lower- leg imaging or a flexible surface coil for thigh imaging. Thigh imaging was not completed in 2 of the control subjects and 2 of the boys with DMD. Three-dimensional transaxial fat-suppressed gradient echo images were acquired with the following parameters: repetition time=24ms, echo time=1.8ms, flip angle=20°, and optimized field of view (calf: 12–14cm^2, thigh: 18cm^2). Individual muscles (quadriceps, soleus, medial, and lateral gastrocnemius and tibialis anterior) were manually outlined using OsiriX[5], an open-source software (Figure 4-1)[131]. To determine the CSA_{max} of a muscle, the axial image with the largest CSA in the series was identified and the mean of 3 consecutive images (ie, the slice with the greatest CSA and the immediate proximal and distal slices) was used to obtain the value for CSA_{max}. The CSA_{max} of the triceps surae muscle group was taken as the sum of the individual CSA_{max} of the soleus, medial, and lateral gastrocnemius muscles. The CSA_{max} of the quadriceps was taken as the sum of the CSA_{max} of the 3 vasti together and the rectus femoris.

Specific torque: The force-generating capacity of the muscle per unit area (ie, specific torque; units=Nm/cm^2) was calculated by dividing the isometric peak torque by the CSA_{max}, measured by MRI. KE peak torque was divided by quadriceps CSA_{max},

[3] Signa; GE Medical Systems, 3000 N Grandview Blvd, Waukesha, WI 53188.

[4] Achieva; Phillips Medical Systems, 3000 Minteman Rd, Andover, MA 01810-1099.

[5] OsiriX Imging Software, available from: http:www.osirix-viewer.com/

while the PF torque was divided by the triceps surae CSA_{max} and DF torque by the tibialis anterior CSA_{max}.

Functional ability: Subjects performed 4 timed functional tasks, in the following order: time to rise from the floor, rise from a chair, walk 9m and ascend 4 stairs.[132] The subject was given rest breaks between tasks to minimize the effects of fatigue. Subjects performed each task 3 times, and the best time was used for analysis. The functional ability of the DMD subjects was ranked using the Vignos Lower Extremity Functional Scale.[133] This scale ranges from grade 1 (able to walk and climb stairs independently) to grade 10 (confined to bed).

Main outcome measures: Maximal muscle cross sectional area (CSA_{max}) assessed by MRI of the quadriceps, plantar flexors and dorsiflexors, peak isometric torque from dynamometry, and timed functional tests. Subjects will perform 4 timed functional tasks: time to rise from floor, rise from chair, walk 9m and ascend 4 stairs. [132]

Statistical Analysis

1. To examine differences in muscle strength, muscle CSA_{max}, and specific torque between boys with DMD and controls, independent sample t tests was used after testing for equality of variance (Levene's test).

2. Analysis of covariance was used to test for differences between groups in the slopes of the relationships between age and muscle strength as well as muscle CSA_{max}, and specific torque. The level of significance for between-group comparisons is set at an alpha of 0.05 and adjusted for multiple comparisons using the modified Bonferroni correction.

3. To examine the relationships between functional test times and muscle strength, bivariate linear correlations was made using Pearson product moment correlations (alpha=0.05).

Results

Boys with DMD were shorter in stature and had a higher body mass index than controls (Figure 4-7); however, BSA was similar between groups. No significant differences were noted for age between the 2 groups. The lower-extremity Vignos score ranged from grade 1 (independence in walking and climbing stairs) to grade 4 (walks unassisted and rises from chair but cannot climb stairs) in boys with DMD.

Muscle Strength: Peak torques of the PFs, DFs, and KEs were significantly lower in boys with DMD compared with controls (PFs: 31.3±13.8Nm vs 84.9±52.1Nm; DFs: 10.9±3.2Nm vs 24.6±12.3Nm; KEs: 20.5±7.9Nm vs 79.5±46.6Nm in boys with DMD and controls, respectively; $P<0.001$). The slopes of peak torque versus age (Figure 4-2) for all three muscle groups were also significantly different between boys with DMD and controls ($P<0.001$). The difference in slopes between the DMD and control groups are the result of a considerable gain in muscle strength as a function of age in the control group, which was largely absent in boys with DMD. In the control group, peak torque was 3 to 4 times greater in all muscle groups across the age range. In boys with DMD, the PFs and DFs showed only a slight increase in peak torque with age, while KE peak torque did not vary with age.

The difference in peak torque between groups was also examined after normalization to body size, using BSA, which incorporates the age, height, and weight of the child.[129, 130] Normalized peak torque of the KE and PF was 3 times higher in controls than boys with DMD (KE: 64.2±27.3Nm/m^2 vs 20.9±7.8Nm/m^2, $P<0.0021$; PFs: 68.6±30.2Nm/m^2 vs 20.9± 7.8Nm/m2, $P<0.001$). Normalized peak torque of the DFs was twice as high in controls as DMD subjects (DFs: 20.4± 6.4Nm/m^2 vs 10.8±2.6Nm/m^2, respectively; $P<0.001$). As expected, normalized torque in controls

showed an increase with age (slopes=0.08 – 8.6), while a negative slope was found in the boys with DMD in all 3 muscle groups (slopes=.22 to -1.4).

Maximal CSA: The average CSA_{max} of the triceps surae muscle group was about 60% higher in boys with DMD compared with controls (39.1±13.6cm^2 vs 24.5±9.3cm^2; P<0.002). In contrast, no significant difference was found between groups in the CSA_{max} of the tibialis anterior muscle (3.8±1.1cm^2 vs 4.0±1.5cm^2, P<0.78). Furthermore, the slopes of lines expressing muscle CSA_{max} versus age for the triceps surae and tibialis anterior were not significantly different between boys with DMD and controls (P<0.44 and 0.31, respectively; Figure 4-3 A and B). However, there was a significant difference in slope for the CSA_{max} of the quadriceps muscle group between boys with DMD and controls (P<0.006; Figure 4-3 C). The CSA_{max} of the quadriceps appeared larger in the boys with DMD under the age of 10 years compared with controls. However, in subjects aged 11 years and older, boys with DMD tended to have a smaller CSA_{max} than controls (see Figure 4-3 C).

Specific torque: Specific torque (ie, peak torque normalized to muscle CSA_{max}) was significantly different between groups for the PFs (0.88±0.41Nm/cm^2 in DMD vs 3.26±1.08Nm/cm^2 in controls; P<.001), DFs (2.95±0.99Nm/cm^2 in DMD vs 6.03±1.52Nm/ cm^2 in controls, P<0.001), and KEs (0.69±0.21Nm/cm^2 in DMD vs 2.76±.77Nm/cm2, P<0.001). The specific torque of the KEs and PFs was approximately 4 times as high in the controls compared with boys with DMD. In contrast, a 2-fold difference was found in the DFs. The change in specific torque with age is shown in Figure 4-4. A significant difference in slope was observed between the boys with DMD and controls for specific torque of the PFs (P<0.001) and DFs (P<0.006). For both

muscle groups, the boys with DMD showed a decline in specific torque with age, whereas controls showed an increase with age. No difference was found between groups for the slope of KE specific torque versus age (P<0.78).

Functional ability: Boys with DMD required significantly more time to com- plete all functional tasks compared with controls (Figure 4-5) (P<0.001). There was a progressive increase in the time required to complete functional tasks with age in the boys with DMD, whereas the controls were relatively consistent in their times to complete all 4 tasks. Out of the sample of 22 boys with DMD, 5 were not able to rise from supine (ages 8.8–14y) and 3 were unable to climb 4 stairs (ages 8.8–14y).

In boys with DMD, significant relationships were observed between time to walk 9m and KE peak torque (r=0.57, P<0.005) (Figure 4-6 A), as well as PF peak torque, (r=0.46) (P<0.031) (Figure 4-6 B). Furthermore, torque normalized to CSA_{max} of the KEs was correlated to both the time to walk 9m and time to rise from a chair (r=.51 and r=0.56, respectively; P<.05, not shown). Similar correlations were seen for PF normalized torque with these 2 functional tasks (r=0.45 and r=0.48, respectively; P<0.05, not shown). Interestingly, no significant relationships were observed between the functional tasks with DF strength.

Discussion

The findings of this study provide new insights into the age-related changes in CSA_{max} and specific torque production of important lower-extremity muscle groups in ambulatory boys with DMD. We found approximately 60% greater CSA_{max} of the triceps surae muscles (soleus, gastrocnemius) of ambulatory boys with DMD compared with controls. The increase in triceps surae CSA_{max} was observed across all ages, and in fact the slope between muscle CSA_{max} and age was similar in boys with DMD and

controls. In contrast, the age-related increase in the tibialis anterior CSA_{max} appeared to be unaffected by dystrophy. The quadriceps muscle showed a distinct pattern with larger muscles in young boys with DMD, whereas boys older than 11 years demonstrated relatively smaller CSAs than controls. Torque production was impaired in all 3 muscle groups, including the DFs in boys with DMD, both when expressed as absolute values as well as after normalization to BSA or to muscle CSA_{max} (ie, specific torque). Specific torque showed a modest decline with age in boys with DMD, while healthy boys showed large gains in specific torque between the ages of 5 and 14 years. The torque production of the KEs and PFs, but not the DFs, was correlated to performance on functional tasks such as walking and rising from a chair.

Muscle weakness was observed in all three-muscle groups in boys with DMD, although KE strength deficits were observed at an earlier age. KE torque in DMD was on average 71% of controls at 5 to 7 years old and declined to 15% of controls in subjects over 11 years old. This difference was primarily the result of a 4-fold increase in KE torque of the controls with age. McDonald et al.[132] reported a sharp decline in KE strength with age in boys with DMD, both by isometric testing and the MMT. In their study, boys aged 4 to 6 years had an MMT grade of 4, which corresponded to an isometric strength of 40% to 50% of control values.[132] The MMT grade continued to decline with age, and isometric strength was reported to be less than 5% of controls by the age of 8 years.[132] In comparison, we found that although the relative difference between controls and boys with DMD increased with age, there was little change in absolute torque production of the KE in DMD.

Our findings showed that peak torque of the PF and DF were about two thirds of controls at ages 5 to 9 years, whereas McDonald et al.[132] reported an earlier loss of DF strength com- pared with PFs using the MMT. This may be attributed to differences in the position of the ankle joint in testing the DFs between studies. In the MMT, the ankle is placed at or near full DF, whereas in our study, the DFs were tested near their optimal angle for force generation (30°plantarflexion).[134,135] Between the ages of 5 and 14, we observed a 3-fold increase in PF and DF muscle strength in controls. Only a small increase in absolute torque was observed among boys with DMD over the same age. Similarly, Beenakker et al. [122] reported that the greater disparity in lower-extremity muscle strength in older boys with DMD was primarily the result of an increase in strength among the controls. Another important factor to consider in muscle strength changes with age in our subjects is that all subjects in our study were taking corticosteroids, whereas the previous study by McDonald et al. [132] did not indicate the use of corticosteroids. However, at the time at which they collected longitudinal data (1982–1992), corticosteroids were not part of the standard clinical care for patients with DMD. Because corticosteroids have been shown to stabilize muscle force[136], this intervention may have contributed to an improved preservation of muscle torque in our subjects compared with the previous study. This theory is substantiated by a recent study by Parreira et al. [137] in which the progressive loss in muscle strength in boys with DMD who had initiated corticosteroids was found to be less than that reported in an older study by Scott et al.[138] in which the cohort of boys with DMD were not taking corticosteroids.

Previous MRI studies have focused on examining fatty- tissue infiltration, and in particular the distribution of muscle involvement in a variety of muscular dystrophies and inherited myopathies.[139-142] We used MRI to measure the total muscle CSA_{max} including both muscle and fat tissue, although we also observed differential fatty-tissue infiltration across the lower- extremity muscles (Figure 4-1), intramuscular fat infiltration was not quantified in the current study. Although advanced MR techniques such as proton spectroscopy can be used to quantify lipid content of muscle,[143] this study was conducted to specifically measure differences in CSA_{max} with age and to examine the relationship between muscle size and muscle strength in boys with DMD. We found that PF CSA_{max} was larger in the boys with DMD relative to controls across all ages. In contrast, DF CSA_{max} was not different between groups and showed a similar increase in size with age in both controls and DMD. For the quadriceps, however, the slope of line relating CSA_{max} to age was lower in boys with DMD compared with controls. From the scatter plot it appears that young boys with DMD (under 10y) had a higher quadriceps CSA_{max} than controls, whereas older boys with DMD (over age 10) had a lower CSA_{max} than controls. This difference between DMD and controls must be considered in light of our limited sample of young controls for quadriceps CSA_{max}, because the 2 control subjects who were under 7 years old did not participate in this measurement.

Peak torque normalized to muscle CSA (ie, specific torque) provides an index of muscle quality. Our findings clearly showed that increases in muscle size were not reflected by proportional increases in muscle strength in boys with DMD, consistent with a decline in muscle quality. This is similar to recent findings using DXA, which show low correlations between muscle strength and regional lean body mass in boys with DMD

between 5 and 13 years of age.15 In our study, specific torque was impaired in all 3 muscle groups, with the average KE and PF muscles showing 4 times higher values in controls compared with boys with DMD. However, absolute specific torque only showed a modest decline with age in boys with DMD, while in controls; large age-related gains in specific torque were noted. Interestingly, even though age-related in- creases in the DF CSA_{max} mirrored those of controls, the average specific torque in controls was 2-fold higher than that of boys with DMD. In addition, the relationship between DF specific torque and age was significantly different in ambulatory boys with DMD compared with controls. These data demonstrate that while muscle growth (increase in CSA_{max}) may appear normal in the tibialis anterior muscle, there is a loss of muscle quality.

In healthy boys, there is a sharp rise in specific torque around the onset of puberty (age 13–15years).[144] This rapid increase in force-generating capacity may be related to increases in anabolic hormone levels [145] and stature.[146] Oral corticosteroid use has been shown to decelerate growth rate in boys and suppress adrenal function.[147] The subjects with DMD in this study were of shorter stature than controls, which may also have contributed to a smaller gain in specific torque with age. Interestingly, we noted that there were differences in the specific torques of the different muscle groups in healthy subjects. There was a 2-fold difference between PFs and DFs in normalized peak torque: approximately $3Nm/cm^2$ in PF and approximately $6Nm/cm^2$ in DF. Specific tension of the DFs has been reported to be higher than PFs in healthy adults and may be partially attributed to differences in muscle architecture.[148]

We found that the ability to rise from the floor and climb stairs was lost in 50% of the boys with DMD over age 10, although their absolute lower-limb muscle strength was

similar to younger boys who were still able to complete these tasks. This is most likely because of an increase in body stature with little increase in absolute muscle strength to compensate, as indicated by the lower muscle torques normalized to BSA in boys with DMD. Furthermore, we did not evaluate the strength of the upper limbs and trunk and their contribution to the ability of the boys with DMD to perform functional tasks. These muscle groups also play an important role in functional ability in boys with DMD, especially as leg muscle strength declines and compensatory movements are required to maintain independent mobility. Relationships between muscle strength and ability to walk and perform sit-to-stand transfers were observed in the KEs and PFs. Previous studies have also found relation- ships between lower-limb muscle strength and ambulation and transfers.[122,149] Furthermore, PF strength has been implicated as a key muscle in maintaining gait in boys with DMD.[150] Interestingly, we did not observe any relationships between DF muscle strength and functional ability, although a previous study[151] found that ankle DF muscle strength of less than grade 4 was a key prognostic factor in determining time to wheelchair dependence in boys with DMD. Because all subjects in our study were ambulatory, DF torque may not have played a role in their current walking ability.

Although we observed differential fatty-tissue infiltration across the lower-extremity muscles (Figure 4-1) in boys with DMD, fibrosis and intramuscular fat infiltration was not quantified in the current study. All magnetic resonance images in this study were acquired using a standard T_1-weighted imaging sequence, with fat suppression, to facilitate segmentation of the muscle boundaries and quantification of the muscle CSA. Advanced MR techniques such as volume-localized spectroscopy and

3-point Dixon can be used to measure the intramuscular lipid composition;[88] however, the quantification of fibrosis in skeletal muscle presents significant challenges because of extremely short T_2 of collagen. MRI of human skeletal muscle also suffers from partial volume filling because of limited spatial resolution, adding to the complexity of quantifying non-contractile tissue in muscular dystrophies.

Summary

Using MRI in combination with dynamometry allowed us to measure the muscle CSA_{max} and specific torque production of primary lower-extremity muscles in children with DMD. Age- related changes in muscle CSA and specific torque production in lower-extremity muscles showed distinctly different patterns in the KE, PF, and DF muscles of boys with DMD. The distal triceps surae muscles showed a larger CSA_{max} by approximately 60% in ambulatory boys with DMD compared with controls across ages, while the tibialis anterior muscle showed age-appropriate increases in CSA_{max}. In the quadriceps muscle, CSA_{max} tended to be higher than controls in younger boys with DMD but lower in older boys with DMD over 10 to 11 years of age. However, all muscles showed significant deficits in specific torque, with a 4-fold difference in the PF and KE, and 2-fold difference in the DFs. Specific torque showed a modest decline with age in boys with DMD, while in controls, large age-related gains in specific torque were noted.

Future clinical trials for therapeutic strategies in DMD should consider examining multiple muscles to evaluate the efficacy of treatment, as well as the inclusion of physiologic measures such as muscle CSA and specific torque. This study also underlines the importance of including age-matched healthy controls in evaluating boys with DMD.

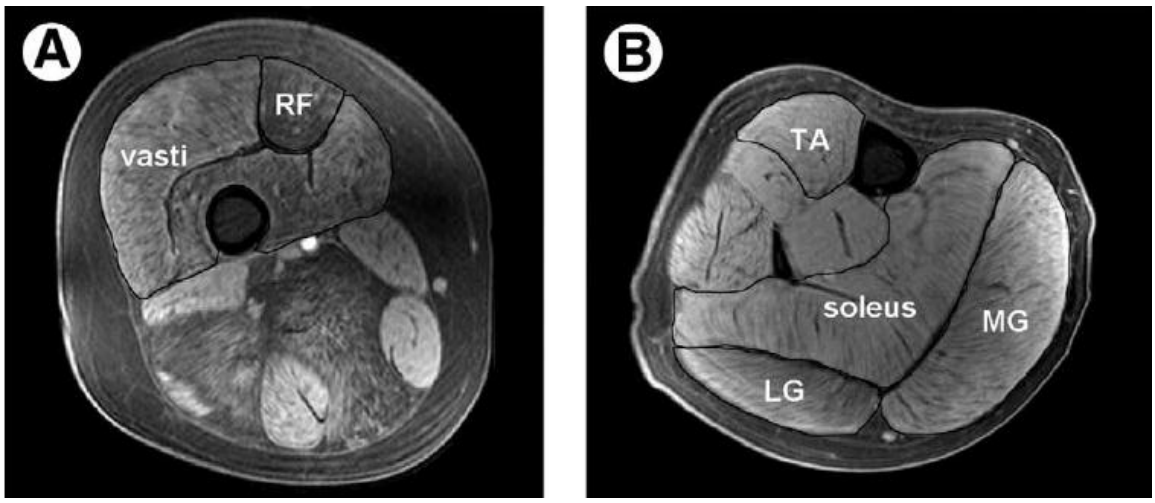

Figure 4-1. T_1-weighted fat-suppressed transaxial images of the thigh (A) and lower leg (B) obtained from an 11-year-old boy with DMD. The rectus femoris and vasti muscles are outlined on the thigh, and the TA, soleus, MG, and LG are outlined on the lower leg. Note the presence of fatty infiltration to a greater extent in the thigh musculature than in the calf. Abbreviations: LG, lateral gastrocnemius; MG, medial gastrocnemius; RF, rectus femoris; TA, tibialis anterior.

Figure 4-2. Scatter plots of age versus peak torque (Nm) in boys with DMD (filled circles, solid line) and controls (open circles, dashed line) (A) PFs (n=22 DMD, n=10 control), (B) DFs (n=21 DMD, n=10 control), and (C) KEs (n=22 DMD, n=10 control). Please note that in A, 2 subjects with DMD had overlapping values for plantar flexion peak torque (age 6.2y, 33.2Nm and 33.4Nm); in B, 1 subject with DMD was unable to perform the dorsiflexion torque measurement.

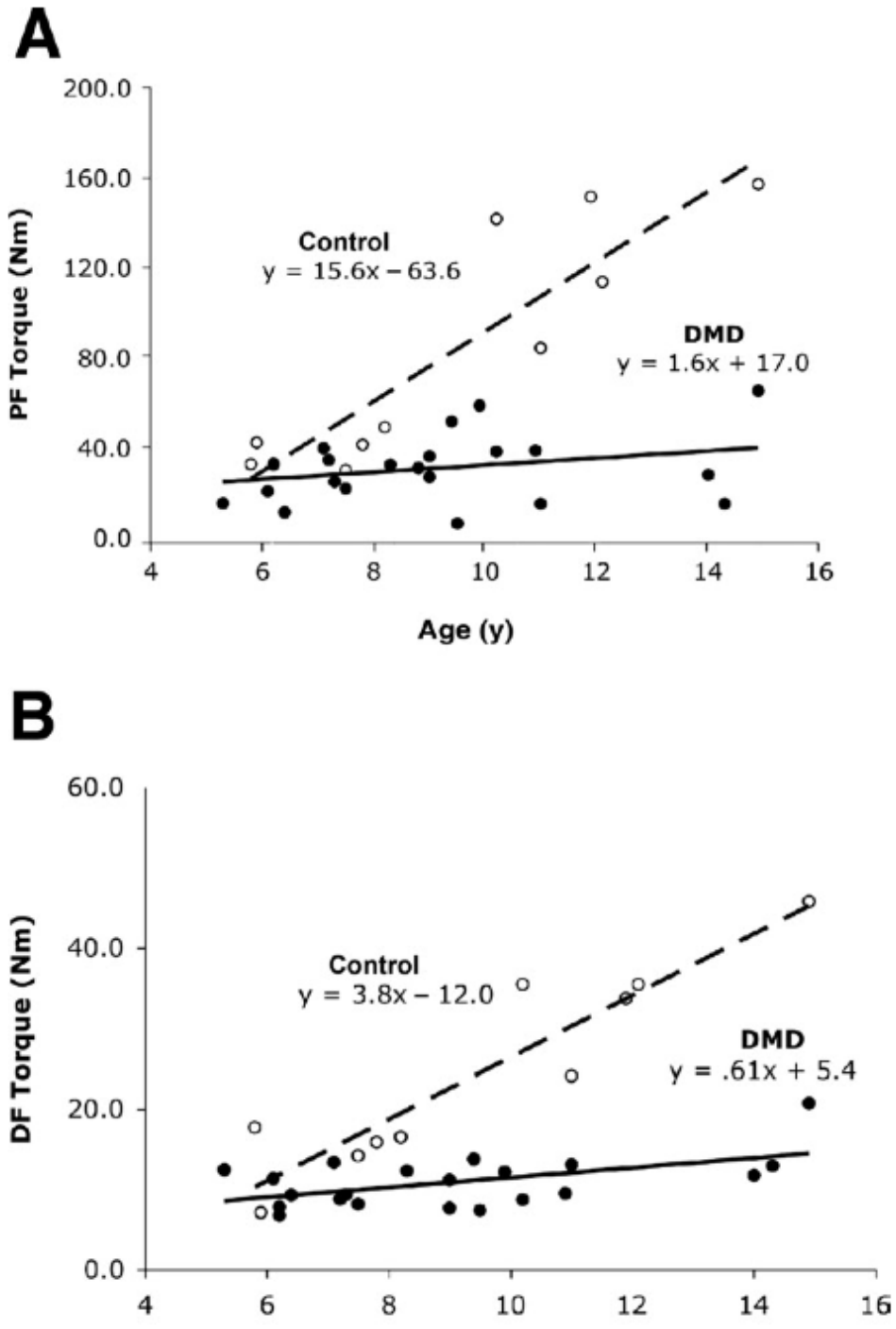
A
200.0
160.0
120.0
80.0
40.0
0.0
PF Torque (Nm)
Control
y = 15.6x – 63.6
DMD
y = 1.6x + 17.0
4
6
8
10
12
14
16
Age (y)
B
60.0
40.0
20.0
0.0
DF Torque (Nm)
Control
y = 3.8x – 12.0
DMD
y = .61x + 5.4
4
6
8
10
12
14
16

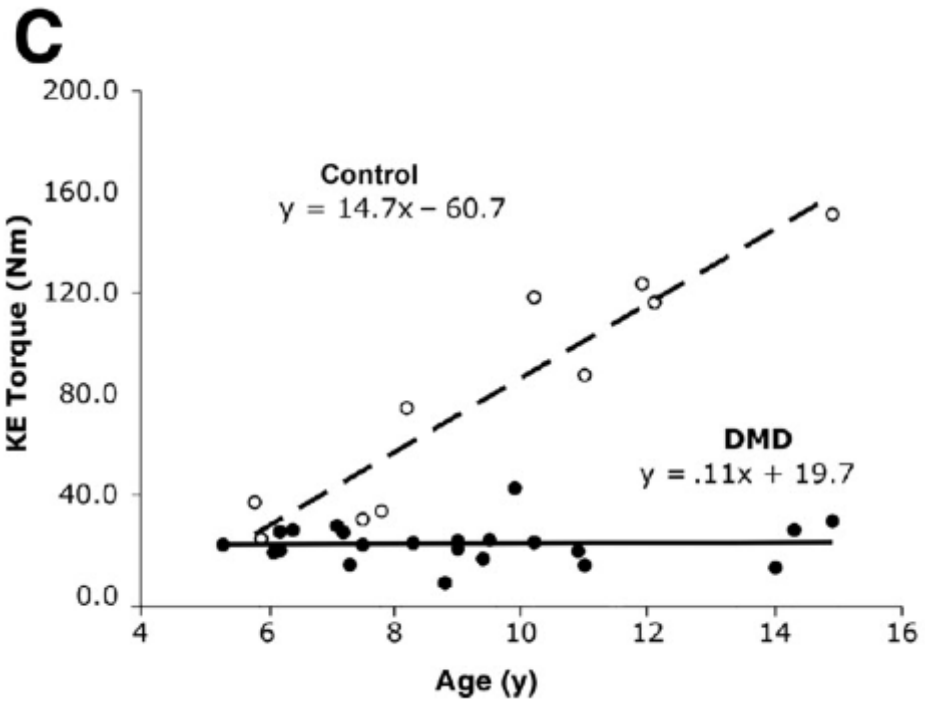
C
200.0
160.0
120.0
80.0
40.0
0.0
KE Torque (Nm)
Control
y = 14.7x – 60.7
DMD
y = .11x + 19.7
4
6
8
10
12
14
16
Age (y)

Figure 4-3. Scatter plots of CSA_{max} (cm^2) versus age in boys with DMD (filled circles, solid line) and controls (open circles, dashed line)

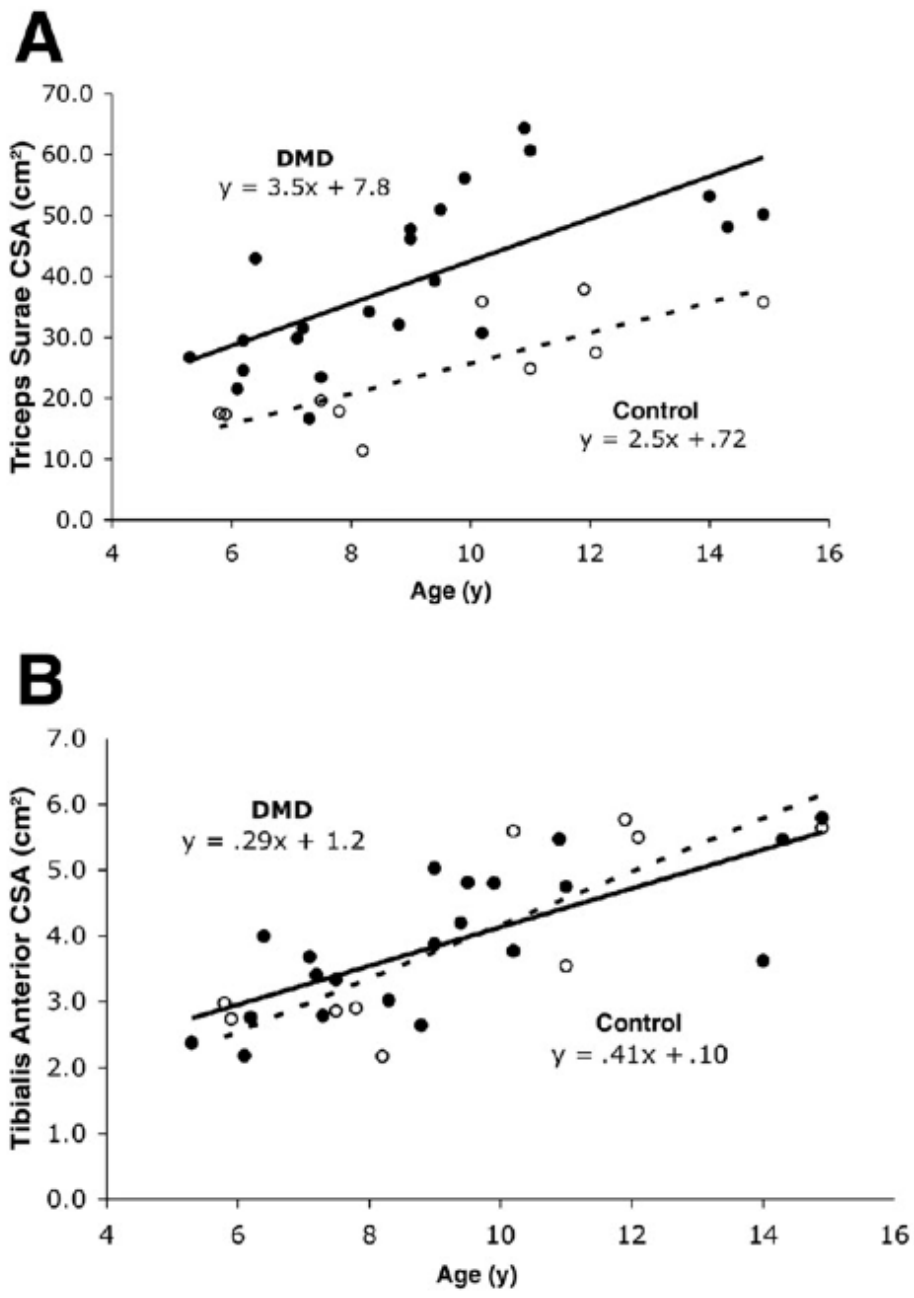
A
Triceps Surae CSA (cm²)
70.0
60.0
50.0
40.0
30.0
20.0
10.0
0.0
DMD
y = 3.5x + 7.8
Control
y = 2.5x + .72
4
6
8
10
12
14
16
Age (y)
B
Tibialis Anterior CSA (cm²)
7.0
6.0
5.0
4.0
3.0
2.0
1.0
0.0
DMD
y = .29x + 1.2
Control
y = .41x + .10
4
6
8
10
12
14
16
Age (y)

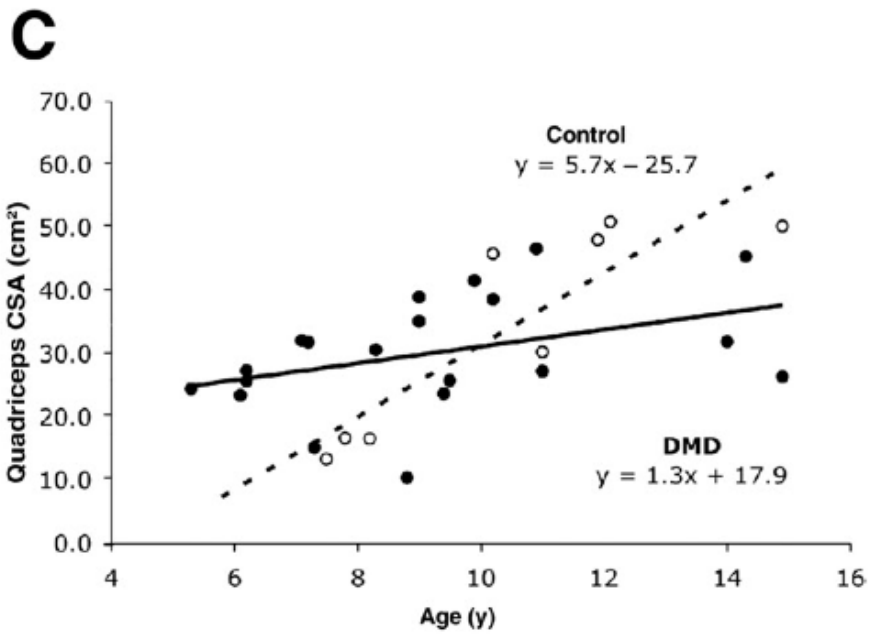
C
70.0
60.0
50.0
40.0
30.0
20.0
10.0
0.0
Quadriceps CSA (cm²)
Control
y = 5.7x – 25.7
DMD
y = 1.3x + 17.9
4
6
8
10
12
14
16
Age (y)

Figure 4-4. Scatter plots of age versus specific torque (torque normalized to CSA_{max} of muscle; Nm/cm^2) in boys with DMD (filled circles, solid line) and controls (open circles, dashed line)

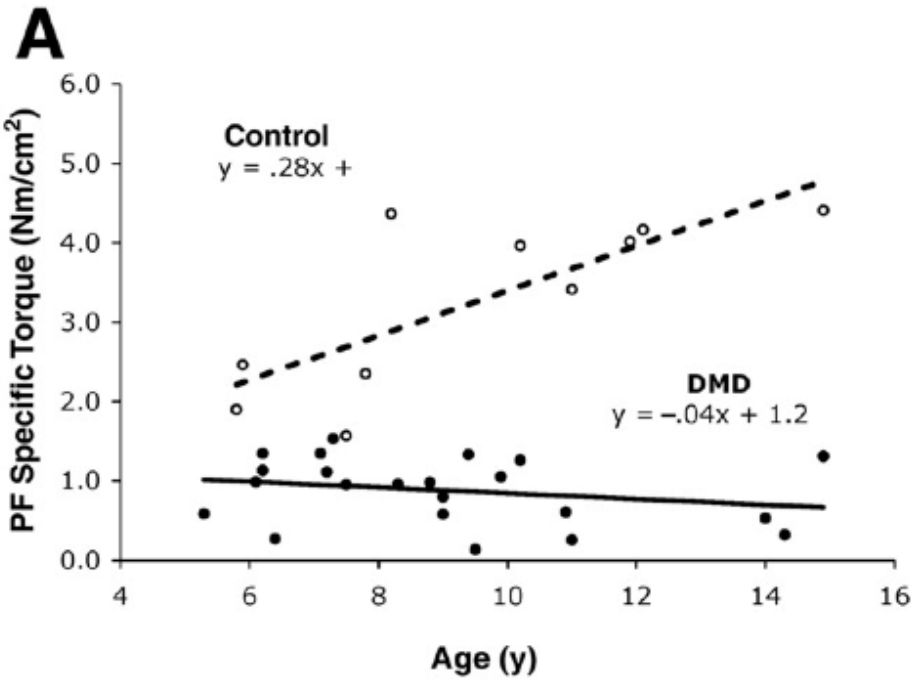
A
PF Specific Torque (Nm/cm²)
Control
y = .28x +
DMD
y = –.04x + 1.2
Age (y)

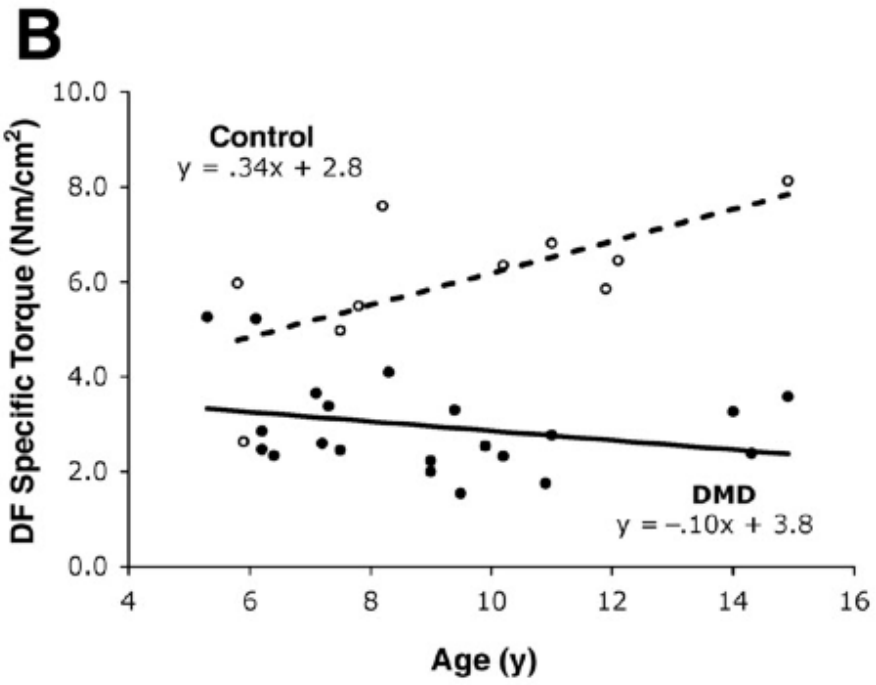
B
DF Specific Torque (Nm/cm²)
Control
y = .34x + 2.8
DMD
y = –.10x + 3.8
Age (y)

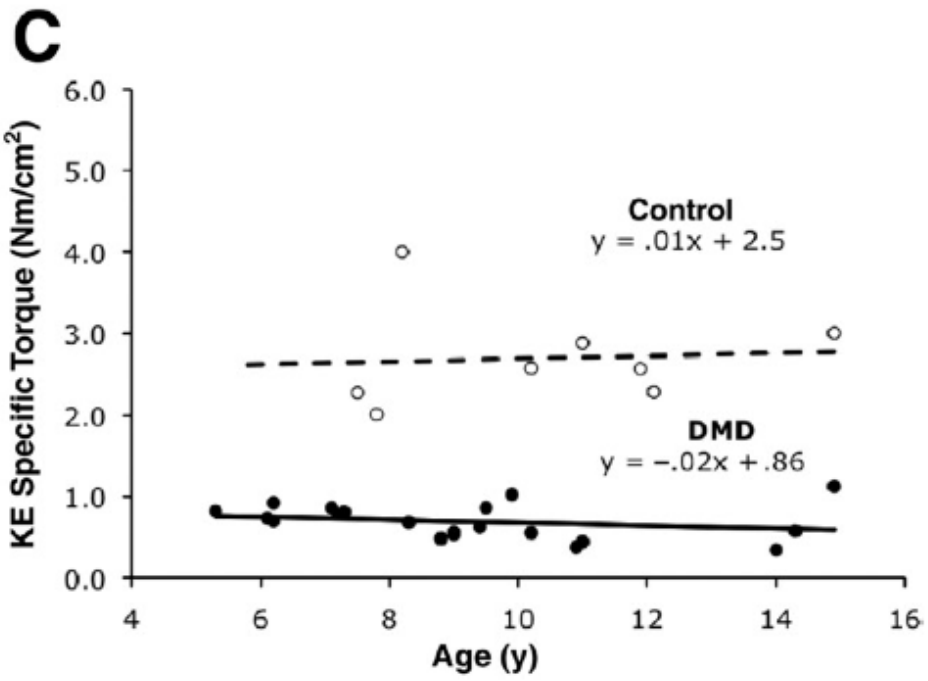
C
KE Specific Torque (Nm/cm²)
6.0
5.0
4.0
3.0
2.0
1.0
0.0
Control
y = .01x + 2.5
DMD
y = −.02x + .86
4
6
8
10
12
14
16
Age (y)

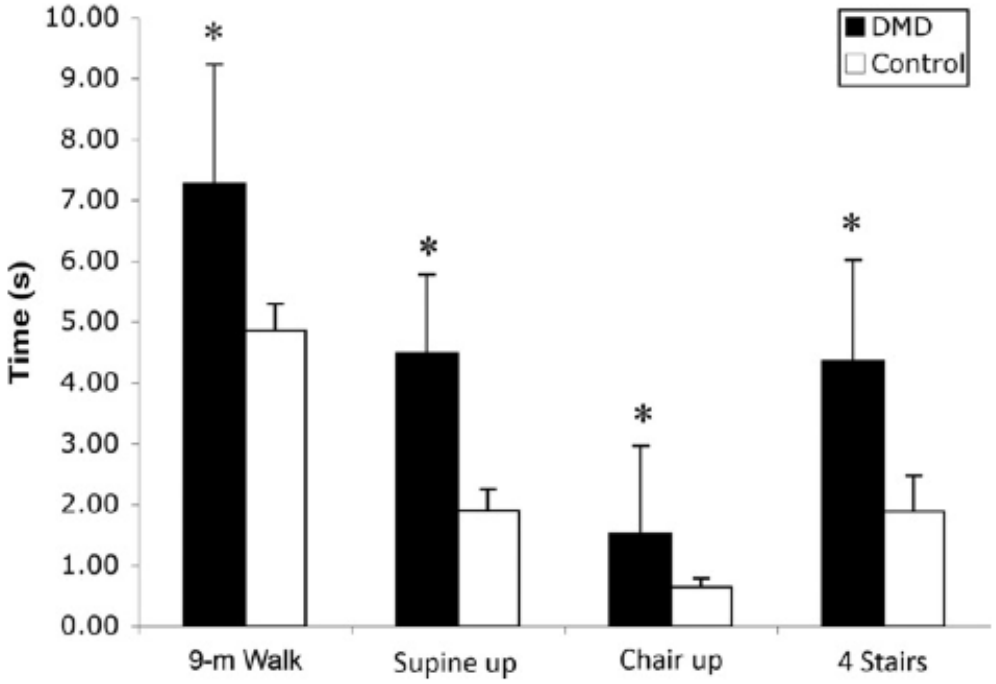

Figure 4-5. Group means ±SD of 4 timed functional tasks in boys with DMD and controls. *P<0.001.

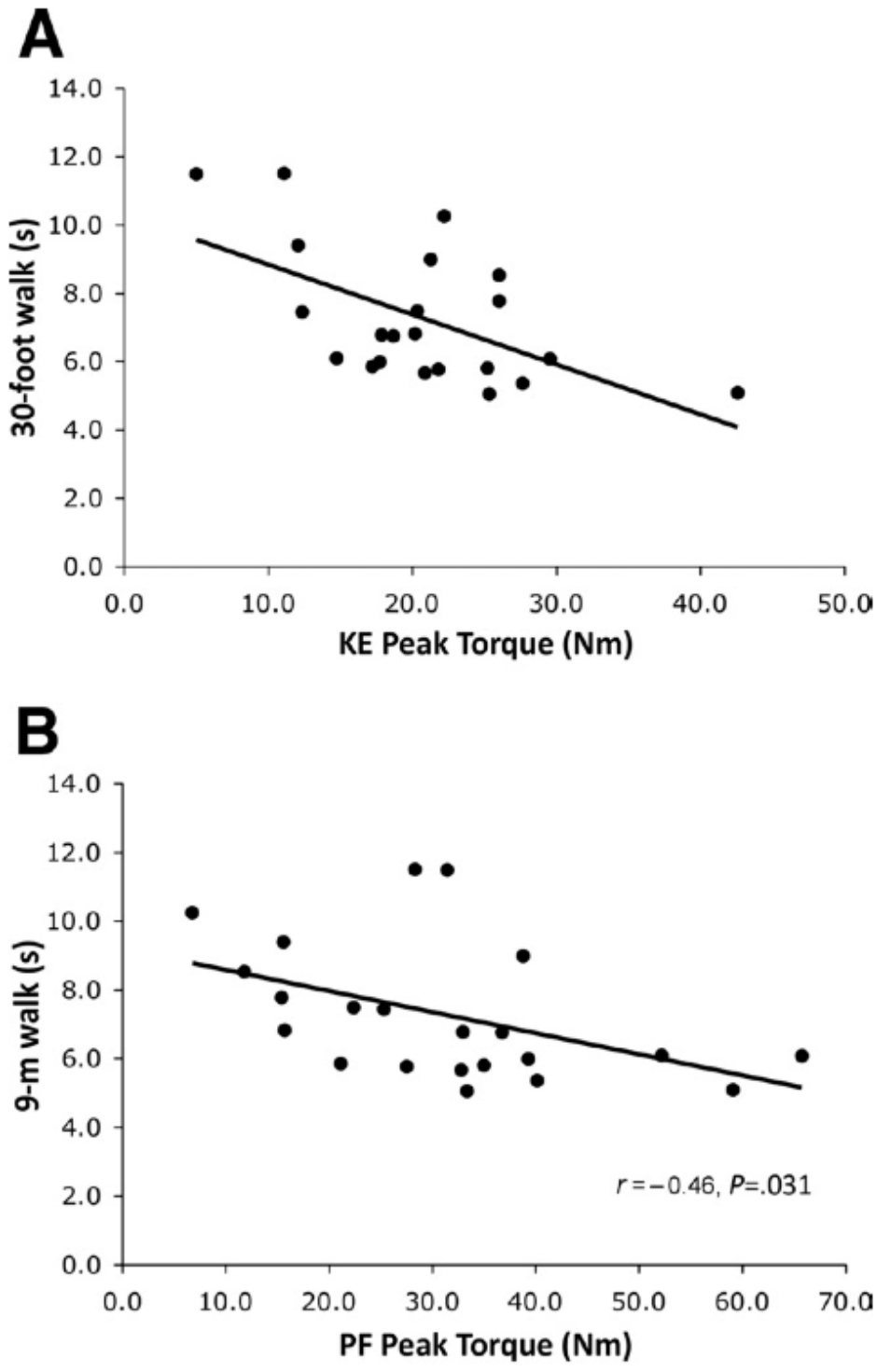

Figure 4-6. Relationships between peak torque of the KEs (A) and PFs (B) and time to walk 9m.

Table 4-1. Demographics of patients.

Characteristics	DMD (n=22)	Controls (n=10)	P
Age (y)	9.6±2.7	9.7±3.0	0.48
Height (m)	1.20± 0.13	1.40±0.18	0.002*
Weight (kg)	31.3±11.2	33.1±11.6	0.67
BMI (kg/m2)	20.7±5.3	16.3±1.7	0.002*
BSA (m2)	1.02±0.23	1.15±0.25	1.6
Vignos score (median)	1.5(1-4)	1	NA

CHAPTER 5
RELATIONSHIP BETWEEN LOWER EXTREMITY MUSCLES CONTRACTILE CROSS SECTIONAL AREA AND FUNCTIONAL MEASUREMENTS IN BOYS WITH DUCHENNE MUSCULAR DYSTROPHY

Muscular dystrophy includes a large group of genetic disorders that result in loss of muscle fibers, leading to progressive skeletal muscle weakness. Duchenne muscular dystrophy (DMD) is one of the most common forms of muscular dystrophy affecting approximately 1 in 3500 newborn males. DMD is caused by a mutation in the dystrophin gene leading to absence or non-functional structural protein, dystrophin (dys).[12] Absence of dystrophin protein affects sarcolemmal integrity leading to progressive fatty tissue infiltration and muscle atrophy.

Loss of muscle strength and skeletal functional muscle mass profoundly leads to an increased risk of disability, morbidity and ultimately quality of life.[152,153] During the initial stages of the disease inflammatory changes and repair are seen which are followed by irreversible fatty tissue infiltration.[154] Progressive fatty tissue infiltration and muscle weakness lead to loss of ambulation between the age of 10 and 15 years. Disease progression and the loss of functional muscle mass ultimately leads to premature death due to cardiopulmonary complications in early twenties.[155]

Selective muscle involvement is an important feature of DMD, with some muscles displaying hypertrophy and others muscle atrophy. In DMD patients, there is a significant loss of skeletal muscle mass [91,118,141,156] especially in proximal muscles including pelvis and thigh muscles. Furthermore, extensor muscles are weaker than flexor muscles.[132] The term ‘pseudo-hypertrophy’ has been used in DMD to describe selective enlargement of the posterior compartment muscles, especially the calf muscles, assuming that a large component of the muscle is occupied by non-contractile

material. Other studies have shown selective sparing of the gracillis (Gr), sartorius (Sar), semimembranosus (SM) muscles[118,141] and tibialis posterior (TP)[97,157] In fact, there are reports of true hypertrophy in Gr and Sar muscles.[141] Assessing changes in muscle cross sectional area is an important measure in muscular dystrophy patients as muscle size is an important determinant of muscle strength [91,141], but differentiating between contractile and non-contractile component holds even more significance.[90]

Magnetic resonance imaging (MRI) has been used to monitor alterations in skeletal muscle in conditions like obesity, [158] sarcopenia,[159] cachexia.[160] Furthermore, MRI has also been used to monitor disease progression in various myopathies.[161,162] MRI methods, such as T_1- and T_2 weighted imaging, and three point DIXON imaging, have been utilized to estimate intramuscular fatty infiltration in DMD patients.[156,161] Recently, we demonstrated the differences in age related changes in lower extremity muscles CSA and specific torque production in boys with DMD compared to controls.[91] Furthermore, we evaluated the contractile and non-contractile tissue in thigh muscles of boys with DMD. [90] However, to our knowledge no study has quantified the amount of contractile and non-contractile tissue in lower extremity muscles, which is the focus of this chapter.

Specific Aims

To assess the non-contractile and contractile content of individual muscles of lower extremity in boys with DMD and age matched healthy controls. 2) To evaluate the relationship between non-contractile content and functional ability of boys with DMD. 3) To evaluate age related changes in contractile and non-contractile content of lower leg muscles in boys with DMD.

Research Design and Methods

Subjects: A cohort of thirty-one boys with DMD (DMD group) and thirteen healthy boys from the general population (CONT group) volunteered to participate in this observational cross-sectional study. Ambulatory status and mean (±SEM) physical characteristics of all subjects are shown in Table 5-1. A report confirming the diagnosis of DMD using molecular genetic testing (e.g. PCR amplification) and/or immunohistochemical staining from muscle biopsy was obtained from each of the DMD subjects. In the DMD group, twenty-nine boys were ambulatory and three boys were non-ambulatory. All DMD subjects were being treated with corticosteroids (either Prednisone or Deflazacort). CONT subjects were relatively sedentary, in that they did not participate in sport specific training 2 or more times per week. This study was approved by the Institutional Review Board at the University of Florida. Written informed consent was obtained from the participants' parents, and written assent was obtained from each participant.

MRI acquisition: MRI was performed on 3.0T (Achieva)[1] whole-body scanner. Subjects were placed in a supine position with their lower leg positioned in either a lower-extremity quadrature coil (1.5T) or an 8-channel sensitivity encoding, receive-only extremity coil (3.0T) for lower leg imaging. Three-dimensional transaxial gradient echo images were acquired with the following parameters: repetition time=24ms, echo time=1.8ms, flip angle=20°, and optimized field of view 12–14cm^2.

Isometric muscle strength testing: Isometric peak torque of the KEs, PFs, and DFs of the right leg was measured using a Biodex[2] dynamometer. For KE testing, the

[1] Achieva; Philips Medical Systems, 3000 Minuteman Rd, Andover, MA 01810-1099.
[2] Biodex Medical Systems, 20 Ramsay Rd, Shirley, NY 11967-4704

knee and hip joints were placed at 90° of flexion. For PFs and DFs, the knee was placed between 0° to 10° of flexion and the ankle was placed in neutral (for PFs) or 30° of plantar-flexion (for DFs). The subject was instructed to push or pull as hard as possible for 5 seconds, followed by a 2-minute rest. Five trials were performed for each muscle group, and the highest torque value was used for analysis (peak torque). This protocol was tested for between-day reliability (2-month interval) by the same tester, in a subset of children with DMD (n=6) and controls (n=10). ICCs were calculated for both groups of subjects. High reliability was found for all 3-muscle groups (KEs: ICC=0.89 in DMD and 0.99 in controls, PFs: ICC=0.88 in DMD and 0.98 in controls, and DFs: ICC=0.87 in DMD and 0.95 in controls; P=. 001 for all ICCs).

Functional abilities: Subjects were asked to perform timed functional tasks. These tasks included the time to walk 30 feet (30 feet Walk), time to rise from floor (Supine up), time to rise from a chair (Chair Up), the pediatric timed up and go (TUG) and ascend four stairs (4 stairs) [132]. Subjects were asked to perform each tests three times and the fastest time was recorded for analysis. The functional ability was also ranked using Brookes Lower Functional scale (Brooke et al., 1981). This scale is ranged from grade 1 (able to walk and climb stairs independently) to grade 10 (confined to bed).

MRI data analysis: Medical Image Processing, Analysis and Visualization (MIPAV)[3] software (version 4.2.1; National Institutes of Health, MD) was used to analyze the MR images. We selected a single image corresponding to the most proximal slice in which Flexor hallucis longus (FHL) could be visually confirmed.

[3] MIPAV imaging software, available from: http://mipav.cit.nih.gov/.

Furthermore, we one immediate proximal and distal slice was used for data analysis. We identified 5 individual muscles on the image: tibialis anterior (TA), extensor digitorum longus (EDL), peroneals (PER), medial gastrocnemius (MG) and soleus (SOL). Representative MR images for DMD and Ctrl subjects are shown in Figure 5-1.

Contractile cross sectional area (C-CSA) and non-contractile cross sectional area (NC-CSA) in the lower leg muscles was calculated using a modified image analysis technique as previously described.[159,163] The first step of the analysis was to correct for image heterogeneity caused by sub- optimal radiofrequency coil uniformity, or gradient-driven eddy currents, using a well-established nonparametric non- uniform intensity normalization (N3) algorithm.[164] This step was essential for subsequent analyses that assume homogenous signal intensity across the images. Optimized image correction parameters (N3) were determined (end tolerance 0.0001; maximum iterations 100, signal threshold 1; field distance 33.33 mm; subsampling factor 2; Kernel full width half maximum of 0.15; Wiener filter noise 0.01), and the same parameters were applied to all images.

To separate contractile and non-contractile tissues in the pixel number-signal intensity histogram with minimal bias, we implemented the Maximum Entropy method. Furthermore, to minimize manual tracing errors, three trials were averaged, and the values were applied to all muscles of interest. After tracing all muscles of interests, following parameters were calculated 1) total number of pixels with in ROI; 2) the number of pixels with a signal intensity lower than the threshold value (contractile tissue) and 3) the number of pixels with a value higher than the threshold value (non-contractile tissue). The proportion of contractile and non-contractile content of each

muscle was calculated as: Contractile content (%) = (CC)/[(CC)+(non-CC)] x 100, Non-contractile content (%) = (non-CC)/[(CC)+(non-CC)] x 100. The contractile and non-contractile CSA was calculated as: Contractile CSA (cm^2) = (CC) x (FOV/matrix size)^2 Non-contractile CSA (cm^2) = (non-CC) x (FOV/matrix size)^2. Where CC = contractile tissue pixel number; non-CC = non-contractile tissue pixel number; FOV= field of view. Intra class correlation coefficient in individual muscles ranged from 0.93 to 1.00 for non-contractile content.

Statistical analysis: All values are reported as means and standard error of the mean. Levene's test showed unequal variances between DMD and Ctrl groups. Non-parametric Mann Whitney tests were used to compare % non-contractile content, contractile CSA and non-contractile CSA between DMD and Ctrl groups. Spearman's rank correlation tests were used to determine the relationships between two independent variables. The level of significance was set at $p<0.05$.

Results

Subject demographics: Boys with DMD were shorter in height and had higher body mass index compared to controls (Table 5-1); however no significant difference was found between age and weight of DMD and CTRL groups. Furthermore, the mean Brookes scale was 2.2±0.4 in DMD boys, indicating that most patients in this group were ambulatory, except for three subjects who were non-ambulatory.

Contractile and non-contractile content of lower leg muscles: Non-contractile content (%) (%NCC), Contractile CSA (cm^2) (C-CSA), and non-contractile CSA (cm^2) (NC-CSA) of lower leg muscles of DMD and Ctrl are shown in Figure 5-2. Both the % NCC and NC-CSA of the Per, MG and SOL differed significantly between

DMD boys and Ctrl ($p<0.05$). On the other hand, no difference was found in the % NCC and NC-CSA of the TA and EDL between DMD and Ctrl group.

Relationships between non-contractile content of lower leg muscles and functional abilities: We used Spearman's rank correlation coefficients to examine the relationship between the % NCC of different muscles, strength measurements, timed functional tests and Brooke's scale in DMD subjects (Table 5-2). (A) We found significant correlation between %NCC of Per ($p<0.05$), MG ($p<0.01$), SOL ($p<0.01$) and plantar flexor peak torque. (B) Furthermore, significant correlations were found between % NCC of all muscles and 30-feet walk ($r_s=0.45$-0.61, $p<0.001$) as well as the Brookes scale (0.43-0.62, $p<0.001$) Figure 5-3 and 5-4. (C) Significant correlations were also found between %NCC of EDL ($p<0.05$), Per ($p<0.05$) and dorsi flexor peak torque, however we did not find a significant correlation between % NCC of TA and dorsi flexor peak torque. In addition, we found that specific torque of DF and PF was significantly reduced in DMD as compared to Ctrl group (Figure 5-5).

Age related changes in contractile and non-contractile CSA: Muscles of the lower limb of DMD boys were evaluated for age related changes in contractile and non-contractile CSA (Figure 5-6, 5-7). All DMD subjects were divided into three sub-groups i.e 5-8 years, 8-10 years and 10 years and above (10 years <). An age dependent progressive increase in both NC-CSA and C-CSA was observed. (A) NC-CSA of all the lower leg muscles was significantly different between 5-8 and 8-10 years old DMD boys ($p<0.01$). (B) Between 8-10 and 10 years < groups, NC-CSA was significantly different in Per, MG, SOL ($p<0.001$). (C) CCSA Per and MG differed significantly between group 5-8 and 10 years < ($p<0.01$).

Discussion

The main findings of this study were (1) DMD boys had a significant increased proportion of % NCC and NC-CSA in lower leg muscles compared to age matched controls, especially in Per, MG and SOL. (2) The proportion of % NCC of leg muscles correlated with functional ability as assessed by the 30 foot walk and Brookes scale, however muscle % NCC did not correlate with strength measurements assessed using dynamometer muscle testing (3) NC-CSA of all the lower leg muscles increased with age in DMD boys, (4) C-CSA of Per and MG differed significantly between 5-8 year and 10 years < age group in DMD boys. (5) The DF and PF specific torque production was significantly reduced in DMD boys as compared to healthy boys.

Assessment of non-contractile content in lower leg muscles of DMD boys: Although, all the lower leg muscles (TA, EDL, Per, MG, SOL) in the DMD group had increased proportion of % NCC, it was significantly greater in Per, MG and SOL muscles compared to Ctrl group. Our findings indicate that TA and EDL muscles were relatively spared with %NCC less than 10%. Similarly, Arai et al.[165] reported that the TA and TP were relatively preserved up to 14 years of age. Similarly, Torriani et al.[97] found that TA, EDL and TP were relatively spared in DMD patients. Furthermore, we have shown that the %NCC ranged from 20%-40% in Per, 18%-42% in MG and 11%-22% in SOL muscle, whereas in healthy boys % NCC ranged from 1-8% in all muscles. These findings are in accordance with previous studies[166] in which the authors reported a percentage of 18-38% increase in fatty-fibrous tissue in gastrocnemius muscle whereas this component never exceeded 8% in normal subjects.

Contractile, Non-contractile CSA and specific torque production in DMD boys: Amount of force generated per unit muscle mass (specific force) is an important

determinant of muscle quality. Our results showed that, NC-CSA of Per, MG (DMD, 92% of Ctrl) and SOL (DMD 82% of Ctrl) were significantly greater in DMD than Ctrl. In contrast, C-CSA of lower leg muscles was not significantly different between DMD and Ctrl subjects. A similar pattern of muscle involvement has been previously reported in DMD patients.[97, 157, 167] It is valuable to differentiate and quantify both C-CSA and NC-CSA because patients having more muscle mass preserved may respond well to various therapies. A study by van Deutekom et al.[167] showed that muscles with less fatty tissue infiltration responded well to antisense oligonucleotide treatment.

Pseudo-hypertrophy of the calf muscles is one of the hallmark signs of DMD. It is assumed to be caused by replacement or infiltration of muscles by collagenous and/or fatty tissue. Although, the most commonly affected muscles are the calf muscles pseudo-hypertrophy has been reported to occur in temporalis muscle as well.[168] Increase in both C-CSA and NC-CSA can lead to an increase in overall size of the muscle which can be measured by assessing calf circumference[169] and CSA.[91] Our results indicate that there is an increase in both C-CSA and NC-CSA in the lower leg muscles in DMD patients compared to healthy boys. However, the increase in NC-CSA is more pronounced especially in Per, MG and SOL muscles. Similar to our results, Jones et al. [170] reported true hypertrophy in the calf muscles of DMD boys using needle biopsy. Furthermore, they reported that despite the presence of hypertrophied fibers it was insufficient to cause muscle enlargement.

Age related changes in C-CSA and NC-CSA in lower leg muscles: We have reported that NC-CSA increases significantly with age in all the examined lower leg

muscles. However, only C-CSA of Per and MG (42% and 45% respectively) differed significantly between 5-8 and 10 < years.

Muscle contractile area and specific torque: Our study showed a significant decrease in DF and PF specific force in DMD patients (43% and 62% respectively) as compared to Ctrl. Furthermore, both PF and DF specific torque strongly correlated with age in Ctrl subjects whereas this relationship was absent in DMD patients. Similar results have been reported in animal studies affirming that specific force (P_0) of EDL and SOL muscles differ significantly between *mdx* and C57Bl mice.[171]

Limitations: There were some limitations to our study. Firstly, even after correcting the images with N3 inhomogeneity correction we were unable to do so completely. We did not include lateral gastrocnemius because of presence of B_1 inhomogeneity. Secondly, because of limited spatial resolution MR images suffer from partial volume filling leading to underestimation of the contractile area.

Summary

We have shown that T_1 weighted images can be used to quantify contractile and non-contractile tissue content in lower leg muscles. The amount of non-contractile content assessed by MRI was significantly greater in lower leg muscles of boys with DMD especially Per, MG and SOL. Moreover, there was a significant correlation between amount of non-contractile tissue present and functional measurements such as 30- foot walk and Brookes scale. We have also shown that C-CSA did not differ significantly between DMD and Ctrl group. In addition, we have shown that there is increase in C-CSA of Per and MG with age which may indicate “compensatory hypertrophy”. However, NC-CSA was significantly greater in DMD boys especially in

Per, MG, and SOL suggesting “pseudo-hypertrophy”. Finally, MRI can provide critical information, which can be used to assess the disease progression in DMD boys.

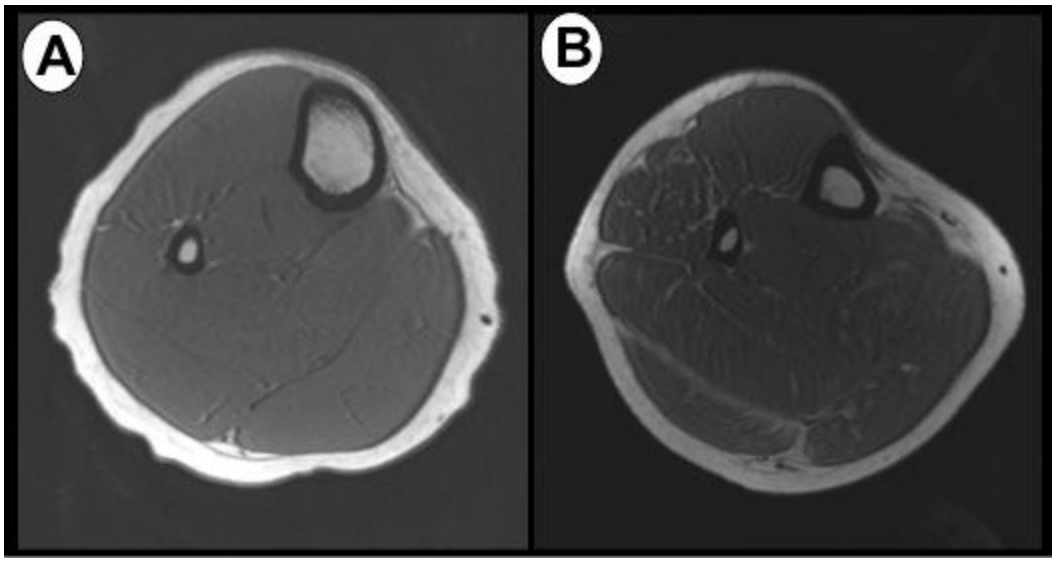

Figure 5-1. T1 weighted fat-unsuppressed trans-axial images of the lower leg of Ctrl (A) and DMD subject (B).

Figure 5-2. Comparison of percent non-contractile content, non-contractile CSA and contractile CSA of lower leg muscles. A) Comparison of non-contractile content of lower leg muscles between DMD and Ctrl boys. TA, tibilais anterior; EDL, extensor digitorum longus; Per, peroneals; MG, meadial gastrocnemius; SOL, soleus. *$p<0.05$. B) Comparison of non-contractile cross sectional area of lower leg muscles between DMD and Ctrl boys. C) Comparison of contractile cross sectional area of lower leg muscles between DMD and Ctrl boys. TA, tibilais anterior; EDL, extensor digitorum longus; Per, peroneals; MG, medial gastrocnemius; SOL, soleus. *$p<0.05$, # $p=0.07$.

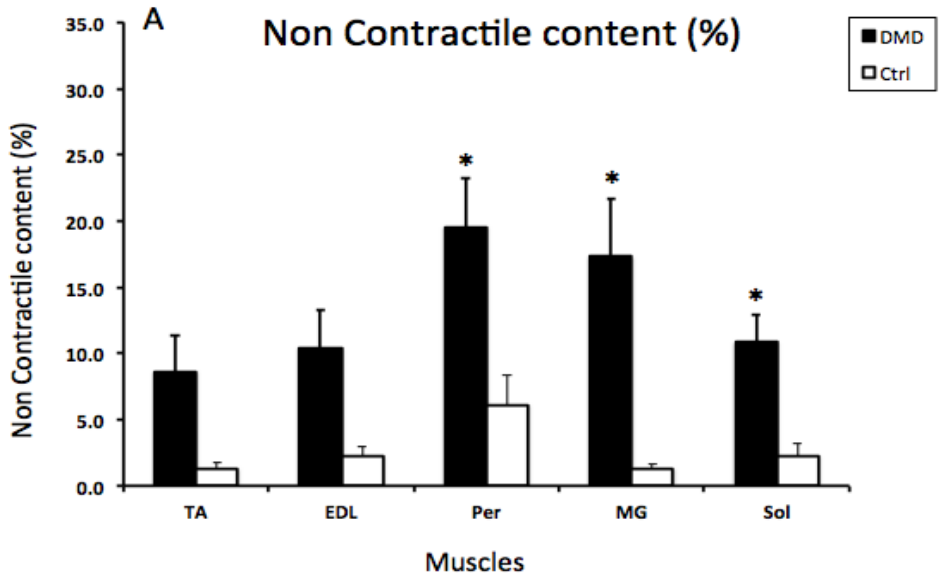
A
Non Contractile content (%)
DMD
Ctrl
Non Contractile content (%)
35.0
30.0
25.0
20.0
15.0
10.0
5.0
0.0
*
*
*
TA
EDL
Per
MG
Sol
Muscles

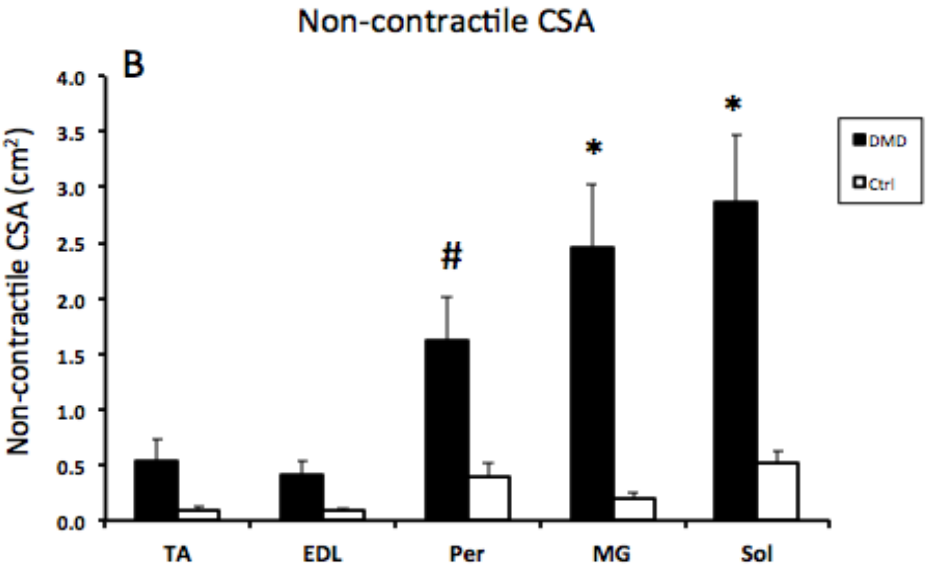
Non-contractile CSA
B
DMD
Ctrl
Non-contractile CSA (cm²)
4.0
3.5
3.0
2.5
2.0
1.5
1.0
0.5
0.0
#
*
*
TA
EDL
Per
MG
Sol

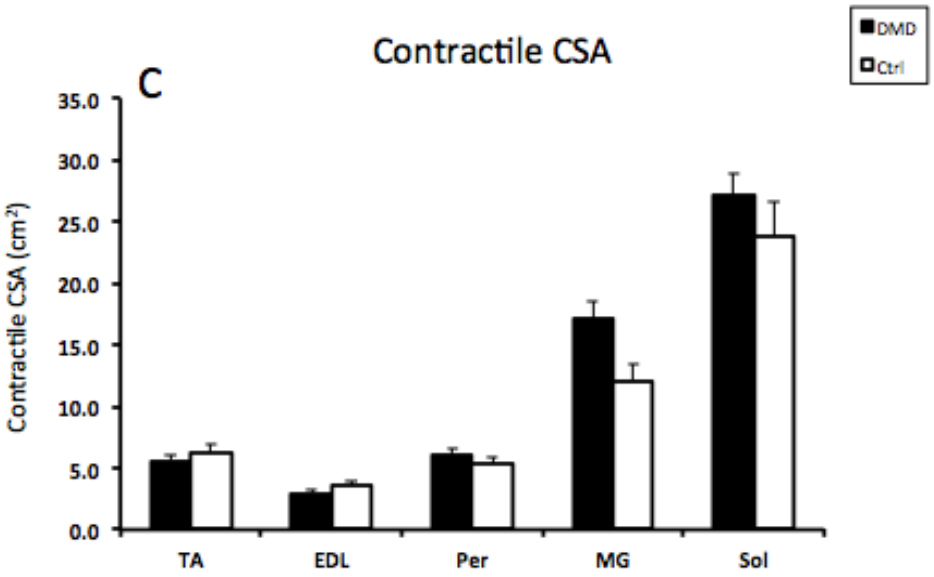
C
Contractile CSA
DMD
Ctrl
Contractile CSA (cm²)
35.0
30.0
25.0
20.0
15.0
10.0
5.0
0.0
TA
EDL
Per
MG
Sol

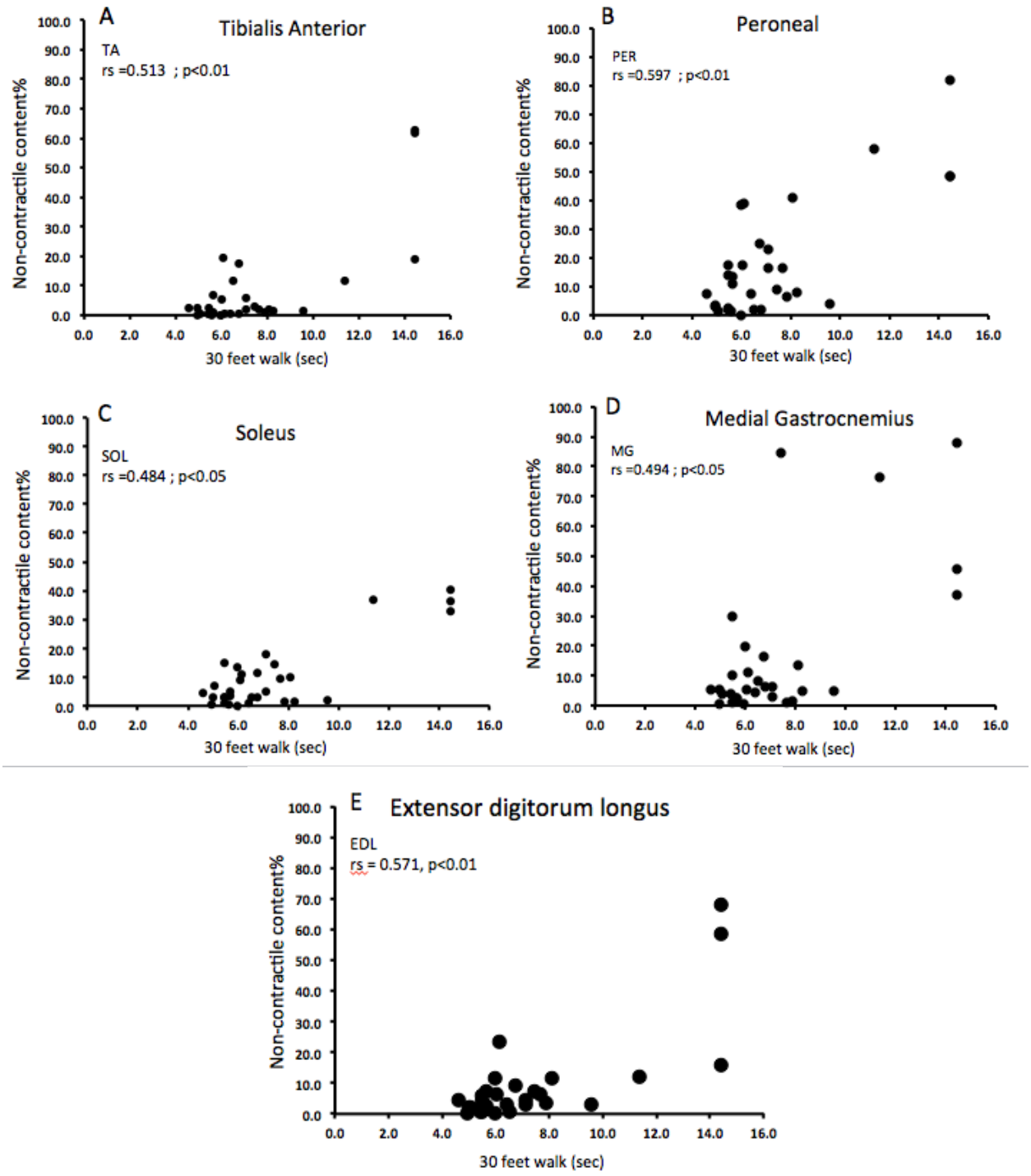

Figure 5-3. Relationship between 30 feet walk and non-contractile content (%) of lower leg muscles. (A)Tibialis anterior (TA), (B) peroneals (Per), (C) soleus (SOL), (D) medial gastrocnemius (MG), and (E) extensor digitorum longus (EDL) in boys with DMD.

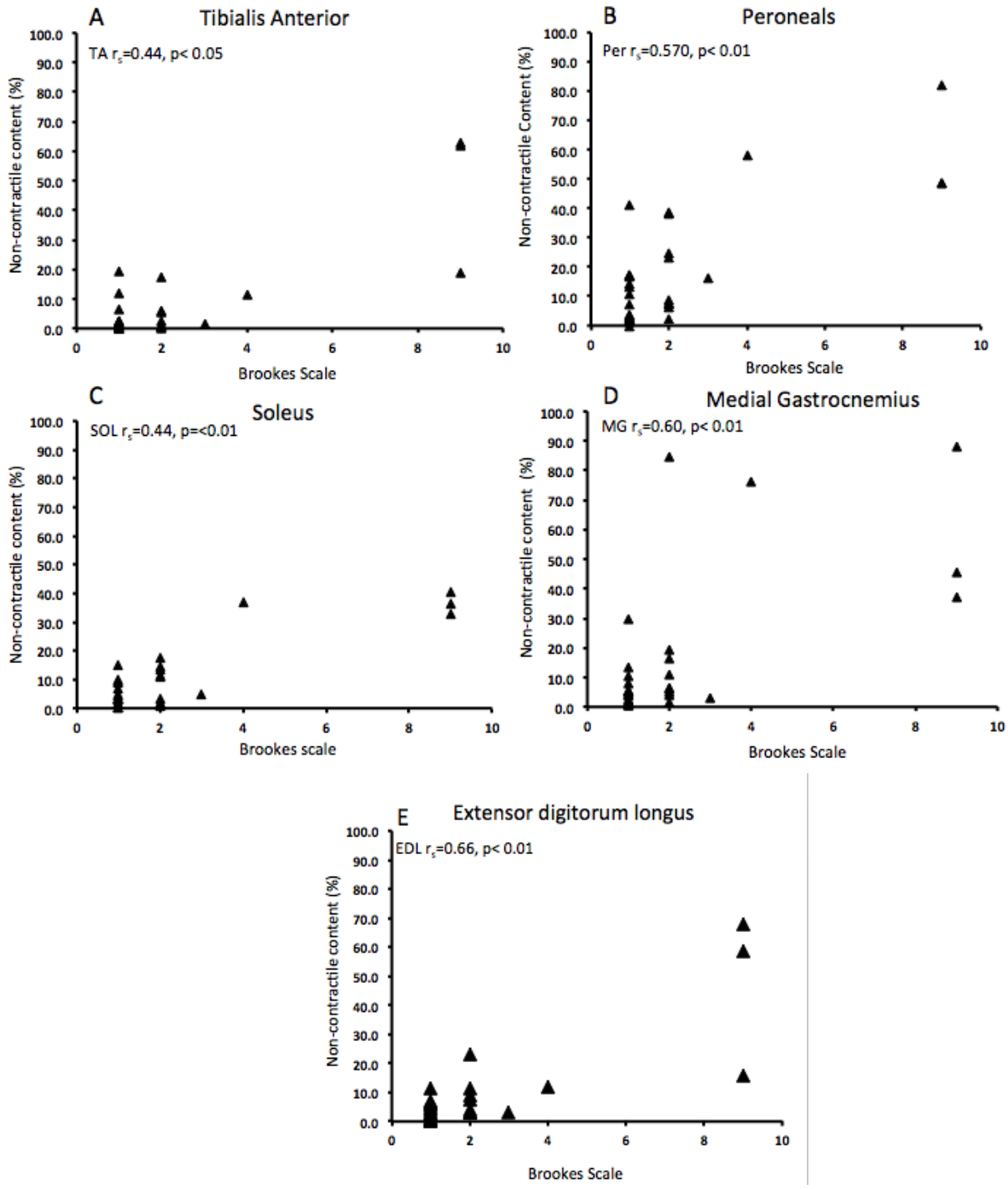

Figure 5-4. Relationship between Brookes scale and non-contractile content (%) of lower leg muscles. (A)Tibialis anterior (TA), (B) peroneals (Per), (C) soleus (SOL), (D) medial gastrocnemius (MG), and (E) extensor digitorum longus (EDL) in boys with DMD.

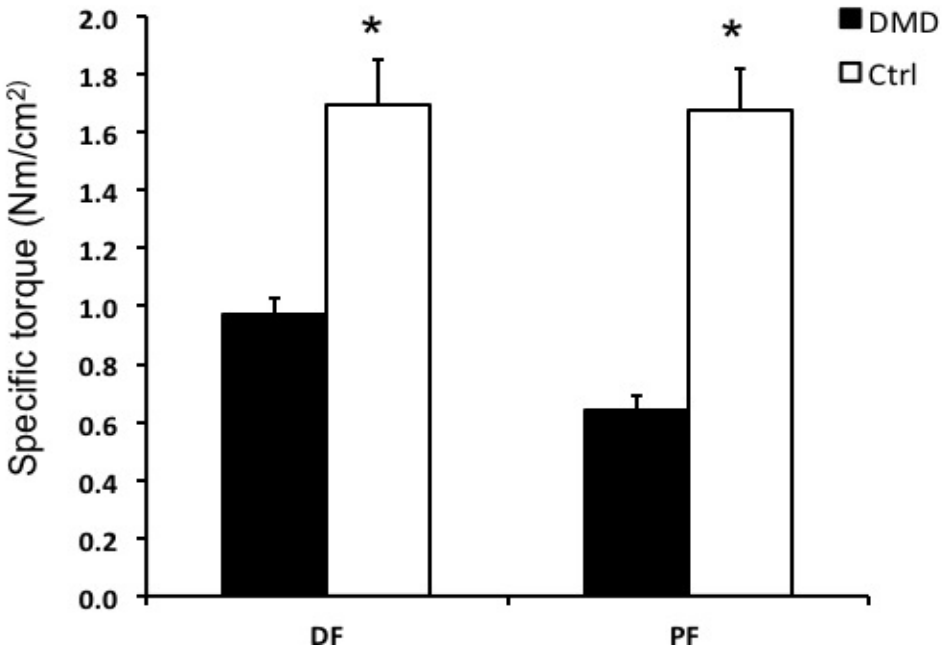

Figure 5-5. Specific torque of dorsiflexors (DF) and plantar flexors (PF) between DMD, Duchenne muscular dystrophy and Ctrl, control group. * $p<0.005$.

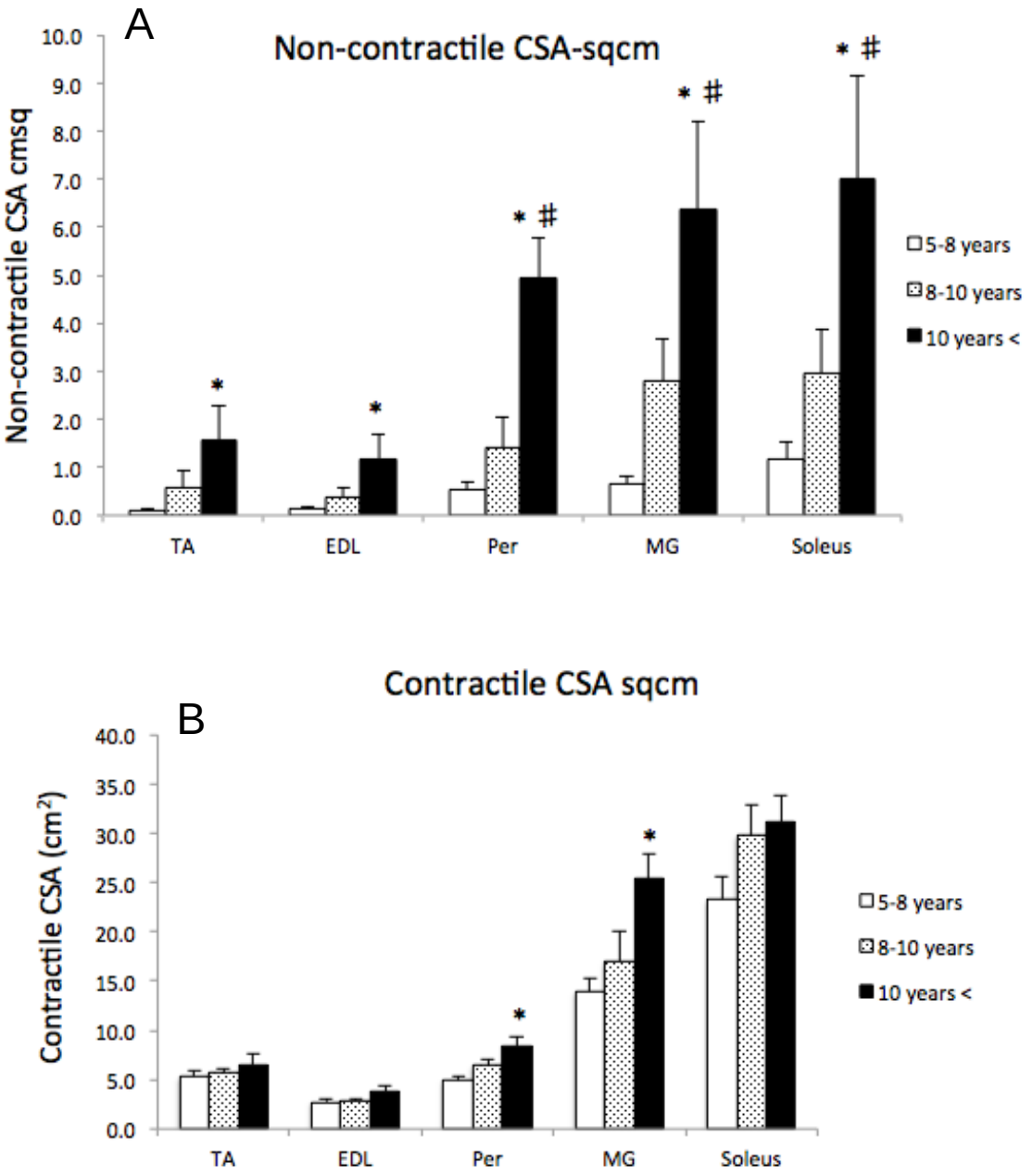

Figure 5-6. Non-contractile and Contractile CSA comparison among different age groups in DMD. Non-contractile CSA (A) and Contractile CSA (B) of lower leg muscles of DMD subjects. * Significant difference between 5-8 years and > 10 years ($p<0.001$), # Significant difference between 8-10 years and > 10 years ($p<0.001$).

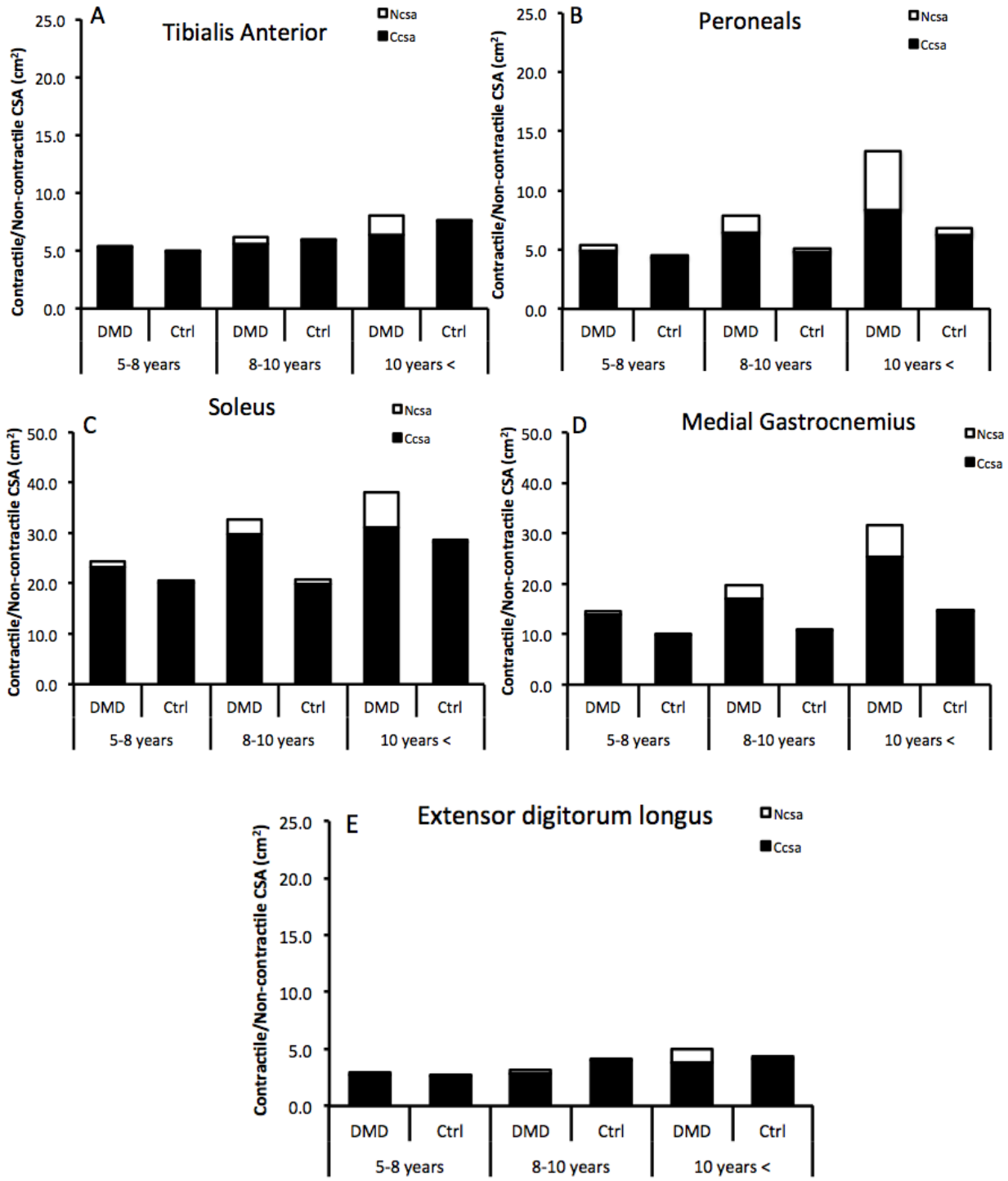

Figure 5-7. A) Non-contractile CSA and Contractile CSA comparison among different age groups in DMD.

Table 5-1. Subjects demographics. Values are mean ± SEM. DMD, Duchenne muscular dystrophy group; Ctrl, control group; BMI, body mass index; BSA, body surface area.

Subject Demographics	DMD	Ctrl
Number of subjects	31	13
Age (years)	8.83 +/- 0.44	9.4 +/-0.81
Height (cm)	124.09 +/-2.39	138.3 +/ 4.31
Weight (Kg)	29.88 +/- 2.04**	31.7 +/- 2.80
BMI (kg/m-sq)	18.84 +/-0.70*	16.2 +/- 0.66

** p<0.01 versus Ctrl group

*p<0.05 versus Ctrl group

Table 5-2. Spearman rank correlation between non-contractile content, strength and functional measurements.

Functional measurements	n	TA	EDL	PER	MG	SOL
Plantar-flexor peak torque	32	NA	NA	-0.32*	-0.47**	-0.41**
Dorsi-flexor peak torque	32	-0.17	-0.32*	-0.31*	NA	NA
30-feet walk	29	0.45**	0.56**	0.48**	0.61**	0.52**
Brooks scale	32	0.43**	0.62**	0.57**	0.61**	0.54**
Fastest supine up	26	0.138	0.12	0.101	-0.201	0.01
Chair up	29	0.191	-0.023	0.012	-0.203	0.039
TUG	29	-0.213	-0.143	-0.248	-0.445*	-0.262
4 stairs	29	0.052	0.231	0.212	-0.019	0.147

**Correlation is significant at 0.01 level (2 tailed)

* Correlation is significant at 0.05 level (2 tailed)

CHAPTER 6
TO MONITOR CHANGES IN T_2 WITH AGE IN HINDLIMB MUSCLES OF *MDX* MICE

While the contractile and non-contractile cross-sectional area can be estimated using T_1 weighted images, another potentially valuable MR marker of disease progression in DMD is transverse relaxation time (T_2). T_2 has been shown to be dependent on a number of compositional changes relevant to DMD, such as fibrosis, muscle damage and edema. In order to examine the potential of T_2 to monitor disease progression the *mdx* mouse model can be utilized. Animal models have the advantage that they enable a more direct histological confirmation of our specific measures. The mouse model, the DMD^{mdx} (*mdx*- 10ScSn) mouse, is the most commonly used animal model of DMD. *mdx* mice, similar to DMD patients lack dystrophin and share some biochemical and histopathological features. The result of many histological studies has confirmed that hind-limb muscles and diaphragm muscle of *mdx* mice show progressive weakness and muscle deterioration with age. Despite these similarities, the phenotype of *mdx* mice is considered less severe than DMD patients. However, the phenotype exhibited by old *mdx* mice closely resembles the myopathy of DMD. In addition, the *mdx* mouse is readily available and offers an economic way for testing possible therapeutic interventions.

Different invasive techniques have been incorporated to measure the efficacy of an intervention to reduce the underlying pathology in DMD. However, the ability to non-invasively measure the pathological features of muscular dystrophy may be valuable for studying the response of different experimental therapeutic strategies. The transverse relaxation time constant (T_2) is a quantitative measure of a basic biophysical property that leads to signal contrast on MRI. Changes in the T_2 of skeletal muscle have been

observed during both acute physiological responses in healthy muscle and under pathophysiological conditions, such as muscle damage and inflammation.[117,118]

Specific Aims

To monitor the progression of dystrophic changes in the hind limb muscles of *mdx* mice based on changes in the transverse relaxation time constant (T_2).

Research Design and Methods

Animals: C57BL/10ScSn-DMD*mdx* (*mdx*; n=18) and wild-type C57BL/10ScSn (n=12) male mice were included in the study. *mdx* and wild type mice were divided equally in three groups: young, adult and old. Mice were obtained from Jackson laboratories (Bar Harbor, ME) and were housed in an AAALAC approved facility with 12 hour light:dark cycle (72^{o}F, 42% humidity and free access to food and water). The University's Institutional Animal Care and Use Committee approved the experimental protocol.

Magnetic resonance imaging: Magnetic resonance imaging (MRI) was performed in a 4.7 T, horizontal bore magnet (Bruker Avance). The animals were anesthetized using an oxygen and isoflurane mixture (3% isoflurane) and maintained under 0.5-1% isoflurane for the duration of the MR procedure. Respiratory rate of the mouse was monitored for the duration of the scan. The lower hindlimbs of the mouse were inserted up to the knee into a 2.0 cm internal diameter, solenoid ^{1}H-coil (200 MHz). T_2 weighted images were acquired with the following parameters: Multiple slice, single spin-echo images, repetition time (TR) =2000ms, echo time (TE)=14ms and 40ms, FOV 10-20mm, slice thickness 0.5-1mm, acquisition matrix = 128 x 256 and two signal averages [112]. Diffusion weighting was fixed at both TEs (diffusion weighting 3 mm^2/s at both 14 and 40 ms). Hahn spin echoes were implemented to avoid the

contribution of stimulated echoes in the T2 measurement. Signal-to-noise ratios were 25:1 at TE = 14 ms and 9:1 at TE= 40 ms.

MRI muscle T_2 Analysis: Muscle T_2 values of the anterior and posterior muscle compartment were computed from a T_2 map, created from two echo times (TEs; 14 and 40 ms) using in-house software as described previously.[112] The T_2 relaxation time of each pixel was calculated using a single exponential decay with the following equation: $T_2 = (26\ ms)/\ ln\ (SI_{14}/SI_{40})$, where SI_{14} and SI_{40} are the pixel intensities at 14 ms and 40 ms respectively.[172] The percent of muscle damage detected by MRI was defined as the percentage of pixels in a region of interest, which had T_2 values over two standard deviations above the mean muscle T_2 found in control mice (> 29ms) up to a maximum value of 100 ms.

Statistical Analysis: All statistical analysis was performed using SPSS for mac (version 20.0)[1]. Results were expressed as mean ± standard error of mean. Research hypothesis was tested at an alpha level of 0.05. One-way analysis of variance (ANOVA) was performed to compare T_2 between mdx and control group at different time points. Furthermore, one-way analysis of variance (ANOVA) for repeated measurements was performed to monitor the changes in hindlimb muscles of young mdx mice.

Results

Assessment of damage in hindlimb muscles mdx mice: Muscle T_2 and the percentage of pixels with elevated T_2 in the lower hindlimb muscles were compared between mdx and control mice using T_2 maps (Figure 6-1). As shown in Figure 6-2, (1) mdx mice had higher mean T_2 values than control mice in both the young and adult age

[1] IBM Corp. Released 2011. IBM SPSS Statistics for Windows, Version 20.0. Armonk, NY: IBM Corp.

groups ($p<0.05$). (2) However, mean T_2 values in old mdx mice did not differ from age matched control group. (3) The percentage of pixels with elevated T_2 in mdx mice was significantly different from age-matched controls in all three groups: young, adult and old age groups. (4) In young mdx mice, there was a three-fold increase in the percentage of pixels with elevated T_2 compared to adult and old mdx mice.

As shown in Figure 6-3, *mdx* mice showed asynchronous, cyclical changes in the T_2 values of both anterior and posterior compartment hind limb muscles with age. We measured mean muscle T_2 and the percent pixels with elevated T_2 in both anterior and posterior compartment. There was a significant increase in the mean muscle T_2 from the 5-week to the 7-week time point. At 10-weeks the mean muscle T_2 was significantly reduced. Furthermore, T_2 and % pixels with elevated T_2 of both anterior and posterior compartment were significantly greater than other time points (Figure 6-4).

In vitro Histological analysis: In vitro histological analysis of hindlimb muscles of *mdx* mice 6 months of age showed a large number of centrally nucleated fibers compared to age matched controls (Figure 6-5). Presence of centrally nucleated fibers was also noted at 96 weeks of age. In addition, Masson's Trichrome staining of hindlimb muscles revealed excessive collagenous tissue accumulation in mdx mice at 96 week of age.

Discussion

The hind limb muscles are the most commonly studied muscles in mdx mice. They include the tibialis anterior (TA) and extensor digitorum longus (EDL) in the anterior compartment, and the gastrocnemius (GAS) and the soleus (SOL) in the posterior compartment. In dystrophin deficient mice pathological changes observed include muscle fiber damage, inflammation, and fibrosis in the later stages. Age related

studies are important to assist in optimal targeting of various pathological processes. Age dependent pathological changes have been well documented in dystrophin deficient muscles using various histopathological techniques.[173,174] However, no one has looked at time-specific responses in mdx mice using a non-invasive measure such as T_2-weighted MRI.

In our study, we found that T_2 is a sensitive biomarker that allows us to follow the longitudinal changes occurring in the skeletal muscles of *mdx* mice. We found that, with age both mean muscle T_2 values and percentage of pixels with elevated T_2 showed asynchronous and cyclical changes in both the anterior and posterior compartments hindlimb muscles of *mdx* mice, especially in young *mdx* mice i.e up to 6 months of age. We found that the mean muscle T_2 and the percentage pixels with elevated T_2 peaks peaked at about 7-8 weeks. This finding has been corroborated in the literature by various studies using histological parameters.[175,176] Furthermore, we observed a decrease in the mean muscle T_2 and percent pixels with elevated T_2 in old *mdx* mice aged 96 week.

Depending on the age of the mice, disease progression can be roughly divided into three phases. First, muscles of young mice undergo repeated cycles of degeneration/regeneration.[177,178] It has been suggested that this phase occurs due to increased exploratory behavior and locomotor activity of young mice. Second, muscles of adult *mdx* mice, despite being bigger and heavier than control mice, have reduced specific force. The skeletal muscles do not show extensive fibrosis, except for in the diaphragm.[179] At this stage the extent of involvement of the muscle groups also

varies and is related to position or use of a muscle group in the body. In the third phase, older *mdx* mice show a progressive dystrophic phenotype.

Muscle necrosis and regeneration is most pronounced between 3-8 weeks of age.[176,180] Evidence from the present study further support this pattern of pathology. The TA typically first manifests muscle necrosis around 21 days after birth and this has been demonstrated to be more pronounced than in the quadriceps.[181,182] Another study observed more necrosis in soleus than EDL at 24 days with greater cumulative muscle damage in soleus (~86%) than EDL (~36%) muscle at 34 days.[183] The precise reason for the acute onset of dystropathology at this age is unknown but speculations include 1) increase in locomotor activity 2) downregulation of various genes including utrophin [184] and genes involved in creatine synthesis [185] 3) and downregulation of proteins involved in excitation–contraction coupling mechanisms.[186,187] Increase in locomotor activity during early phase of life has a temporal relationship with the histological abnormalities in mdx mice. Furthermore, it has been shown that locomotor activity varies considerably with age in mdx mice reducing significantly at 9 week post natal time period.[188] Moreover, levels of utrophin protein have been shown to be greatest in the fetal stages and decrease significantly at 2 week post natal time point and stay at lower levels throughout adult life[184]. Furthermore, Bertocchini et al. [186] found an increase in RyR3 levels at the 2-3 week time point, which corresponds to a period where skeletal muscles undergo morphological and biochemical changes. Expression of RyR3 starts to decrease at the 3 week time point, as the levels of other proteins such as RyR1 start increasing steadily.

Activity induced changes in muscle T_2 have been well documented. For example, after a single bout of exercise, the activated muscles show an increase in T_2, which may last up to an hour. The exact mechanism is still not clear but changes in T_2 have been attributed to redistribution of water molecules in muscle cells. Furthermore, eccentric exercise has been shown to increase muscle T_2, which remains elevated untill at least 7 days after the initial bout. Our results show that T_2 in hindlimb muscles of mdx mice change with age, which may be related to the increase in voluntary activity. Furthermore, any change in biophysical properties such as upregulation or downregulation of different proteins may also cause changes in muscle T_2.

Age related studies are critical because there are a number of pathological changes occurring in mdx muscles and treatment strategies may be more effective in certain time windows. For example, therapies improving membrane stability (gene repair, drug therapy) should be targeted with in the time period when there is excessive damage in the muscles. On the other hand, therapies involving antifibrotic treatment should be given after 6 months of age when early signs of collagen accumulation are noticed.

Summary

MRI is non-invasive tool that has the ability to examine several muscles simultaneously. We used T_2- weighted MRI to distinguish muscles of mdx and control mice. Furthermore, we used MRI to monitor asynchronous and cyclical changes occurring in hindlimb muscles of young mdx mice. The mean muscle T_2 and percent pixels with elevated T_2 peaked between 7-8 weeks and they remained fairly leveled after 6 months of age.

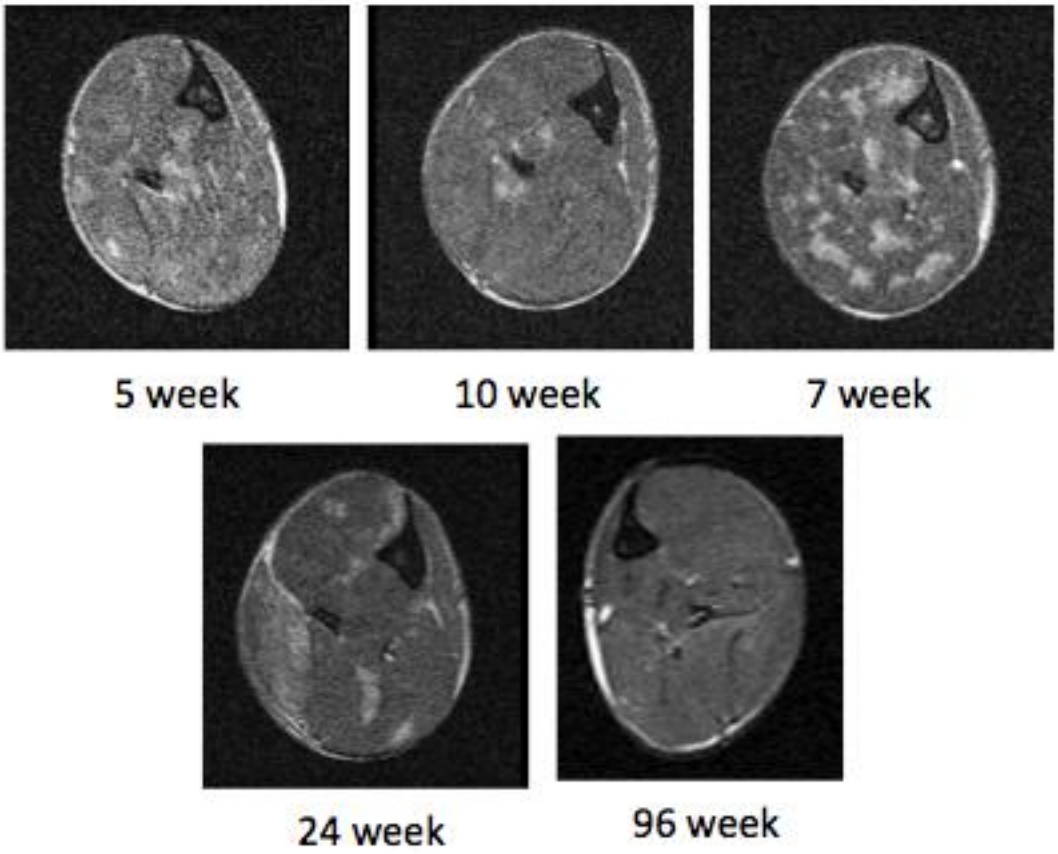

Figure 6-1. T_2 weighted images of *mdx* mouse hindlimb at different time points.

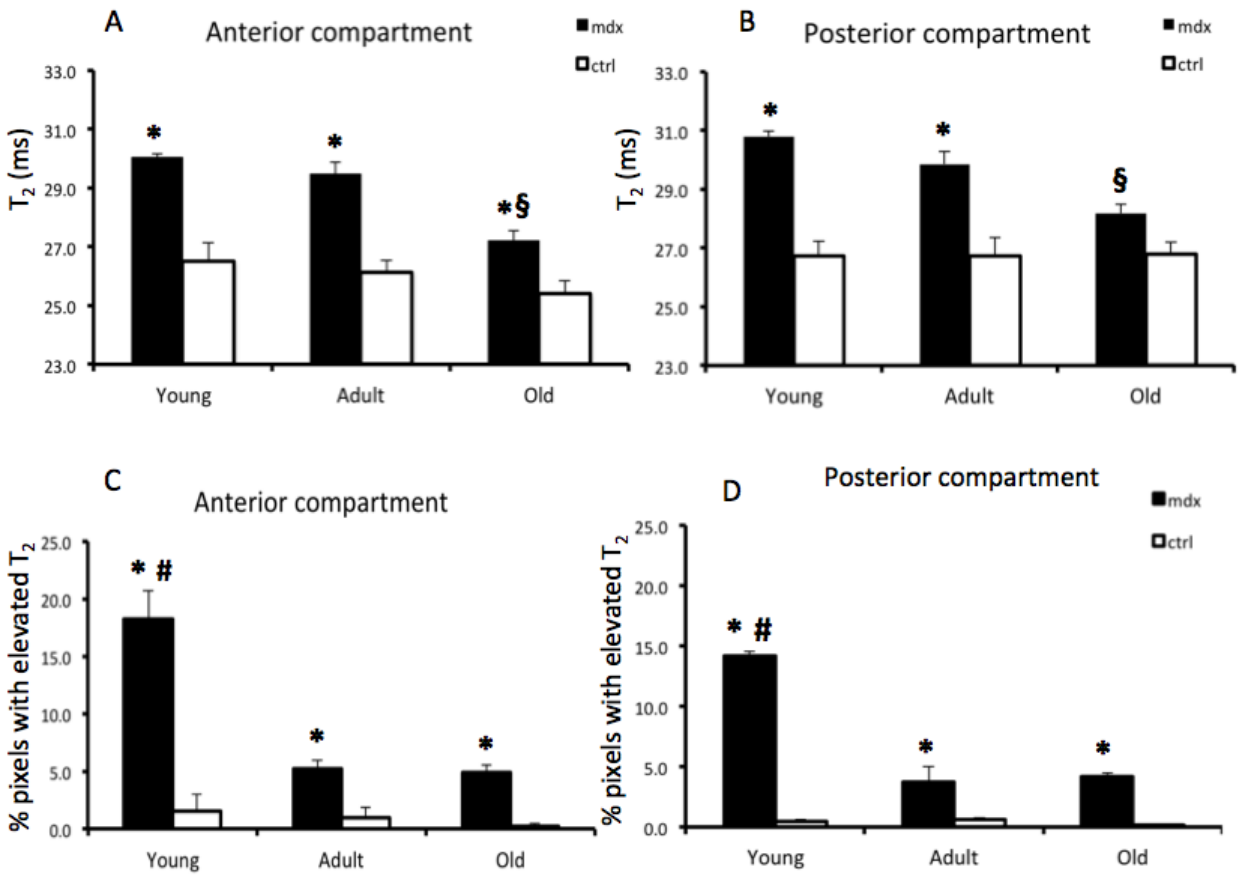

Figure 6-2. Hindlimb muscle T_2 values and % pixels with elevated T_2 of anterior and posterior region. Mean muscle T_2 values and % pixels with elevated T_2 of anterior region (A and C). Mean muscle T_2 values and % pixels with elevated T_2 of anterior region and (B and D) posterior region of mdx and age matched control mice.

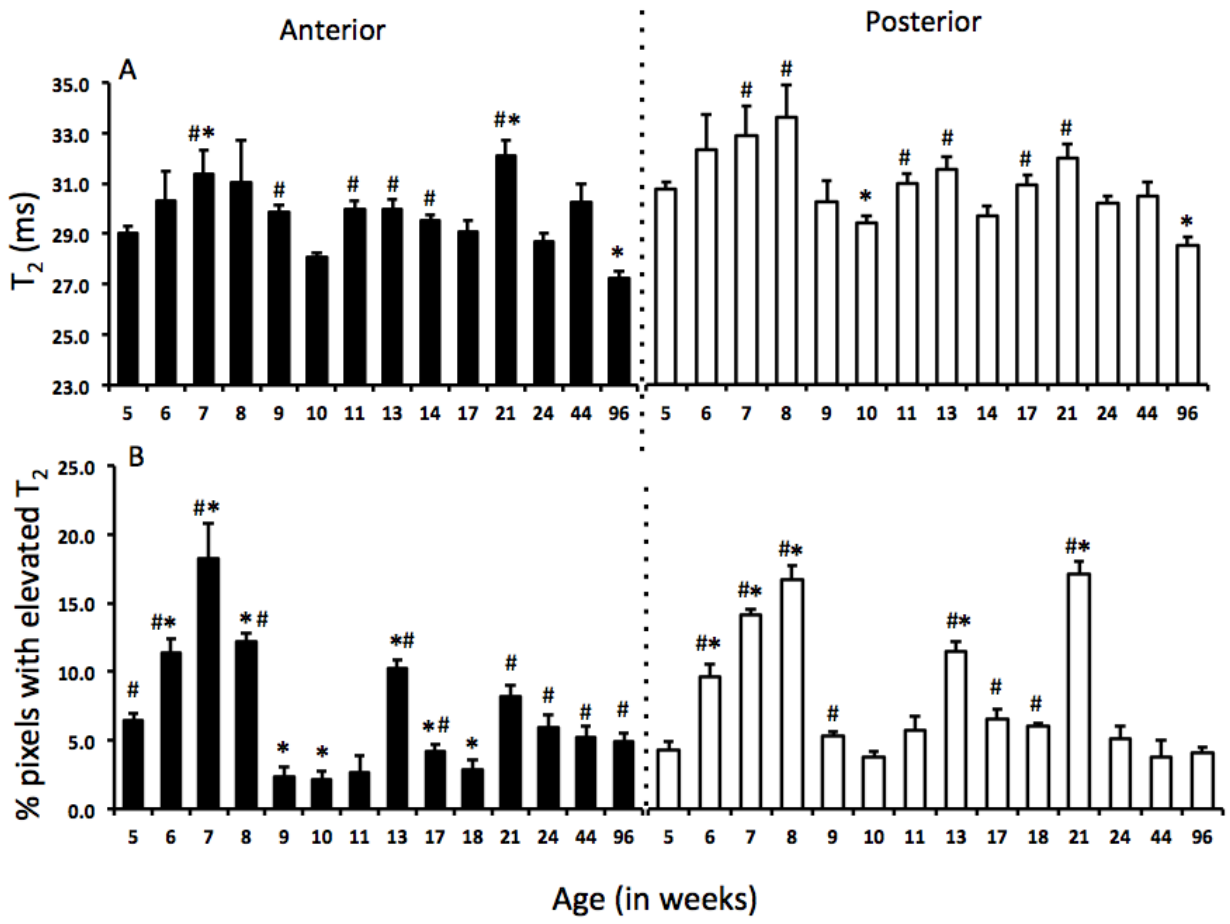

Figure 6-3. Mean muscle T_2 values and % pixels with elevated T_2 of anterior region at different time points. Mean muscle T_2 (A) and % pixels with elevated T_2 (B) in anterior and posterior compartment of hindlimb muscles of *mdx* mice at different time points.* represents significant difference from 5 week time point, # represents significant difference from 10 week time point and ($p<0.05$).

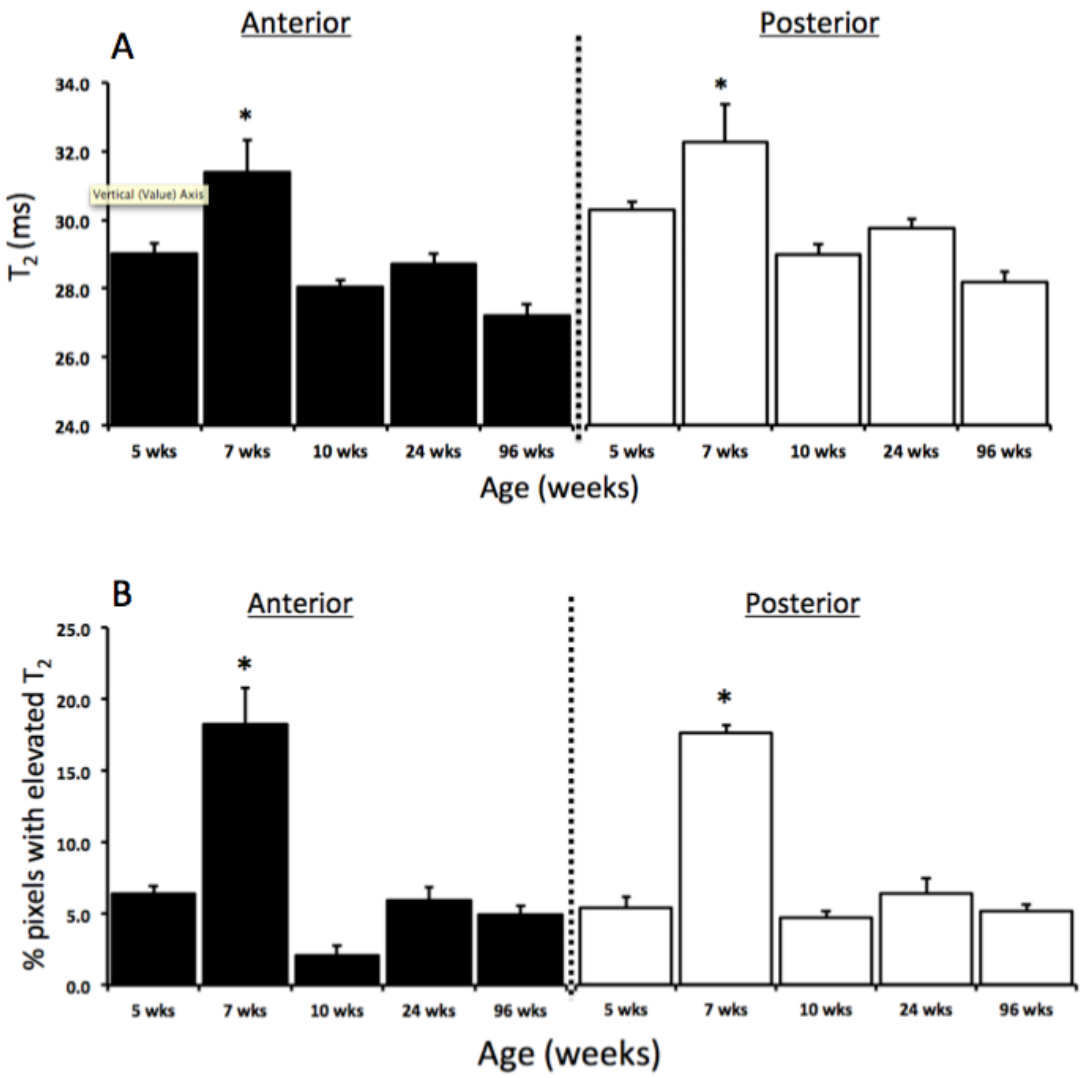

Figure 6-4. Mean muscle T_2 values and % pixels with elevated T_2 of anterior and posterior hindlimb muscle compartments of mdx mice. Mean muscle T_2 (A) and % pixels with elevated T_2 (B) in anterior and posterior compartment of hindlimb muscles of *mdx* mice at different time points. * Represents significant difference from 7-week time point ($p<0.05$).

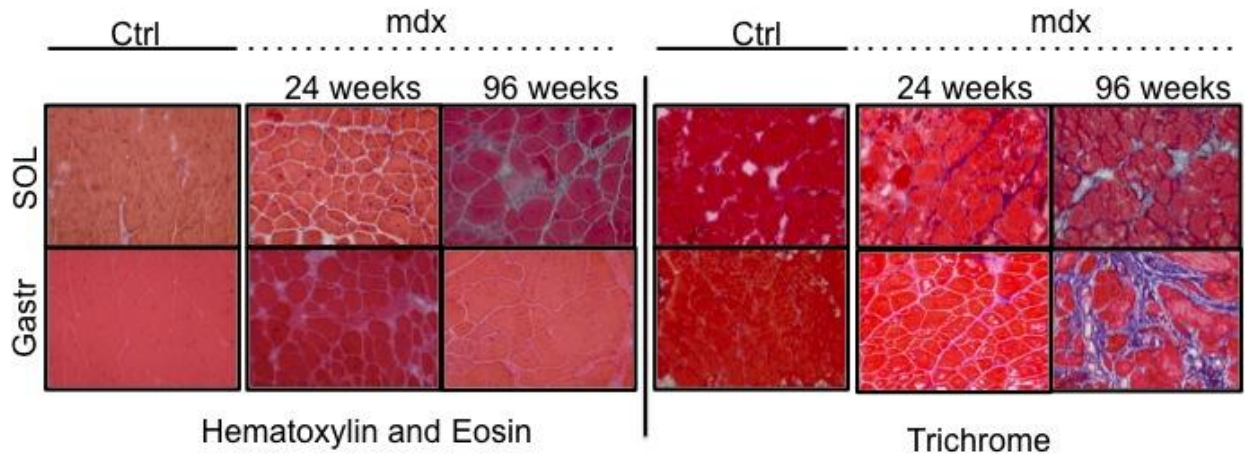

Figure 6-5. Figure showing H&E and trichrome staining of SOL and gastr in *mdx* and Ctrl mice at different time points.

CHAPTER 7
CHANGES IN MUSCLE T_2 AND TISSUE DAMAGE IN HINDLIMBS OF *MDX* MICE AFTER DOWNHILL RUNNING[1]

The absence of dystrophin compromises the entire dystrophin glycoprotein complex, leading to an increased vulnerability to muscle damage during contractions. Furthermore, exercise-induced muscle damage occurs after high-force, unaccustomed exercise, particularly after eccentric (i.e., lengthening) muscle contractions. The initial mechanical damage is followed by an inflammatory response and subsequent reparative and regenerative process within the muscle.

Models of eccentric loading commonly employed in animal models, such as direct electrical stimulation of an excised muscle under passive stretch[4,189] or electrical stimulation of intact muscles under lengthening conditions[190,191] can be used to produce marked damage to individual muscles. However, these models are invasive and require termination of the animal to examine muscle structure, and therefore they cannot be used for longitudinal studies. In contrast, downhill treadmill running has been used as a physiologically relevant model of eccentric loading in *mdx* mice[192,193] other rodent models and humans. Downhill running has several advantages over eccentric contractions produced from electrical stimulation of muscles. First, it incorporates a physiological load and voluntary muscle contractions, which may translate into more relevant findings for studies involving human subjects. Second, downhill running has been used to accelerate muscle weakness and fibrosis in the limb muscles of the *mdx* mouse to more closely mirror the muscle pathology seen in patients

[1] Sunita Mathur, Ravneet S Vohra, Sean A Germain, Sean Forbes, Nahan D Bryant, Krista Vandenborne, Glenn A Walter. Changes in muscle T2 and tissue damage after downhill running in mdx mice. Muscle Nerve. 2011 Jun;43(6):878-86.

with DMD.[61,194] Finally, this method can be used for repeated bouts of muscle damage in the same animal, allowing for longitudinal studies of muscle damage and repair.[195]

Downhill treadmill running has previously been shown to produce muscle damage in the gastrocnemius and soleus muscles, as well as the tibialis anterior and extensor digitorum longus (EDL) of *mdx* mice.[192] A limitation of this earlier work is that the change in muscle damage after downhill running was compared between *mdx* mice that underwent downhill running to a group of *mdx* mice that did not run. This comparison has inherent limitations, because *mdx* mice have damaged muscle fibers even under conditions of normal cage activity, and there is high variability in muscle degeneration between animals.[194] Ideally, the response of dystrophic muscle to downhill running should be examined in the same animal both pre- and postexercise. This can be achieved using a noninvasive approach such as MRI.

The transverse relaxation time constant (T_2) is a quantitative measure of a basic biophysical property that leads to signal contrast on MRI. Changes in the T_2 of skeletal muscle have been observed during both acute physiological responses in healthy muscle and under pathophysiological conditions. For example, acute and transient increases in muscle T_2 lasting approximately 1 hour have been observed in activated muscles after a bout of exercise.[196,197] Although the exact mechanisms that account for these changes have not been fully elucidated, T_2 changes have been attributed to a redistribution of water molecules in the muscle cells.[198] Furthermore, after bouts of eccentric exercise, a later phase of increased muscle T_2 occurs after the initial increase, and it peaks approximately 2–7 days after the initial exercise bout.[109,197] Chronic

changes in muscle T_2 have also been detected in resting muscles of individuals with incomplete spinal cord injury,[199] stroke,[200] DMD,[118] and dermatomyositis,[201] all conditions associated with muscle damage and inflammation.

Specific Aims

4. To monitor the response of muscle T_2 over a time course of 48 hours after a single bout of downhill running in *mdx* mice to wild-type (control) mice
5. To compare the effects of horizontal vs. downhill running on muscle damage, assessed by T_2 MRI in *mdx* mice.
6. To compare the effects of downhill running on the lower anterior vs. posterior hindlimb muscles of *mdx* mice.

Hypotheses

Our hypotheses are as follows 1) After a single bout of downhill running muscles of *mdx* mice will show greater increase in T_2 than control mice. 2) A single bout of downhill running will cause greater increase in T_2 than horizontal running. 3) The anterior compartment muscles will show greater increase in T_2 than the posterior compartment after a bout of downhill running.

Research Design and Methods

Both C57BL/10ScSn-DMD*mdx* (*mdx*; n = 27) and wild-type C57BL/10ScSn (controls n = 6) adult male mice (aged 5–15 months) will be included in the study. Wild-type mice and breeding pairs from the *mdx* colony were obtained from Jackson Laboratories (Bar Harbor, Maine) and thereafter maintained in-house. Animals were housed in an AAALAC-approved facility with a 12-hour light:dark cycle (72^{o}F, 42% humidity) and free access to food and water. The institutional animal care and use committee of University of Florida approved the experimental protocol.

MRI was be conducted prior to treadmill running in both *mdx* and control mice to determine baseline muscle T_2 values of the lower hindlimb muscles. The methods of the MRI protocol and T_2 analysis are outlined in what follows. After the initial MRI, each mouse underwent one of two treadmill-running protocols: a bout of downhill running or a bout of horizontal-grade running. Specifically, mice were run either on a downhill-slope (14 degrees decline) or a horizontal (0% grade) motorized treadmill at a speed of 8–10 m/min, for 45 minutes. To ensure the mice ran for the entire duration of the protocol, they were observed continuously. If necessary, a short burst of compressed air or the use of a brush at the base of the tail was used to encourage running. From a total of 18 *mdx* mice screened, 11 were able to complete the downhill running protocol with some encouragement needed during the first 5–10 minutes of running and near the end of the 45-minute period. All control mice (6 of 6) were able to complete the downhill running protocol without encouragement. All *mdx* mice (9 of 9) were able to complete the horizontal running protocol without external stimulation. MRI of the lower hindlimbs will be conducted immediately post-exercise (approximately 20 minutes after the exercise bout), and at 24 and 48 hours post-exercise. In 5 of the *mdx* mice that ran downhill, a 10-day postexercise follow-up MRI scan was also conducted. Lower hindlimb muscles were extracted in a subset of *mdx* (n = 8) and control mice (n = 5) at the end of the study for histological confirmation of muscle damage.

Magnetic resonance imaging: MRI was performed in a 4.7-T horizontal bore magnet (Bruker Avance, ParaVision 3.02; Bruker). The animal was anesthetized using an oxygen and isoflurane mixture (3% isoflurane) and maintained under 0.5–1% isoflurane for the duration of the MR procedure. The respiratory rate of the mouse was

monitored for the duration of the scan (SA Instruments)[2]. The lower hindlimbs of each mouse were inserted up to the knee into a custom-built solenoid 1H-coil (200 MHz) with a 2.0-cm internal diameter. Multiple-slice, diffusion- controlled, single spin–echo images were acquired with the following parameters: repetition time (TR) = 2000 ms; echo time (TE) = 14 ms and 40 ms; field of view (FOV) = 10–20 mm; slice thickness = 1 mm; acquisition matrix = 128 X 256; and with two signal averages, as previously described [112]. Diffusion weighting was fixed at both TEs (diffusion weighting 3 mm2/s at both 14 and 40 ms). Hahn spin echoes were implemented to avoid the contribution of stimulated echoes in the T2 measurement. Signal-to-noise ratios were 25:1 at TE = 14 ms and 9:1 at TE = 40 ms.

Muscle T_2 analysis from MRI: Muscle T_2 values of the entire lower hindlimb (excluding bone), as well as of individual muscle compartments (anterior, posterior, and medial; Figure 7-1), were computed from a T_2 map, created from two TEs (14 and 40 ms) using in-house software as previously described.[20,112] T_2 relaxation time was calculated using single exponential decay with the following equation: $T_2 = (26\ ms) / \ln(SI_{14} / SI_{40})$, where SI_{14} and SI_{40} are the pixel intensities at 14 and 40 ms, respectively.[172] The percentage of muscle damage detected by MRI was defined as the percentage of pixels in a region of interest that had T_2 values over 2 standard deviations above the mean muscle T2 found in control mice (>29 ms) up to a maximum value of 100 ms.

Histological confirmation of muscle damage: Histological confirmation of muscle damage was conducted in a subset of *mdx* and control mice from each of the

[2] SA instruments, Inc., Stony Brook, New york.

protocols: downhill running (n = 4 *mdx*, n = 5 control) and horizontal-grade running (n = 4 *mdx* only). Twenty-four hours after the exercise bout, mice were injected with EBD (0.10 mL per 10 g of body weight) via intraperitoneal injection. Forty-eight hours after exercise (i.e., 24 hours postinjection), the following muscles of the lower hindlimb were harvested: tibialis anterior (TA); extensor digitorum longus (EDL); flexor digitorum longus (FDL); soleus; and gastrocnemius. Muscles were coated with OCT, frozen in iso pentane cooled with liquid nitrogen, and stored at -80^{0}C. Each muscle was sectioned at the mid-belly region, at 10 μm thickness, and mounted on slides using a fluorescence-mounting medium with 4,6- diamidino-2-phenylindole (DAPI; VectaShield, Vector Labs). Slides were viewed using fluorescence microscopy, optimized for EBD (Texas red filter). Images of the entire muscle cross-section were captured at 10 X magnification using a light microscope (Leica Microsystems, Bannockburn, Illinois) attached to a digital camera with slightly overlapping fields to obtain images from the entire muscle. The cross-section of the muscle was reconstructed in Adobe Photoshop from the digital images. EBD-positive fibers were outlined using NIH Image J[3], and the total area occupied by EBD-positive fibers was calculated as a percentage of the total muscle area.

Statistical analysis: Data were analyzed using SPSS, version 11.0[4]. The descriptive data are presented using mean and standard error of the mean (SEM). To compare the differences in muscle T_2 and percent muscle damage between *mdx* and control mice after a single bout of downhill running (study objective 1), independent-

[3] Image J available from http://rsbweb.nih. gov/ij/

[4] SPSS Inc, 233 S. Wacker Drive, 11th floor, Chicago, Illinois 60606.

sample t-tests were used to make comparisons at each time-point between groups (p= 0.05, adjusted for multiple comparisons using a modified Bonferroni correction). Paired t-tests were used to compare differences in muscle T_2 and percent damage from pre-exercise values to post-exercise time-points (immediately post-exercise, 24 and 48 hours post-exercise), in each of the *mdx* and control groups (alpha = 0.05, adjusted for multiple comparisons). A comparison of the response of muscle T_2 and percent damage in *mdx* mice between downhill running and horizontal running (study objective 2) was conducted using independent-sample t-tests at each time-point ($P < 0.05$). To examine study objective 3, the response of each muscle compartment to one bout of downhill treadmill running in *mdx* mice was compared using a two-way, repeated-measures analysis of variance (ANOVA) and the Tukey post hoc tests (main factors: time-point and muscle, $P < 0.05$). Finally, the Spearman rank correlation was used to examine the relationship between the percentage of muscle cross-sectional area positive for EBD and the percentage of pixels with elevated T_2.

Results

Downhill running in *mdx* compared with control mice: Muscle T_2 and the percentage of pixels with elevated T_2 in the lower hindlimb muscles was compared between *mdx* and control mice after a single bout of downhill running over a period of 48 hours. As shown in Figure 7-2A, *mdx* mice had a higher muscle T_2 compared with control mice both pre-exercise and at each time-point after downhill running ($P < 0.001$). A twofold increase in the number of pixels with elevated T_2 was detected immediately post-exercise in *mdx* mice (14.5 6 2.9% of pixels with elevated T_2 post-exercise vs. 7.1 6 1.5% pre-exercise) and remained elevated vs. baseline values at 24 and 48 hours post-exercise ($P < 0.001$; Figure 7-2B). Muscle T_2 was higher immediately post-exercise

in the *mdx* mice ($P < 0.05$; Figure 7-2A), but not at 24 or 48 hours. The percentage of pixels with elevated T_2 consistently returned to baseline values 10 days after downhill running in *mdx* mice (Figure 7-3). Immediately after downhill running and 24 and 48 hours later, the control mice did not show any difference in their muscle T_2 or percentage of elevated pixels compared with their pre-exercise values. An example of transaxial T_2-weighted images from an *mdx* mouse after downhill running is shown in Figure 7-4, with follow-up MRI taken 10 days after the exercise bout. A distinct hyperintense region is observed on the T_2-weighted images of the medial muscle compartment. Figure 7-5 shows a projection from a three-dimensional rendering of the medial compartment with elevated muscle T_2 after downhill running.

Downhill vs. Horizontal running in *mdx* mice: The response of muscle T_2 and percentage of muscle damage was compared in two independent groups of *mdx* mice that underwent either a bout of downhill or horizontal treadmill running. As shown in Figure 7-6, muscle T_2 increased only in the group of *mdx* mice immediately after downhill running, whereas no change in T_2 was observed in those that underwent horizontal treadmill running. The percentage of pixels with elevated T_2 showed an increase in the horizontally run mice immediately postexercise (5.0 6 1.0% at baseline vs. 6.8 6 1.5% immediately postexercise, $P < 0.05$), but remained elevated only in the downhill running group at 24 and 48 hours after the exercise bout.

Comparison between muscle compartments in *mdx* mice after downhill running: As *mdx* mice showed an increase in muscle damage of their lower hind- limb muscles after downhill running, a further examination of response in the three muscle compartments (anterior, medial, and posterior) was conducted. As shown in Figure 7-7,

the medial muscle compartment had a significantly higher percentage of pixels with elevated T_2 at baseline compared with the anterior and posterior muscle groups. Furthermore, the medial compartment showed a significant increase in the percentage of elevated pixels at each time-point after exercise compared with pre-exercise values ($P < 0.05$). However, a significant change was not observed in the anterior and posterior muscle compartments.

Histological confirmation of muscle damage using evan's blue dye:

Individual muscles from the lower hind limb of *mdx* and control mice were extracted following the 48-hour MRI scan and examined for EBD uptake (Figure 7-8), indicative of muscle damage. The percent of the total muscle cross-sectional area positive for EBD fibers was compared to the percent of pixels with elevated T_2 from the corresponding muscle compartment (i.e. tibialis anterior and extensor digitorum longus muscles were compared to the anterior muscle compartment; gastrocnemius and soleus muscles to the posterior muscle compartment and flexor digitorum muscle to the medial muscle compartment). Bivariate correlational analysis demonstrated a strong relationship between the percent of muscle cross-sectional area that was EBD positive and the percent of pixels with elevated T_2 ($r = 0.79$, $p < 0.001$; see Figure 7-9).

Discussion

The findings of our study demonstrate that increases in muscle T_2 can be visualized using MRI following downhill running in *mdx* mice. Furthermore, T_2 elevation was evident in *mdx* following downhill running but not control mice after downhill running or *mdx* mice after horizontal (flat) treadmill running, which did not experience muscle damage. A relationship between histological evidence of muscle damage (Evan's Blue Dye positive fibers) and T_2 elevation was found in this study. However, a limitation of

this study was that we were not able to determine the relative contributions of muscle fiber damage, edema and/or inflammation to the measured elevated muscle T_2. Furthermore, MRI allowed for individual muscle compartments to be examined simultaneously in the same animal. The medial muscle compartment had greater changes in muscle T_2 following downhill running in *mdx* mice and therefore may be more prone to muscle damage than the anterior and posterior muscle compartments.

The effects of two standardized, exercise-based perturbations resulted in different responses in *mdx* mice. Downhill treadmill running consistently caused muscle T_2 elevation above baseline in *mdx* mice (measured as the percent of pixels with elevated T_2), whereas horizontal running resulted in no change in muscle T_2 in *mdx* mice. These physiologically relevant protocols may prove useful in pre-clinical testing of the effects of therapeutic interventions, which are aimed at improving the integrity of dystrophic muscle. Activity-based outcomes such as treadmill running have been identified as relevant endpoints for translational research as they parallel the outcome measures used in clinical trials. The addition of MRI assessment following a known exercise perturbation would allow for the direct visualization of tissue damage and inflammation.[194]

Muscle T_2 was higher in the *mdx* mice compared to controls at baseline, and is likely due to regions of muscle degeneration and damage in the dystrophic mice.[114,202,203] Elevated muscle T_2 has been observed in the pelvic and thigh muscles, particularly the gluteus maximum, of children with DMD.[118] However, the high T_2 values in the muscles of children with DMD were attributed to fatty infiltration, which does not occur in young *mdx* mice.[204] In other animal models of DMD that are

characterized by large amounts of fatty tissue replacement similar to the human condition (e.g. golden retriever dog model), changes in muscle T_2 have been used to visualize both the corrective[205] and inflammatory[206] aspects of therapeutic intervention.

In our study, we found that *mdx* mice showed an additional increase in the percent of pixels with elevated T_2 from baseline values following a bout of downhill running, which remained elevated up to 48 hours. On the other hand, following the same exercise protocol in control mice, the percent of elevated pixels did not show an immediate (20 min post) or prolonged increase. An acute elevation of muscle T_2 observed immediately after exercise has been attributed to changes in intra- and extramyocellular water content[98,207] and redistribution of water molecules within muscle[198,208] and typically dissipates within one hour post-exercise.[109] T_2 elevation that lasts longer than 24 hours post-exercise is most likely due to the inflammatory response and increased membrane permeability, resulting from the initial muscle damage.[112,195] In our study, the control mice did not show an acute increase in muscle T_2, which may indicate that their level of exercise was not intense enough to cause a prolonged shift in water compartmentalization.[209] This is consistent with previous findings of Kobyashi et al.[20] who reported that *mdx* mice have an accumulation of muscle water content in their hindlimbs after mild treadmill exercise, which is not seen in wild-type mice. Vilquin et al.[193] also showed that wild type mice that ran downhill for 5 minutes did not experience muscle damage as measured by an increase in plasma creatine kinase (CK) whereas *mdx* mice did. However using a more intense protocol, Lynch et al.[210] reported histological signs of muscle damage in the

soleus and EDL muscles wild type mice (60 min at 16% decline). Similarly, Carter et al.[211] reported a large increase in plasma CK in wild type mice that ran downhill until exhaustion. Therefore, the amount of muscle damage that occurs in controls is likely dependent on the intensity of the running protocol and this was not achieved with the current protocol.

We found that the percent of pixels with elevated T_2 48 hours after downhill running in *mdx* mice was associated with a histological measurement of increased uptake of Evan's Blue Dye, which is indicative of increased permeability of the sarcolemma from membrane damage.[212] Muscle T_2 elevation occurring 48 hours following exercise is likely due to multiple causes including fiber damage, inflammatory responses, and subsequent edema. Marqueste et al.[195] reported that increased plasma markers of muscle damage (creatine kinase and lactate dehydrogenase) were correlated to increased muscle T_2, 3 to 17 days after downhill running in rabbits. However the authors also noted an increase in muscle edema, which could also contribute to elevated T_2.[195] The process of muscle damage is associated with an inflammatory response as well as edema within the muscle,[195] both of which can independently result in increased T_2.[201,213] Future studies using other imaging methods, such as those that enable multiexponential analysis, along with histological analysis of inflammation and edema may be able to further elucidate the mechanisms accounting for increases in muscle T_2.

In comparison to downhill running, *mdx* mice that ran on a horizontal grade treadmill only demonstrated an acute increase in the percentage of pixels with an elevated T_2, which then returned to baseline levels by 24 hours post-exercise. This

indicates that although horizontal running caused significant muscle activation in *mdx* mice, it did not result in muscle damage to the same extent as downhill running. This result is consistent with the well-established finding that downhill running, an eccentrically-biased activity,[214] is more damaging than horizontal running, which is predominately concentric. The comparison between horizontal and downhill running in *mdx* mice is an interesting model by which to compare the effects of dystrophin replacement as it provides an option for an exercised “control” that does not cause muscle damage in untreated *mdx* mice.

Previous studies on downhill running in mice and rats have shown that the tibialis anterior muscle is damaged to a lesser extent than the gastrocnemius and soleus muscles,[192,195] which was attributed to the plantarflexor muscles undergoing a longer period of eccentric work than the dorsiflexors during downhill running.[214] We found no difference between the anterior and posterior muscle compartments in T_2 elevation following downhill running in *mdx* mice. However muscles of the medial compartment of the lower hindlimb showed a higher muscle T_2 at baseline than both the anterior or posterior compartment muscles. There was also an increase in muscle T_2 in the medial compartment following downhill running, which was not observed in other two muscle compartments. These findings imply that the medial compartment muscles may be more susceptible to contraction-induced muscle damage both during regular cage activity (i.e. baseline) and during exercise. The medial compartment muscles consist of the long toe flexors located between the tibia and fibula (flexor digitorum longus and flexor hallucis longus), tibialis posterior and the peroneals. We have not identified other studies that have examined the response of these muscles to downhill

running in rodents. It is plausible that one or more of these muscles undergoes greater strain or eccentric activity during downhill running than the others, resulting in greater muscle damage and T_2 elevation. Furthermore, these muscles are primarily composed of fast-twitch fibers in rodents[215] which also increases their susceptibility to muscle damage. The functional role of these muscles during downhill running and their susceptibility to muscle damage in *mdx* mice warrants further investigation.

We utilized two measures from T_2-weighted imaging to examine changes in signal intensity after exercise: mean T_2 relaxation time (ms) from a region of interest and the percentage of pixels exceeding a pre-defined threshold. We found that the threshold method used in this study (% of pixels between 30 and 100 ms) was more sensitive for detecting differences in T_2 between *mdx* and control mice after downhill running than the mean T_2 of the ROI. Threshold methods for pixel intensity from MRI have previously been used to examine dystrophic muscle[114] and muscle activation following exercise.[216] This method differs from the calculation of the mean T_2 from a specified region, as it identifies the proportion of pixels that exceed a given threshold. In our study the threshold was set two standard deviations above the mean T_2 of uninjured, control muscle, therefore was used to identify muscle, which had particularly high signal intensity on T_2-weighted imaging.

About 60% of *mdx* mice in our study were able to complete the downhill running protocol with encouragement and 100% of control mice were able to run downhill and did not require any external encouragement. Previous reports have indicated that *mdx* mice have a greater fatigue response to treadmill or free wheel running than wild type mice.[20, 217] Vilquin et al.[193] reported that *mdx* mice aged 9 to14 months were

unable to run for more than 5 minutes without external stimulation on a more intense downhill running protocol than used in our study (-16^{o} decline at 10m/min). They also found that although there were a few “natural runners” in their group (5 out of 15), two of the mice died one hour post-exercise. We did not have any fatalities from running in our study, although the protocol was much longer in length (45 minutes) and the mice were of a similar age. We also found that all of the *mdx* mice were able to complete the horizontal running protocol, even though downhill running is less energy consuming than horizontal or uphill activity. Therefore, this difference may not have only to do with muscle fatigue but also a protective response to muscle damage. The tolerance of *mdx* mice to downhill running has important implications when planning studies to examine the response to intervention. Depending on the age of the animal and the intensity of the protocol a proportion of mice may not be able to complete the protocol, therefore a “drop-out” rate must be established and accounted for in sample size estimations.

The limitations of this study must also be considered when interpreting the results. First, we did not include a group of control mice in the horizontal running protocol to compare with the *mdx* group. However, since there was no prolonged T_2 elevation observed in the *mdx* mice following horizontal running, the comparison to controls may not have provided any additional information regarding susceptibility to muscle damage. Second, the T_2 measurements were made using single exponential analysis from two echo times, which has previously been employed by our group[112,213] and others.[216] Although the experiment may have benefitted from multi-exponential analysis in order to further differentiate muscle damage from inflammation, it is challenging to obtain images at multiple TEs during in-vivo

experiments. Therefore this approach was beyond the scope of this study. Finally, the correlation between EBD positive fibers and percent of pixels with elevated T_2 is limited by the fact that perfect registration between the histological cross-section and trans-axial MR image was not obtained, although the mid-belly of the muscle was sampled for both measures. However, we observed macroscopically that bundles damaged muscle fibers, positive for EBD, ran continuously along the entire length of a muscle and were therefore captured on multiple cross-sections. This has also been shown using longitudinal muscle sections of EBD positive fibers in *mdx* mice by Straub et al.[218] Similarly, areas of elevated muscle T_2 were observed in the same spatial location on multiple trans-axial images of the muscle. Although the cross-sections were not exactly registered, the correlation between histology and MRI findings of muscle damage based on using the mid-belly region of the muscle seems acceptable based on the distribution of damaged fibers along the entire length of a muscle.

Summary

The protocol for downhill running used in this study provides a stimulus to induce muscle damage in the lower hindlimbs of *mdx* mice, which can be noninvasively visualized using T_2-weighted MRI. Using MRI to examine T_2 changes following exercise allows for repeated and longitudinal measurements to be made from multiple muscles in a single animal. The ability to examine several muscles simultaneously is particularly important since not all muscles respond in the same way to downhill running. Therefore MRI may be used to complement histological studies by determining which muscles experience the most damage and should be examined further. An important aspect of the downhill running protocol used in this study was its ability to differentiate *mdx* mice that experience muscle T_2 changes from downhill run wild type mice and *mdx* mice run

on a horizontal grade treadmill, which do not experience elevated T_2 after running. In addition, this protocol allowed for the examination of acute muscle damage following a known and timed perturbation event, in the presence of asynchronous bouts muscle damage and recovery that are typically observed in dystrophic mice.

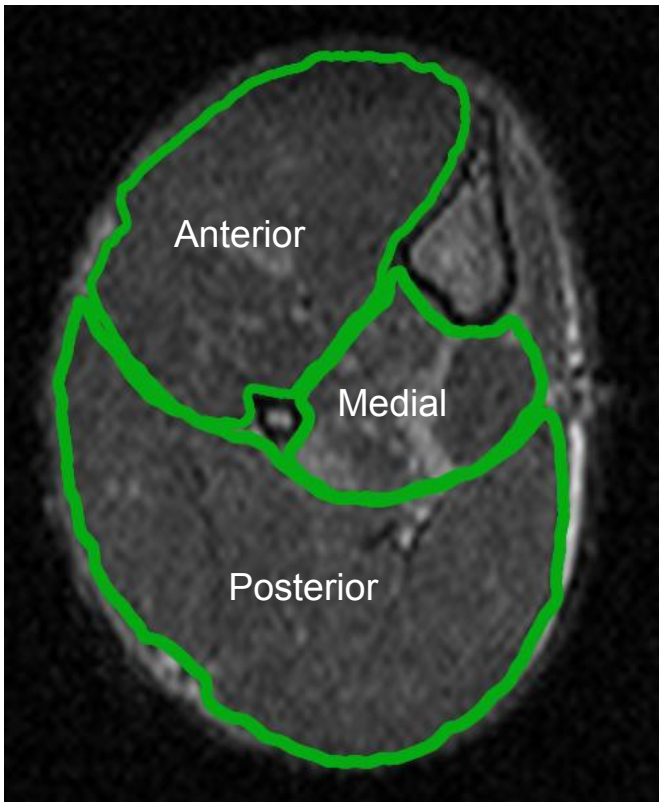

Figure 7-1. Trans-axial MR image of the lower hindlimb showing regions of interest (ROIs) for muscle T_2 analysis. Muscles in each region include: tibialis anterior and extensor digitorum longus in the anterior compartment, flexor hallucis and flexor digitorum in the medial compartment and gastrocnemius, soleus and plantaris in the posterior compartment.

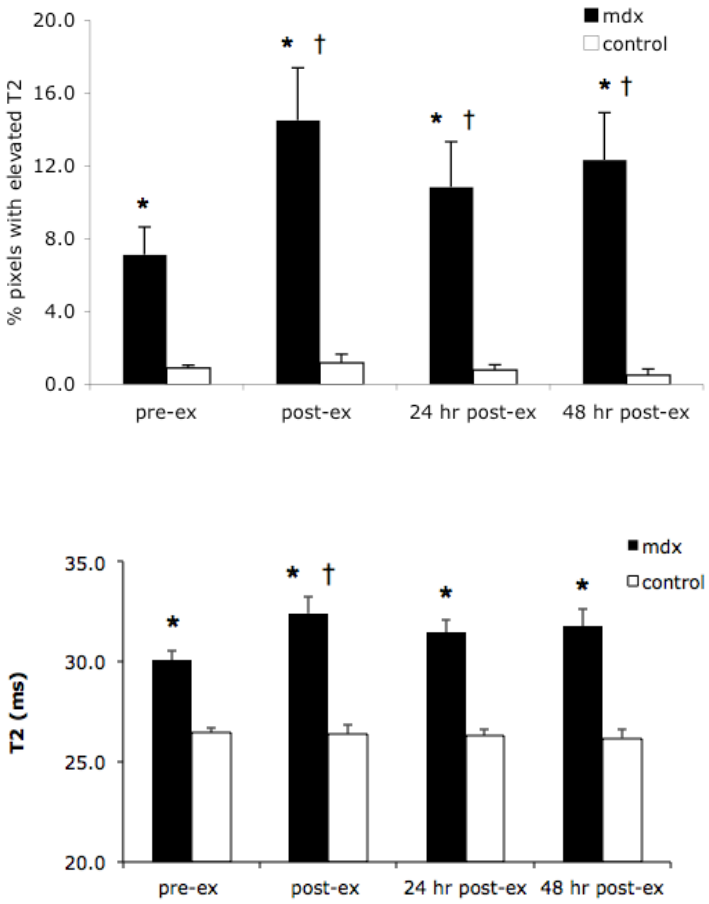

Figure 7-2. Percentage of pixels with elevated T_2 and muscle T_2. A) Percentage of pixels with elevated T_2 (% damaged muscle; mean ± SEM) in the lower hindlimb muscles of *mdx* and control mice before and after downhill running. B) Muscle T_2 of the lower hindlimb muscles of *mdx* and control mice before and after a single bout of downhill running. The *mdx* mice had higher T_2 values at all timepoints (pre and post-exercise) than controls ($p < 0.001$; denoted by *). The *mdx* mice showed a significant increase in muscle T_2 immediately post-exercise ($p < 0.05$, denoted by †). No significant difference was observed in T_2 values of control mice following a bout of downhill running.

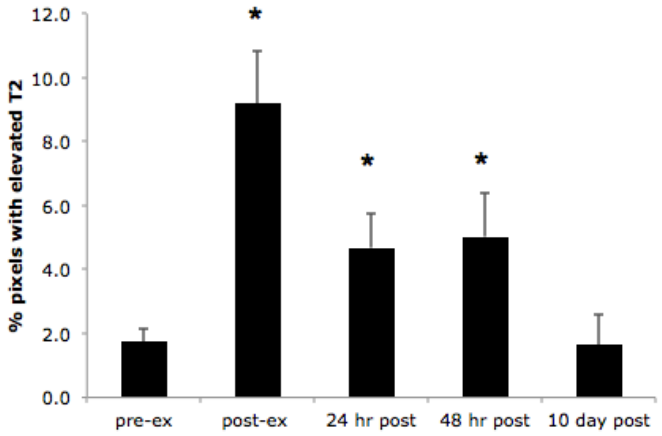

Figure 7-3. Percentage of pixels with elevated T_2 (% damaged muscle; mean ± SEM) returned to baseline values ten days after downhill running in mdx mice (n = 5). The *mdx* mice showed a significant increase in % damaged muscle immediately post-exercise, 24 hr and 48 hrs post-exercise, compared to pre-exercise values ($p < 0.05$, denoted by *), however no significant difference was seen 10 days after downhill running compared to baseline.

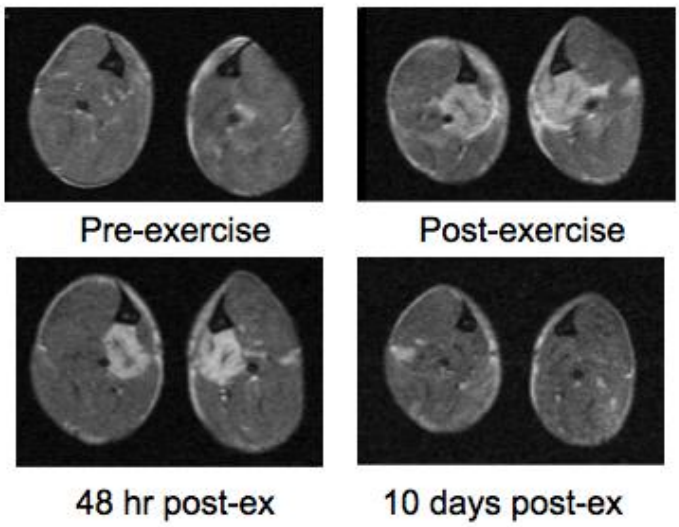

Figure 7-4. Transaxial, T_2-weighted images from the lower hindlimb of an *mdx* mouse before and after a single bout of downhill running for 45 min (-14% grade, 8m/min). Note specific area of hyperintensity in the medial region, between the tibia and fibula, which is recovered after 10 days.

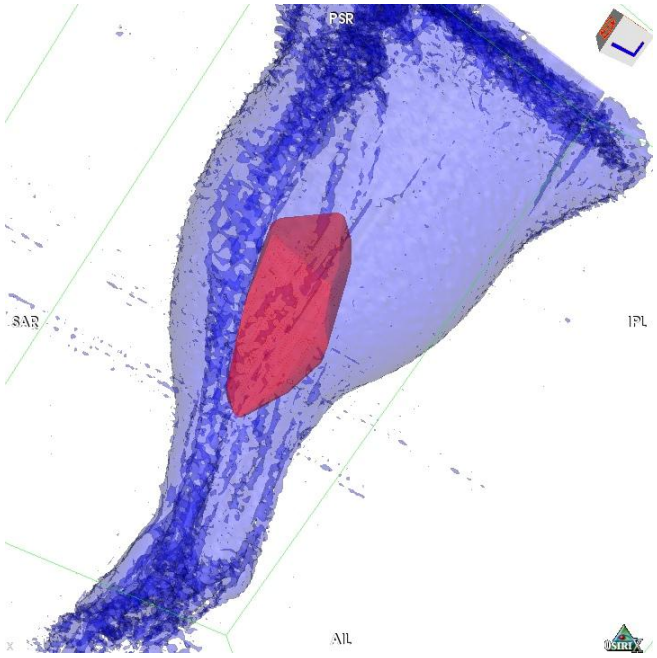

Figure 7-5. Three-dimensional rendering of regional muscle damage in the hindlimb of an *mdx* mouse following downhill running.

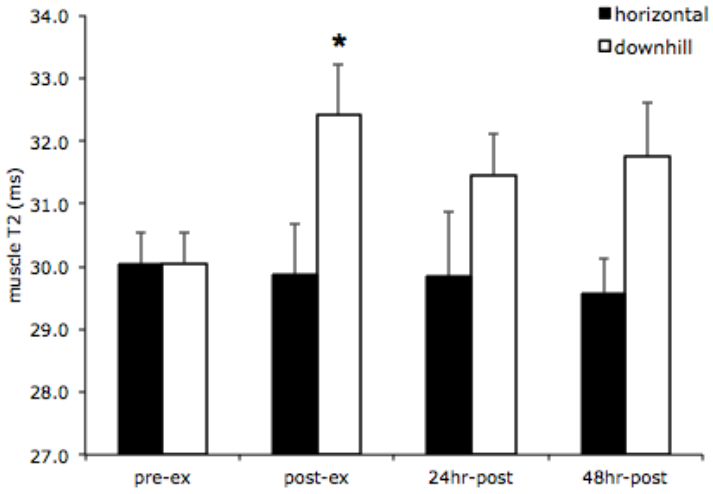

Figure 7-6. Muscle T_2 values in *mdx* mice following a single bout of downhill running compared to horizontal running. Muscle T_2 showed a significant increase immediately following downhill running (compared to pre-exercise, $p < 0.05$, denoted by *) but not following horizontal grade running.

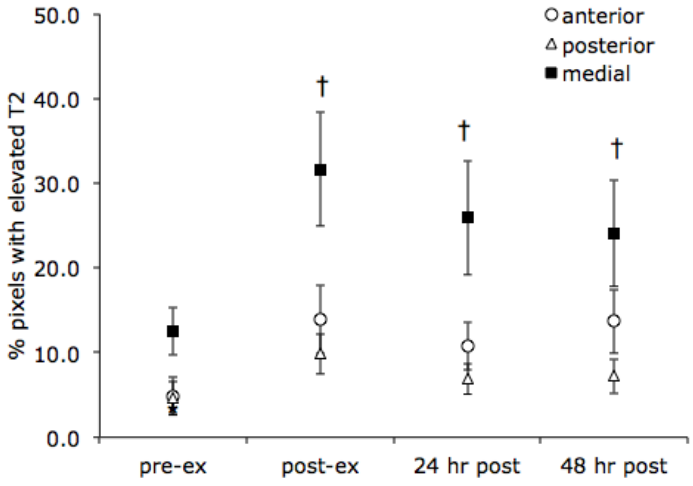

Figure 7-7. Change in % muscle damage in individual muscle compartments of *mdx* mice following a single bout of downhill running. The medial muscle compartment (flexor hallucis/digitorum longus muscles) had a higher % of damaged muscle at baseline than the anterior and posterior muscle compartments ($p < 0.05$; denoted by *) and also showed significant increases in % damage from pre-exercise values, immediately post-exercise and at 24 and 48 hours ($p < 0.05$, denoted by †).

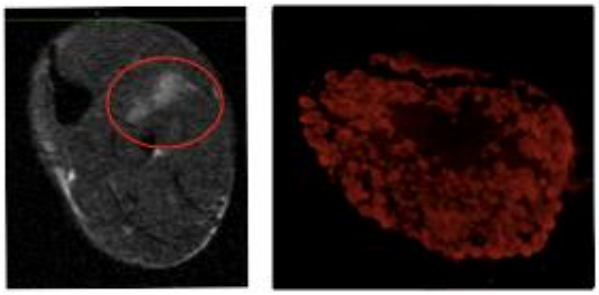

Figure 7-8. EDL muscle of *mdx* mouse 48 hr following 1 bout of downhill treadmill running.

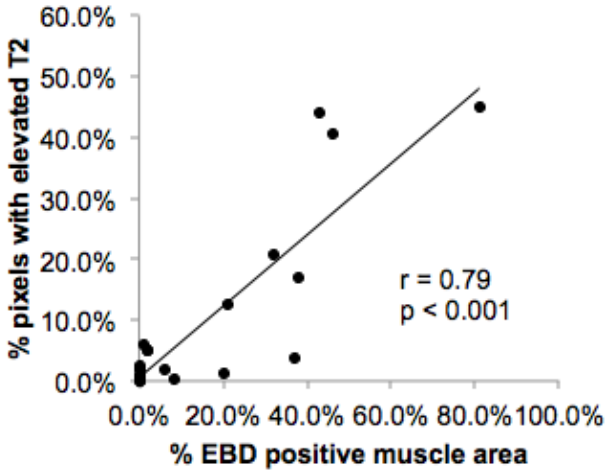

Figure 7-9 Correlation between % of pixels with elevated T_2 and % of area showing damaged fibers using Evan's Blue Dye.

CHAPTER 8
EFFECT OF UPHILL RUNNING ON MYOCARDIUM T_2 IN *MDX* MICE

Duchenne muscular dystrophy patients exhibit progressive skeletal and cardiac muscle pathology. Skeletal muscles of DMD patients display signs of weakness at approximately 5 years of age. Furthermore, loss of diaphragm function leads to respiratory failure and this account for more than 75% of deaths in DMD patients. As a result, research has been more focused on understanding the manifestation of DMD in skeletal muscles. Improvement in ventilator support techniques over the past decade has lead to prolongation in the life expectancy of DMD children. Moreover, novel experiment strategies have shown promise in restoring skeletal muscle function. On the other hand, these strategies often leave the dystrophic cardiac muscle essentially untreated. Clinically apparent cardiomyopathy usually occurs after 10 years of age and almost all the patients are affected by the age of 18 years [219]. As a result of increased life expectancy complications arising from cardiac involvement dominate the later part of life in DMD children. With the improvement in strategies involving skeletal and respiratory systems, it is estimated that approximately 20% of DMD patients die of heart failure.[220,221]

Research on DMD has vastly benefited from animal models, particularly the murine model, the *mdx* mouse, which results from a nonsense mutation exon 23 of the dystrophin gene [222]. *Mdx* mice display histological signs of skeletal muscle pathology as early as 3 weeks of age, which becomes more prominent between 3rd and 8th week of life. On the other hand, *mdx* mice do not demonstrate any signs of cardiac pathology till later stages of life [223]. Novel gene and cell therapies have been utilized to increase

levels of dystrophin and thereby restoring both skeletal and cardiac function in *mdx* mouse.[224-227]

Cardiac stress testing has been widely used to identify cardiac abnormalities that are undetectable at rest.[227,228] Several methods of performing stress testing have been used in the animal models, including administration of a low dose dobutamine.[229] However, uphill running is a more physiological relevant model of cardiac stress test. This model has been utilized to study changes in both skeletal [230] and cardiac muscles.[231]. Furthermore, uphill running has several advantages over other methods, such as, it incorporates the physiological load on the heart and it can be used repeatedly during longitudinal studies of damage and repair.[195]

Magnetic resonance imaging (MRI) has been proposed as a non-invasive method of monitoring tissue structure in DMD patients. The measure of transverse relaxation (T_2) of tissue has been well documented and it has been used to detect various soft tissue pathologies. T_2 is believed to increase with fatty tissue accumulation and increase in water content and edema whereas it decreases with collagen accumulation or fibrosis. Because T_2 relaxation time changes with the disease progression it may be used to monitor disease progression and response to therapy. T_2 weighted imaging has been demonstrated to be a valuable tool in cardiac imaging of DMD patients.[232,233]

Methods

Both C57BL/10ScSn-DMD*mdx* (*mdx*; n = 5) and wild-type C57BL/10ScSn (controls n = 5) adult male mice (aged 3-4 months) were included in the study. Wild-type mice and breeding pairs from the *mdx* colony were obtained from Jackson Laboratories (Bar Harbor, Maine) and thereafter maintained in-house. Animals were housed in an

AAALAC-approved facility with a 12-hour light: dark cycle (72^{o}F, 42% humidity) and free access to food and water. The institutional animal care and use committee of University of Florida approved the experimental protocol.

MRI was conducted prior to treadmill running in both *mdx* and control mice to determine baseline muscle T_2 values of the lower hindlimb muscles. After the initial MRI, each mouse underwent a bout of uphill running. Specifically, mice were run on a uphill-slope (14 degrees decline) motorized treadmill at a speed of 8–13 m/min, for up to one hour. To ensure the mice ran for the entire duration of the protocol, they were observed continuously. If necessary, a short burst of compressed air or a brush was applied at the base of the tail was used to encourage running. Cardiac magnetic resonance (CMR) was conducted at 24 hours post-exercise.

Magnetic resonance imaging: A 4.7T Oxford Magnet with an Agilent/Varian operating system was used to acquire gated T_2-weighted single spin–echo (SE) images of the left ventricle in the short axis view (TR 750 ms; TE 12.5 ms and TE 30 ms; field of view, 25X25 mm^2; slice thickness, 1.0 mm; acquisition matrix size, 256 X 128; averages, 8) with a custom built quadrature volume coil (3.3 cm inner diameter). The animal was anesthetized using an oxygen and isoflurane mixture (3% isoflurane) and maintained under 0.5–1% isoflurane for the duration of the MR procedure. The respiratory rate of the mouse was monitored for the duration of the scan (SA Instruments, Inc., Stony Brook, New York). Diffusion weighting was fixed at both TEs (diffusion weighting 3 mm^2/s at both 14 and 40 ms).

Cardiac MR T_2 analysis: Short axis slices from the mid-papillary region were used to calculate mean T_2. Mean T_2 was calculated using the average signal intensity at

each TE by manually tracing the myocardium. T_2 relaxation time was calculated using a single exponential decay with the following equation: T_2 = (26 ms) / ln (SI12.5 / SI30), where SI12.5 and SI30 are the pixel intensities at 12.5 and 30 ms, respectively[172].

Histological confirmation of myocardial membrane damage: Twenty-four hours after the exercise bout, mice were injected with EBD (0.10 mL per 10 g of body weight) via intraperitoneal injection. Forty-eight hours after the exercise bout (i.e 24 hours post injection), heart was excised, coated with OCT, frozen in isopentane cooled with liquid nitrogen and stored at -80^{o}C. Frozen heart sections were sectioned at 10 microns in a cryostat and mounted on slides using a fluorescence-mounting medium with 4', 6- diamidino-2-phenylindole (DAPI; VectaShield, Vector Labs). Slides were viewed using fluorescence microscopy, optimized for EBD (Texas red filter). Images of the entire muscle cross-section were captured at 10X magnification using a light microscope (Leica Microsystems)[1], attached to a digital camera with slightly overlapping fields to obtain images from the entire muscle. The cross-section of the muscle was reconstructed in Adobe Photoshop from the digital images.

Statistical analysis: Data were analyzed using SPSS, version 20.0[2]. The descriptive data are presented using mean and standard error of the mean (SEM). To compare the differences in myocardium T_2 between *mdx* and control mice after a single bout of downhill running, independent-sample t-tests were used to make comparisons at each time-point between groups (alpha = 0.05, adjusted for multiple comparisons using a modified Bonferroni correction). Paired t-tests were used to compare differences in

[1] Leica Microsystems, Bannockburn, Illinois.

[2] IBM Corp. Released 2011. IBM SPSS Statistics for Windows, Version 20.0. Armonk, NY: IBM Corp.

muscle T_2 and percent damage from pre-exercise values to post-exercise time-points, in each of the *mdx* and control groups (alpha = 0.05, adjusted for multiple comparisons).

Results

Myocardium T_2 was compared between *mdx* and control mice after a single bout of uphill running. As shown in Figure 8.3, muscle T_2 significantly differed between control and *mdx* mice post exercise. At the pre- exercise time point the muscle T_2 did not differ significantly between the two groups. Each control mouse completed one hour of uphill running (800 meters), while there was considerable variability in the amount of time and distance run by *mdx* mice (33±21 minutes; 329±227 meters), with only one mouse completing one hour.

Discussion

This study was the first to examine the myocardium after uphill running in dystrophy using MRI-T_2. The main finding of this study was that uphill running results in an increase in T_2 in the myocardium of dystrophic mice, but not in wild-type mice. As a result, this protocol may be valuable to non-invasively test interventions aimed at improving sarcolemmal integrity in dystrophic myocardium using murine models.

MRI-T_2: T_2 has been well established to be sensitive to muscle damage, as confirmed with the other histological markers of muscle damage i.e. presence of Evan's Blue positive fibers (chapter 7) and presence of central nuclei (chapter 6). Keeping this in account, we used T_2 weighted images as an index of myocardial injury in *mdx* mice. The measure of transverse relaxation time (T_2) of tissue has been well characterized. T_2 weighted MR images of skeletal muscles have been shown to be sensitive to both acute injury and exercise induced contrast enhancement. Furthermore, elevated T_2 may be due to an increase in tissue fluid content or decreased muscle integrity. In recent years,

T_2 weighted imaging has been utilized in cardiac imaging of acute myocardial process such as myocardial infarct [234] and myocarditis.[235,236] T_2 has also shown promise in monitoring cardiac involvement in boys with Duchenne muscular dystrophy[232].

Disease progression in Dystrophy: Both DMD patients and *mdx* mice have complete loss of dystrophin from skeletal muscle fibers as well as cardiomyocyte. Unlike skeletal muscles of *mdx* mice, the heart does not show any abnormal functional pathological signs until 9-11 months.[237] In this study we utilized mean T_2 of myocardium to quantify myocardial damage in *mdx* mice after a single bout of uphill running. MR measurements of T_2 in myocardium were significantly higher in *mdx* mice compared to control mice after a single bout of uphill running. The elevated T_2 of cardiac muscle after a single bout of uphill running were suggestive of an increase in myocardial damage. Furthermore, this was supported by presence of EBD positive fibers.

Model to test interventions: Uphill running has previously been used in murine model to test the sarcolemmal integrity of muscle fibers in myocardium. For example Michele et al.[231] used an uphill running protocol similar to this study and found that muscles lacking normal dystroglycan function were more susceptible to damage. Furthermore, they found an increase in the number of EBD positive fibers in cardiac myocytes after an acute bout of uphill running. Uphill running has been used as a physiological relevant model for cardiac stress testing. Accumulation of EBD has been shown to be one the earliest indicator of cardiac disease. By 3 months of age there is an increase in accumulation of dye as compared to controls. However, the extent of damage remains low because of resealing mechanisms that take place thorough our

lifetime.[238,239] Furthermore, accumulation of fibrotic tissue has been reported to occur in 6 months old mdx mice. Therefore mdx mice aged between 3-5 months may be preferential for a therapy that improves the membrane stability, whereas older mdx mice may be valuable for anti-fibrotic studies.

Summary

The uphill running protocol used in this study is sufficient to induce myocardium damage in mdx mice. T_2-weighted MRI and histological studies can be used to visualize myocardium damage. This protocol allowed us to examine acute myocardium damage after a timed perturbation, which may provide valuable information regarding potential therapeutic agents.

Figure 8-1 Custom built quadrature volume coil with 3.3 cm inner diameter.

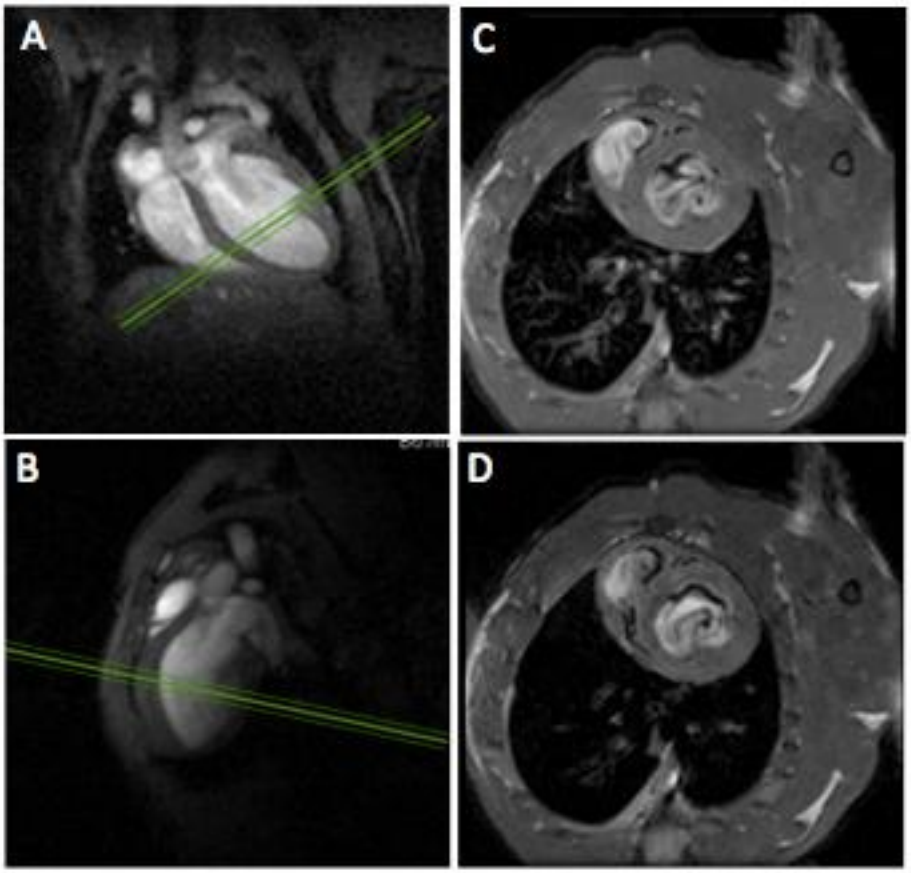

Figure 8-2 Representative four and two chamber long axis images. (A) Four chamber and (B) two chamber image used to position scans in the short axis view. Short axis SE images were acquired at TE=12.5 ms (C) and TE=30 ms (D) to estimate myocardial T_2 from the mid papillary region of the left ventricle.

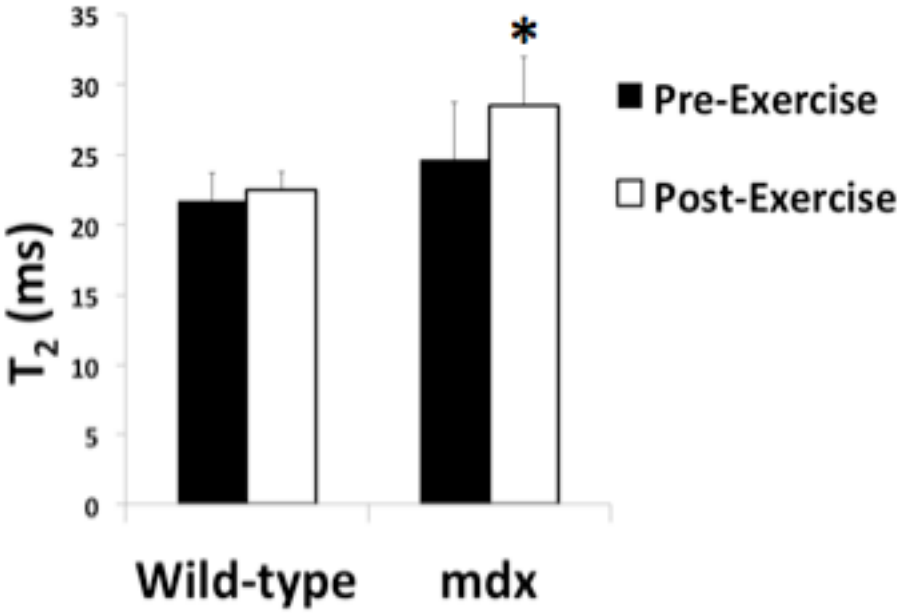

Figure 8-3 Myocardial T_2 values in *mdx* mice after a single bout of uphill running compared to wild-type mice. Myocardial T_2 showed significant increase in *mdx* mice compared to wild type after a single bout of uphill running (*$p<0.05$).

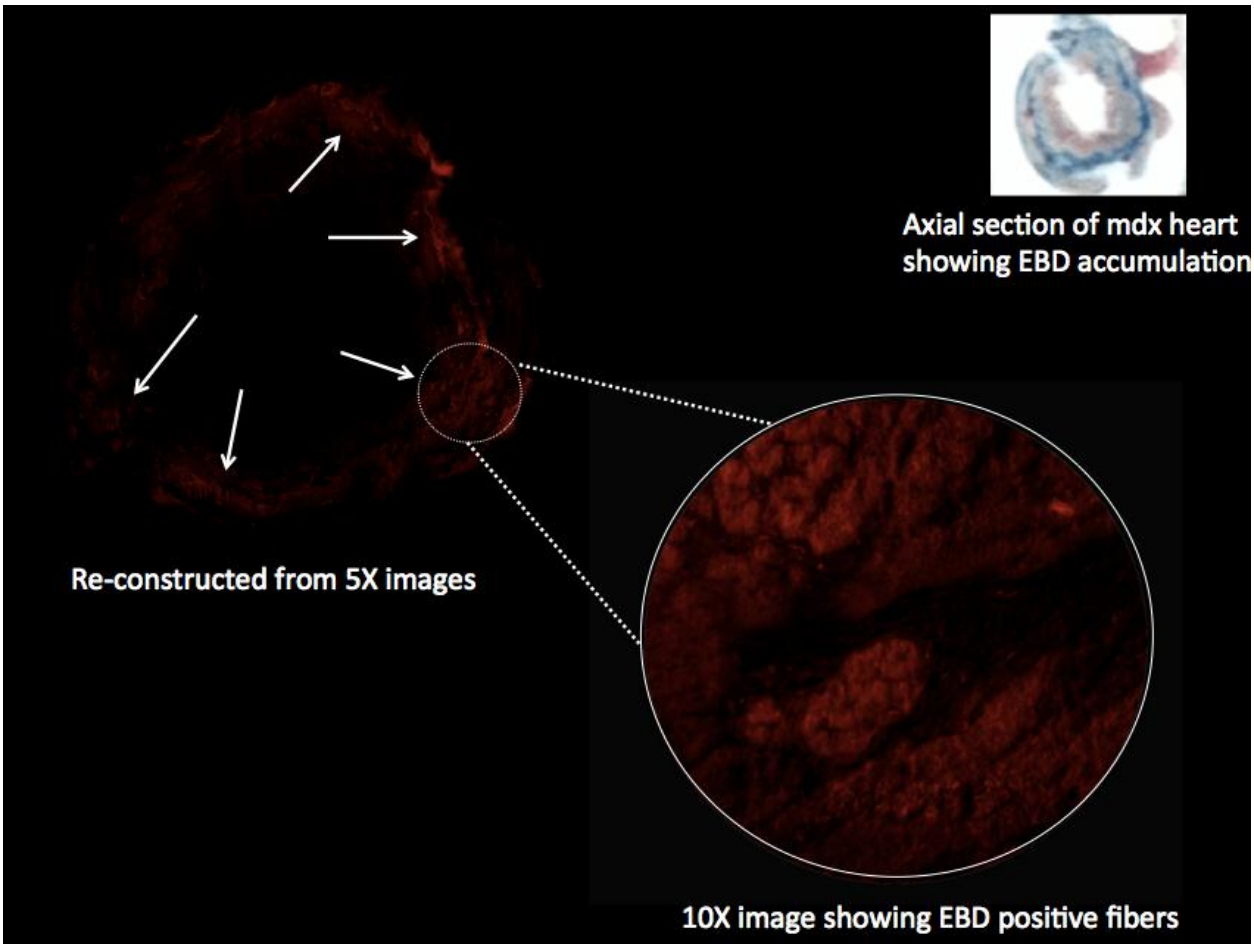

Figure 8-4 Myocardium of mdx mouse 48 hours following a single bout of uphill running.

CHAPTER 9
CONCLUSIONS

Overview

The muscular dystrophies are a group of heterogeneous genetic disorders characterized by muscle wasting. During the last decade, new avenues have opened up both in gene and drug based therapies. In order to monitor the disease progression and response to a therapy a reliable and quantitative non-invasive method is required. In the present work I have used MRI as a non-invasive technique in order to monitor the pathological changes occurring in DMD.

Summary of Conclusions

Relationship between lower-limb muscle cross sectional area and torque production in boys with Duchenne muscular dystrophy: MRI along with dynamometry was implemented to measure CSA max and specific torque production of lower extremity muscles in children with DMD. Age- related changes in muscle CSA and specific torque production in lower-extremity muscles displayed different patterns in the knee extensor, plantar flexor, and dorsi flexor muscles of boys with DMD. The distal triceps surae muscles showed a larger CSA_{max} by approximately 60% in ambulatory boys with DMD compared with controls across ages, while the tibialis anterior muscle showed age-appropriate increases in CSA_{max}. Furthermore, in the quadriceps muscle, CSA_{max} tended to be higher than controls in younger boys with DMD but lower in older boys with DMD over 10 to 11 years of age. All muscles showed significant deficits in specific torque, with a 4-fold difference in the PF and KE, and 2-fold difference in the DFs.

Relationship between lower extremity muscle contractile cross sectional area and functional measurements in boys with DMD: The amount of non-contractile content, measured by MRI was greater in dystrophic peroneal, medial gastrocnemius and soleus muscles. The increase in non-contractile tissue lead to deterioration in timed functional tasks such as 30 feet walk and Brooke's scale. An increase in contractile cross sectional area was seen in the peroneal and medial gastrocnemius muscle, suggestive of "compensatory hypertrophy". Both dorsiflexor and plantar flexor muscles showed a 2-fold difference in specific torque.

To monitor changes in T_2 with age in hindlimb muscles of mdx mice: MRI is non-invasive tool that has the ability to examine several muscle simultaneously. We used T_2- weighted MRI to distinguish muscles of mdx and control mice and evaluate time dependent changes. Using T_2 MRI we found asynchronous and cyclical changes in both the anterior and posterior hindlimb muscles of young mdx mice. The mean muscle T_2 and percent pixels with elevated T_2 peaked between 7-8 weeks.

Changes in muscle T_2 and tissue damage in hindlimb muscles of mdx mice after downhill running: The protocol for downhill running used in this study provides a stimulus to induce muscle damage in the lower hindlimbs of *mdx* mice, which can be noninvasively visualized using T_2-weighted MRI. The ability to examine several muscles simultaneously is particularly important since not all muscles respond in the same way to downhill running. Therefore MRI may be used to complement histological studies by determining which muscles experience the most damage and should be examined further. Using the downhill running protocol we were able to differentiate between *mdx* mice and wild type mice, with mdx mice experiencing extensive muscle T_2 changes

following downhill running. The increase in T_2 in mdx mice was observed for an extended period, consistent with the presence of muscle damage. *mdx* mice that ran on a horizontal grade treadmill did not experience elevated T_2 after running.

Effect of uphill running on myocardium T_2 in mdx mice: The uphill running protocol used in this study is sufficient to induce myocardium damage in mdx mice. T_2-weighted MRI in combination with histological studies can be used to visualize myocardium damage. This protocol allowed us to examine acute myocardium damage after a timed perturbation.

LIST OF REFERENCES

[1] Emery AE. Population frequencies of inherited neuromuscular diseases--a world survey. Neuromuscul Disord. 1991;1:19-29.

[2] Fuchs E, Weber K. Intermediate filaments: structure, dynamics, function, and disease. Annu Rev Biochem. 1994;63:345-82.

[3] Ervasti JM. Dystrophin, its interactions with other proteins, and implications for muscular dystrophy. Biochim Biophys Acta. 2007;1772:108-17.

[4] Petrof BJ, Shrager JB, Stedman HH, Kelly AM, Sweeney HL. Dystrophin protects the sarcolemma from stresses developed during muscle contraction. Proc Natl Acad Sci U S A. 1993;90:3710-4.

[5] Monaco AP, Neve RL, Colletti-Feener C, Bertelson CJ, Kurnit DM, Kunkel LM. Isolation of candidate cDNAs for portions of the Duchenne muscular dystrophy gene. Nature. 1986;323:646-50.

[6] Kunkel LM, Beggs AH, Hoffman EP. Molecular genetics of Duchenne and Becker muscular dystrophy: emphasis on improved diagnosis. Clin Chem. 1989;35:B21-4.

[7] Mandel JL. Dystrophin. The gene and its product. Nature. 1989;339:584-6.

[8] Monaco AP, Bertelson CJ, Liechti-Gallati S, Moser H, Kunkel LM. An explanation for the phenotypic differences between patients bearing partial deletions of the DMD locus. Genomics. 1988;2:90-5.

[9] Monaco AP, Kunkel LM. Cloning of the Duchenne/Becker muscular dystrophy locus. Adv Hum Genet. 1988;17:61-98.

[10] Worton RG, Thompson MW. Genetics of Duchenne muscular dystrophy. Annu Rev Genet. 1988;22:601-29.

[11] Coffey AJ, Roberts RG, Green ED, Cole CG, Butler R, Anand R, et al. Construction of a 2.6-Mb contig in yeast artificial chromosomes spanning the human dystrophin gene using an STS-based approach. Genomics. 1992;12:474-84.

[12] Hoffman EP, Brown RH, Jr., Kunkel LM. Dystrophin: the protein product of the Duchenne muscular dystrophy locus. Cell. 1987;51:919-28.

[13] Bushby KM, Gardner-Medwin D. The clinical, genetic and dystrophin characteristics of Becker muscular dystrophy. I. Natural history. J Neurol. 1993;240:98-104.

[14] Manzur AY, Muntoni F. Diagnosis and new treatments in muscular dystrophies. J Neurol Neurosurg Psychiatry. 2009;80:706-14.

[15] Moens P, Baatsen PH, Marechal G. Increased susceptibility of EDL muscles from mdx mice to damage induced by contractions with stretch. J Muscle Res Cell Motil. 1993;14:446-51.

[16] Hopf FW, Turner PR, Denetclaw WF, Jr., Reddy P, Steinhardt RA. A critical evaluation of resting intracellular free calcium regulation in dystrophic mdx muscle. Am J Physiol. 1996;271:C1325-39.

[17] Spencer MJ, Montecino-Rodriguez E, Dorshkind K, Tidball JG. Helper (CD4(+)) and cytotoxic (CD8(+)) T cells promote the pathology of dystrophin-deficient muscle. Clin Immunol. 2001;98:235-43.

[18] Merlini L, Cicognani A, Malaspina E, Gennari M, Gnudi S, Talim B, et al. Early prednisone treatment in Duchenne muscular dystrophy. Muscle Nerve. 2003;27:222-7.

[19] Biggar WD, Politano L, Harris VA, Passamano L, Vajsar J, Alman B, et al. Deflazacort in Duchenne muscular dystrophy: a comparison of two different protocols. Neuromuscul Disord. 2004;14:476-82.

[20] Kobayashi YM, Rader EP, Crawford RW, Iyengar NK, Thedens DR, Faulkner JA, et al. Sarcolemma-localized nNOS is required to maintain activity after mild exercise. Nature. 2008;456:511-5.

[21] Adams ME, Mueller HA, Froehner SC. In vivo requirement of the alpha-syntrophin PDZ domain for the sarcolemmal localization of nNOS and aquaporin-4. J Cell Biol. 2001;155:113-22.

[22] Bredt DS, Snyder SH. Nitric oxide: a physiologic messenger molecule. Annu Rev Biochem. 1994;63:175-95.

[23] Nathan C. Nitric oxide as a secretory product of mammalian cells. FASEB J. 1992;6:3051-64.

[24] Brenman JE, Chao DS, Xia H, Aldape K, Bredt DS. Nitric oxide synthase complexed with dystrophin and absent from skeletal muscle sarcolemma in Duchenne muscular dystrophy. Cell. 1995;82:743-52.

[25] Chang WJ, Iannaccone ST, Lau KS, Masters BS, McCabe TJ, McMillan K, et al. Neuronal nitric oxide synthase and dystrophin-deficient muscular dystrophy. Proc Natl Acad Sci U S A. 1996;93:9142-7.

[26] Asai A, Sahani N, Kaneki M, Ouchi Y, Martyn JA, Yasuhara SE. Primary role of functional ischemia, quantitative evidence for the two-hit mechanism, and phosphodiesterase-5 inhibitor therapy in mouse muscular dystrophy. PLoS ONE. 2007;2:e806.

[27] Genome sequence of the nematode C. elegans: a platform for investigating biology. Science. 1998;282:2012-8.

[28] Sonnhammer EL, Durbin R. Analysis of protein domain families in Caenorhabditis elegans. Genomics. 1997;46:200-16.

[29] Bessou C, Giugia JB, Franks CJ, Holden-Dye L, Segalat L. Mutations in the Caenorhabditis elegans dystrophin-like gene dys-1 lead to hyperactivity and suggest a link with cholinergic transmission. Neurogenetics. 1998;2:61-72.

[30] Bier E. Drosophila, the golden bug, emerges as a tool for human genetics. Nat Rev Genet. 2005;6:9-23.

[31] Hoffman EP, Dressman D. Molecular pathophysiology and targeted therapeutics for muscular dystrophy. Trends in pharmacological sciences. 2001;22:465-70.

[32] Vainzof M, Ayub-Guerrieri D, Onofre PC, Martins PC, Lopes VF, Zilberztajn D, et al. Animal models for genetic neuromuscular diseases. Journal of molecular neuroscience : MN. 2008;34:241-8.

[33] Chapman VM, Miller DR, Armstrong D, Caskey CT. Recovery of induced mutations for X chromosome-linked muscular dystrophy in mice. Proc Natl Acad Sci U S A. 1989;86:1292-6.

[34] Im WB, Phelps SF, Copen EH, Adams EG, Slightom JL, Chamberlain JS. Differential expression of dystrophin isoforms in strains of mdx mice with different mutations. Hum Mol Genet. 1996;5:1149-53.

[35] Cox GA, Phelps SF, Chapman VM, Chamberlain JS. New mdx mutation disrupts expression of muscle and nonmuscle isoforms of dystrophin. Nat Genet. 1993;4:87-93.

[36] Schatzberg SJ, Olby NJ, Breen M, Anderson LV, Langford CF, Dickens HF, et al. Molecular analysis of a spontaneous dystrophin 'knockout' dog. Neuromuscular disorders : NMD. 1999;9:289-95.

[37] Cooper BJ, Winand NJ, Stedman H, Valentine BA, Hoffman EP, Kunkel LM, et al. The homologue of the Duchenne locus is defective in X-linked muscular dystrophy of dogs. Nature. 1988;334:154-6.

[38] Sharp NJ, Kornegay JN, Van Camp SD, Herbstreith MH, Secore SL, Kettle S, et al. An error in dystrophin mRNA processing in golden retriever muscular dystrophy, an animal homologue of Duchenne muscular dystrophy. Genomics. 1992;13:115-21.

[39] Nguyen F, Cherel Y, Guigand L, Goubault-Leroux I, Wyers M. Muscle lesions associated with dystrophin deficiency in neonatal golden retriever puppies. Journal of comparative pathology. 2002;126:100-8.

[40] Whitehead NP, Yeung EW, Allen DG. Muscle damage in mdx (dystrophic) mice: role of calcium and reactive oxygen species. Clin Exp Pharmacol Physiol. 2006;33:657-62.

[41] Rando TA, Disatnik MH, Zhou LZ. Rescue of dystrophin expression in mdx mouse muscle by RNA/DNA oligonucleotides. Proc Natl Acad Sci U S A. 2000;97:5363-8.

[42] Bertoni C, Rando TA. Dystrophin gene repair in mdx muscle precursor cells in vitro and in vivo mediated by RNA-DNA chimeric oligonucleotides. Hum Gene Ther. 2002;13:707-18.

[43] Dunckley MG, Manoharan M, Villiet P, Eperon IC, Dickson G. Modification of splicing in the dystrophin gene in cultured Mdx muscle cells by antisense oligoribonucleotides. Hum Mol Genet. 1998;7:1083-90.

[44] van Deutekom JC, Bremmer-Bout M, Janson AA, Ginjaar IB, Baas F, den Dunnen JT, et al. Antisense-induced exon skipping restores dystrophin expression in DMD patient derived muscle cells. Hum Mol Genet. 2001;10:1547-54.

[45] Wang B, Li J, Xiao X. Adeno-associated virus vector carrying human minidystrophin genes effectively ameliorates muscular dystrophy in mdx mouse model. Proceedings of the National Academy of Sciences of the United States of America. 2000;97:13714-9.

[46] Watchko J, O'Day T, Wang B, Zhou L, Tang Y, Li J, et al. Adeno-associated virus vector-mediated minidystrophin gene therapy improves dystrophic muscle contractile function in mdx mice. Hum Gene Ther. 2002;13:1451-60.

[47] Barton-Davis ER, Cordier L, Shoturma DI, Leland SE, Sweeney HL. Aminoglycoside antibiotics restore dystrophin function to skeletal muscles of mdx mice. J Clin Invest. 1999;104:375-81.

[48] Wagner KR, Hamed S, Hadley DW, Gropman AL, Burstein AH, Escolar DM, et al. Gentamicin treatment of Duchenne and Becker muscular dystrophy due to nonsense mutations. Annals of neurology. 2001;49:706-11.

[49] Dunant P, Walter MC, Karpati G, Lochmuller H. Gentamicin fails to increase dystrophin expression in dystrophin-deficient muscle. Muscle Nerve. 2003;27:624-7.

[50] Welch EM, Barton ER, Zhuo J, Tomizawa Y, Friesen WJ, Trifillis P, et al. PTC124 targets genetic disorders caused by nonsense mutations. Nature. 2007;447:87-91.

[51] McPherron AC, Lawler AM, Lee SJ. Regulation of skeletal muscle mass in mice by a new TGF-beta superfamily member. Nature. 1997;387:83-90.

[52] Zimmers TA, Davies MV, Koniaris LG, Haynes P, Esquela AF, Tomkinson KN, et al. Induction of cachexia in mice by systemically administered myostatin. Science. 2002;296:1486-8.

[53] Hadjipavlou G, Matika O, Clop A, Bishop SC. Two single nucleotide polymorphisms in the myostatin (GDF8) gene have significant association with muscle depth of commercial Charollais sheep. Animal genetics. 2008;39:346-53.

[54] Kambadur R, Sharma M, Smith TP, Bass JJ. Mutations in myostatin (GDF8) in double-muscled Belgian Blue and Piedmontese cattle. Genome research. 1997;7:910-6.

[55] Lee SJ, McPherron AC. Regulation of myostatin activity and muscle growth. Proc Natl Acad Sci U S A. 2001;98:9306-11.

[56] Rebbapragada A, Benchabane H, Wrana JL, Celeste AJ, Attisano L. Myostatin signals through a transforming growth factor beta-like signaling pathway to block adipogenesis. Mol Cell Biol. 2003;23:7230-42.

[57] Fenichel GM, Florence JM, Pestronk A, Mendell JR, Moxley RT, 3rd, Griggs RC, et al. Long-term benefit from prednisone therapy in Duchenne muscular dystrophy. Neurology. 1991;41:1874-7.

[58] Dubowitz V, Kinali M, Main M, Mercuri E, Muntoni F. Remission of clinical signs in early duchenne muscular dystrophy on intermittent low-dosage prednisolone therapy. European journal of paediatric neurology : EJPN : official journal of the European Paediatric Neurology Society. 2002;6:153-9.

[59] Sharma KR, Mynhier MA, Miller RG. Cyclosporine increases muscular force generation in Duchenne muscular dystrophy. Neurology. 1993;43:527-32.

[60] De Luca A, Nico B, Liantonio A, Didonna MP, Fraysse B, Pierno S, et al. A multidisciplinary evaluation of the effectiveness of cyclosporine a in dystrophic mdx mice. The American journal of pathology. 2005;166:477-89.

[61] Granchelli JA, Pollina C, Hudecki MS. Pre-clinical screening of drugs using the mdx mouse. Neuromuscular disorders : NMD. 2000;10:235-9.

[62] Rolland JF, De Luca A, Burdi R, Andreetta F, Confalonieri P, Conte Camerino D. Overactivity of exercise-sensitive cation channels and their impaired modulation by IGF-1 in mdx native muscle fibers: beneficial effect of pentoxifylline. Neurobiology of disease. 2006;24:466-74.

[63] Grounds MD, Torrisi J. Anti-TNFalpha (Remicade) therapy protects dystrophic skeletal muscle from necrosis. FASEB J. 2004;18:676-82.

[64] Hodgetts S, Radley H, Davies M, Grounds MD. Reduced necrosis of dystrophic muscle by depletion of host neutrophils, or blocking TNFalpha function with Etanercept in mdx mice. Neuromuscul Disord. 2006;16:591-602.

[65] Rando TA. Oxidative stress and the pathogenesis of muscular dystrophies. Am J Phys Med Rehabil. 2002;81:S175-86.

[66] Buetler TM, Renard M, Offord EA, Schneider H, Ruegg UT. Green tea extract decreases muscle necrosis in mdx mice and protects against reactive oxygen species. Am J Clin Nutr. 2002;75:749-53.

[67] Dorchies OM, Wagner S, Vuadens O, Waldhauser K, Buetler TM, Kucera P, et al. Green tea extract and its major polyphenol (-)-epigallocatechin gallate improve muscle function in a mouse model for Duchenne muscular dystrophy. American journal of physiology Cell physiology. 2006;290:C616-25.

[68] Badalamente MA, Stracher A. Delay of muscle degeneration and necrosis in mdx mice by calpain inhibition. Muscle & nerve. 2000;23:106-11.

[69] Sawada H, Nagahiro K, Kikukawa Y, Ban S, Kakefuda R, Shiomi T, et al. Therapeutic effect of camostat mesilate on Duchenne muscular dystrophy in mdx mice. Biological & pharmaceutical bulletin. 2003;26:1025-7.

[70] Morris CA, Selsby JT, Morris LD, Pendrak K, Sweeney HL. Bowman-Birk inhibitor attenuates dystrophic pathology in mdx mice. J Appl Physiol. 2010;109:1492-9.

[71] Zhang G, Budker V, Williams P, Subbotin V, Wolff JA. Efficient expression of naked dna delivered intraarterially to limb muscles of nonhuman primates. Hum Gene Ther. 2001;12:427-38.

[72] Cho WK, Ebihara S, Nalbantoglu J, Gilbert R, Massie B, Holland P, et al. Modulation of Starling forces and muscle fiber maturity permits adenovirus-mediated gene transfer to adult dystrophic (mdx) mice by the intravascular route. Hum Gene Ther. 2000;11:701-14.

[73] Liang KW, Nishikawa M, Liu F, Sun B, Ye Q, Huang L. Restoration of dystrophin expression in mdx mice by intravascular injection of naked DNA containing full-length dystrophin cDNA. Gene Ther. 2004;11:901-8.

[74] Blankinship MJ, Gregorevic P, Allen JM, Harper SQ, Harper H, Halbert CL, et al. Efficient transduction of skeletal muscle using vectors based on adeno-associated virus serotype 6. Mol Ther. 2004;10:671-8.

[75] Chirmule N, Propert K, Magosin S, Qian Y, Qian R, Wilson J. Immune responses to adenovirus and adeno-associated virus in humans. Gene therapy. 1999;6:1574-83.

[76] Heckmatt JZ, Dubowitz V, Leeman S. Detection of pathological change in dystrophic muscle with B-scan ultrasound imaging. Lancet. 1980;1:1389-90.

[77] Fischer AQ, Carpenter DW, Hartlage PL, Carroll JE, Stephens S. Muscle imaging in neuromuscular disease using computerized real-time sonography. Muscle Nerve. 1988;11:270-5.

[78] Maurits NM, Bollen AE, Windhausen A, De Jager AE, Van Der Hoeven JH. Muscle ultrasound analysis: normal values and differentiation between myopathies and neuropathies. Ultrasound Med Biol. 2003;29:215-25.

[79] Pillen S, Verrips A, van Alfen N, Arts IM, Sie LT, Zwarts MJ. Quantitative skeletal muscle ultrasound: diagnostic value in childhood neuromuscular disease. Neuromuscul Disord. 2007;17:509-16.

[80] Heckmatt JZ, Pier N, Dubowitz V. Assessment of quadriceps femoris muscle atrophy and hypertrophy in neuromuscular disease in children. J Clin Ultrasound. 1988;16:177-81.

[81] Heckmatt JZ, Leeman S, Dubowitz V. Ultrasound imaging in the diagnosis of muscle disease. J Pediatr. 1982;101:656-60.

[82] Heckmatt JZ, Pier N, Dubowitz V. Real-time ultrasound imaging of muscles. Muscle Nerve. 1988;11:56-65.

[83] Elsayes KM, Lammle M, Shariff A, Totty WG, Habib IF, Rubin DA. Value of magnetic resonance imaging in muscle trauma. Curr Probl Diagn Radiol. 2006;35:206-12.

[84] Olsen NJ, Qi J, Park JH. Imaging and skeletal muscle disease. Curr Rheumatol Rep. 2005;7:106-14.

[85] Berg HE, Dudley GA, Haggmark T, Ohlsen H, Tesch PA. Effects of lower limb unloading on skeletal muscle mass and function in humans. J Appl Physiol. 1991;70:1882-5.

[86] Ploutz-Snyder LL, Tesch PA, Crittenden DJ, Dudley GA. Effect of unweighting on skeletal muscle use during exercise. J Appl Physiol. 1995;79:168-75.

[87] Stevens JE, Walter GA, Okereke E, Scarborough MT, Esterhai JL, George SZ, et al. Muscle adaptations with immobilization and rehabilitation after ankle fracture. Medicine and science in sports and exercise. 2004;36:1695-701.

[88] Boesch C. Molecular aspects of magnetic resonance imaging and spectroscopy. Molecular aspects of medicine. 1999;20:185-318.

[89] Mulkern RV, Chung T. From signal to image: magnetic resonance imaging physics for cardiac magnetic resonance. Pediatr Cardiol. 2000;21:5-17.

[90] Akima H, Lott D, Senesac C, Deol J, Germain S, Arpan I, et al. Relationships of thigh muscle contractile and non-contractile tissue with function, strength, and age in boys with Duchenne muscular dystrophy. Neuromuscul Disord. 2012;22:16-25.

[91] Mathur S, Lott DJ, Senesac C, Germain SA, Vohra RS, Sweeney HL, et al. Age-related differences in lower-limb muscle cross-sectional area and torque production in boys with Duchenne muscular dystrophy. Arch Phys Med Rehabil. 2010;91:1051-8.

[92] Vandenborne K, Elliott MA, Walter GA, Abdus S, Okereke E, Shaffer M, et al. Longitudinal study of skeletal muscle adaptations during immobilization and rehabilitation. Muscle Nerve. 1998;21:1006-12.

[93] Stevens JE, Pathare NC, Tillman SM, Scarborough MT, Gibbs CP, Shah P, et al. Relative contributions of muscle activation and muscle size to plantarflexor torque during rehabilitation after immobilization. J Orthop Res. 2006;24:1729-36.

[94] Lamminen AE. Magnetic resonance imaging of primary skeletal muscle diseases: patterns of distribution and severity of involvement. Br J Radiol. 1990;63:946-50.

[95] Matsumura K, Nakano I, Fukuda N, Ikehira H, Tateno Y, Aoki Y. Proton spin-lattice relaxation time of Duchenne dystrophy skeletal muscle by magnetic resonance imaging. Muscle Nerve. 1988;11:97-102.

[96] Liu M, Chino N, Ishihara T. Muscle damage progression in Duchenne muscular dystrophy evaluated by a new quantitative computed tomography method. Arch Phys Med Rehabil. 1993;74:507-14.

[97] Torriani M, Townsend E, Thomas BJ, Bredella MA, Ghomi RH, Tseng BS. Lower leg muscle involvement in Duchenne muscular dystrophy: an MR imaging and spectroscopy study. Skeletal radiology. 2012;41:437-45.

[98] Fleckenstein JL, Canby RC, Parkey RW, Peshock RM. Acute effects of exercise on MR imaging of skeletal muscle in normal volunteers. AJR Am J Roentgenol. 1988;151:231-7.

[99] Adams GR, Duvoisin MR, Dudley GA. Magnetic resonance imaging and electromyography as indexes of muscle function. J Appl Physiol. 1992;73:1578-83.

[100] Fleckenstein JL, Watumull D, McIntire DD, Bertocci LA, Chason DP, Peshock RM. Muscle proton T2 relaxation times and work during repetitive maximal voluntary exercise. J Appl Physiol. 1993;74:2855-9.

[101] Saab G, Thompson RT, Marsh GD. Effects of exercise on muscle transverse relaxation determined by MR imaging and in vivo relaxometry. J Appl Physiol. 2000;88:226-33.

[102] Patten C, Meyer RA, Fleckenstein JL. T2 mapping of muscle. Semin Musculoskelet Radiol. 2003;7:297-305.

[103] Ploutz-Snyder LL, Nyren S, Cooper TG, Potchen EJ, Meyer RA. Different effects of exercise and edema on T2 relaxation in skeletal muscle. Magn Reson Med. 1997;37:676-82.

[104] Vandenborne K, Walter G, Ploutz-Snyder L, Dudley G, Elliott MA, De Meirleir K. Relationship between muscle T2* relaxation properties and metabolic state: a combined localized 31P-spectroscopy and 1H-imaging study. European journal of applied physiology. 2000;82:76-82.

[105] Hayashi M, Hanakawa S, Senda M, Takahara Y. Evaluation of the thigh muscles after knee exercise on a Cybex II. Acta medica Okayama. 1998;52:155-60.

[106] Shellock FG, Fukunaga T, Mink JH, Edgerton VR. Exertional muscle injury: evaluation of concentric versus eccentric actions with serial MR imaging. Radiology. 1991;179:659-64.

[107] Takahashi H, Kuno S, Miyamoto T, Yoshioka H, Inaki M, Akima H, et al. Changes in magnetic resonance images in human skeletal muscle after eccentric exercise. Eur J Appl Physiol Occup Physiol. 1994;69:408-13.

[108] Bickel CS, Slade J, Mahoney E, Haddad F, Dudley GA, Adams GR. Time course of molecular responses of human skeletal muscle to acute bouts of resistance exercise. J Appl Physiol. 2005;98:482-8.

[109] Foley JM, Jayaraman RC, Prior BM, Pivarnik JM, Meyer RA. MR measurements of muscle damage and adaptation after eccentric exercise. J Appl Physiol. 1999;87:2311-8.

[110] Sorichter S, Mair J, Koller A, Muller E, Kremser C, Judmaier W, et al. Creatine kinase, myosin heavy chains and magnetic resonance imaging after eccentric exercise. J Sports Sci. 2001;19:687-91.

[111] Bryan WW, Reisch JS, McDonald G, Herbelin LL, Barohn RJ, Fleckenstein JL. Magnetic resonance imaging of muscle in amyotrophic lateral sclerosis. Neurology. 1998;51:110-3.

[112] Frimel TN, Walter GA, Gibbs JD, Gaidosh GS, Vandenborne K. Noninvasive monitoring of muscle damage during reloading following limb disuse. Muscle & nerve. 2005;32:605-12.

[113] Dunn JF, Zaim-Wadghiri Y. Quantitative magnetic resonance imaging of the mdx mouse model of Duchenne muscular dystrophy. Muscle Nerve. 1999;22:1367-71.

[114] Walter G, Cordier L, Bloy D, Sweeney HL. Noninvasive monitoring of gene correction in dystrophic muscle. Magnetic resonance in medicine : official journal of the Society of Magnetic Resonance in Medicine / Society of Magnetic Resonance in Medicine. 2005;54:1369-76.

[115] Kasper CE, Talbot LA, Gaines JM. Skeletal muscle damage and recovery. AACN clinical issues. 2002;13:237-47.

[116] Huang Y, Majumdar S, Genant HK, Chan WP, Sharma KR, Yu P, et al. Quantitative MR relaxometry study of muscle composition and function in Duchenne muscular dystrophy. Journal of magnetic resonance imaging : JMRI. 1994;4:59-64.

[117] Elder CP, Apple DF, Bickel CS, Meyer RA, Dudley GA. Intramuscular fat and glucose tolerance after spinal cord injury--a cross-sectional study. Spinal Cord. 2004;42:711-6.

[118] Kim HK, Laor T, Horn PS, Racadio JM, Wong B, Dardzinski BJ. T2 mapping in Duchenne muscular dystrophy: distribution of disease activity and correlation with clinical assessments. Radiology. 2010;255:899-908.

[119] Mathur S, Vohra RS, Germain SA, Forbes S, Bryant ND, Vandenborne K, et al. Changes in muscle T2 and tissue damage after downhill running in mdx mice. Muscle Nerve. 2011;43:878-86.

[120] LeBlanc A, Lin C, Shackelford L, Sinitsyn V, Evans H, Belichenko O, et al. Muscle volume, MRI relaxation times (T2), and body composition after spaceflight. J Appl Physiol. 2000;89:2158-64.

[121] Kobayashi M, Nakamura A, Hasegawa D, Fujita M, Orima H, Takeda S. Evaluation of dystrophic dog pathology by fat-suppressed T2-weighted imaging. Muscle & nerve. 2009;40:815-26.

[122] Beenakker EA, Maurits NM, Fock JM, Brouwer OF, van der Hoeven JH. Functional ability and muscle force in healthy children and ambulant Duchenne muscular dystrophy patients. Eur J Paediatr Neurol. 2005;9:387-93.

[123] Escolar DM, Henricson EK, Mayhew J, Florence J, Leshner R, Patel KM, et al. Clinical evaluator reliability for quantitative and manual muscle testing measures of strength in children. Muscle Nerve. 2001;24:787-93.

[124] Goodpaster BH, Carlson CL, Visser M, Kelley DE, Scherzinger A, Harris TB, et al. Attenuation of skeletal muscle and strength in the elderly: The Health ABC Study. J Appl Physiol. 2001;90:2157-65.

[125] Mayhew JE, Florence JM, Mayhew TP, Henricson EK, Leshner RT, McCarter RJ, et al. Reliable surrogate outcome measures in multicenter clinical trials of Duchenne muscular dystrophy. Muscle Nerve. 2007;35:36-42.

[126] Skalsky AJ, Han JJ, Abresch RT, Shin CS, McDonald CM. Assessment of regional body composition with dual-energy X-ray absorptiometry in Duchenne muscular dystrophy: correlation of regional lean mass and quantitative strength. Muscle Nerve. 2009;39:647-51.

[127] Gorgey AS, Dudley GA. Skeletal muscle atrophy and increased intramuscular fat after incomplete spinal cord injury. Spinal Cord. 2007;45:304-9.

[128] Trappe TA, Lindquist DM, Carrithers JA. Muscle-specific atrophy of the quadriceps femoris with aging. J Appl Physiol. 2001;90:2070-4.

[129] Gehan EA, George SL. Estimation of human body surface area from height and weight. Cancer chemotherapy reports Part 1. 1970;54:225-35.

[130] Mosteller RD. Simplified calculation of body-surface area. N Engl J Med. 1987;317:1098.

[131] Rosset A, Spadola L, Ratib O. OsiriX: an open-source software for navigating in multidimensional DICOM images. Journal of digital imaging : the official journal of the Society for Computer Applications in Radiology. 2004;17:205-16.

[132] McDonald CM, Abresch RT, Carter GT, Fowler WM, Jr., Johnson ER, Kilmer DD, et al. Profiles of neuromuscular diseases. Duchenne muscular dystrophy. Am J Phys Med Rehabil. 1995;74:S70-92.

[133] Vignos PJ, Jr., Spencer GE, Jr., Archibald KC. Management of progressive muscular dystrophy in childhood. JAMA. 1963;184:89-96.

[134] Maganaris CN. Force-length characteristics of in vivo human skeletal muscle. Acta Physiol Scand. 2001;172:279-85.

[135] Manal K, Roberts DP, Buchanan TS. Optimal pennation angle of the primary ankle plantar and dorsiflexors: variations with sex, contraction intensity, and limb. Journal of applied biomechanics. 2006;22:255-63.

[136] Angelini C. The role of corticosteroids in muscular dystrophy: a critical appraisal. Muscle Nerve. 2007;36:424-35.

[137] Parreira SL, Resende MB, Della Corte Peduto M, Marie SK, Carvalho MS, Reed UC. Quantification of muscle strength and motor ability in patients with Duchenne muscular dystrophy on steroid therapy. Arq Neuropsiquiatr. 2007;65:245-50.

[138] Scott OM, Hyde SA, Goddard C, Dubowitz V. Quantitation of muscle function in children: a prospective study in Duchenne muscular dystrophy. Muscle Nerve. 1982;5:291-301.

[139] Jungbluth H, Davis MR, Muller C, Counsell S, Allsop J, Chattopadhyay A, et al. Magnetic resonance imaging of muscle in congenital myopathies associated with RYR1 mutations. Neuromuscul Disord. 2004;14:785-90.

[140] Kornblum C, Lutterbey G, Bogdanow M, Kesper K, Schild H, Schroder R, et al. Distinct neuromuscular phenotypes in myotonic dystrophy types 1 and 2 : a whole body highfield MRI study. J Neurol. 2006;253:753-61.

[141] Marden FA, Connolly AM, Siegel MJ, Rubin DA. Compositional analysis of muscle in boys with Duchenne muscular dystrophy using MR imaging. Skeletal Radiol. 2005;34:140-8.

[142] Mercuri E, Bushby K, Ricci E, Birchall D, Pane M, Kinali M, et al. Muscle MRI findings in patients with limb girdle muscular dystrophy with calpain 3 deficiency (LGMD2A) and early contractures. Neuromuscul Disord. 2005;15:164-71.

[143] Boesch C. Musculoskeletal spectroscopy. J Magn Reson Imaging. 2007;25:321-38.

[144] Kanehisa H, Yata H, Ikegawa S, Fukunaga T. A cross-sectional study of the size and strength of the lower leg muscles during growth. Eur J Appl Physiol Occup Physiol. 1995;72:150-6.

[145] Ramos E, Frontera WR, Llopart A, Feliciano D. Muscle strength and hormonal levels in adolescents: gender related differences. Int J Sports Med. 1998;19:526-31.

[146] Wood LE, Dixon S, Grant C, Armstrong N. Elbow flexion and extension strength relative to body or muscle size in children. Med Sci Sports Exerc. 2004;36:1977-84.

[147] Lai HC, FitzSimmons SC, Allen DB, Kosorok MR, Rosenstein BJ, Campbell PW, et al. Risk of persistent growth impairment after alternate-day prednisone treatment in children with cystic fibrosis. N Engl J Med. 2000;342:851-9.

[148] Fukunaga T, Roy RR, Shellock FG, Hodgson JA, Edgerton VR. Specific tension of human plantar flexors and dorsiflexors. J Appl Physiol. 1996;80:158-65.

[149] Uchikawa K, Liu M, Hanayama K, Tsuji T, Fujiwara T, Chino N. Functional status and muscle strength in people with Duchenne muscular dystrophy living in the community. J Rehabil Med. 2004;36:124-9.

[150] Armand S, Mercier M, Watelain E, Patte K, Pelissier J, Rivier F. A comparison of gait in spinal muscular atrophy, type II and Duchenne muscular dystrophy. Gait Posture. 2005;21:369-78.

[151] Bakker JP, De Groot IJ, Beelen A, Lankhorst GJ. Predictive factors of cessation of ambulation in patients with Duchenne muscular dystrophy. Am J Phys Med Rehabil. 2002;81:906-12.

[152] Baiardini I, Minetti C, Bonifacino S, Porcu A, Klersy C, Petralia P, et al. Quality of life in Duchenne muscular dystrophy: the subjective impact on children and parents. J Child Neurol. 2011;26:707-13.

[153] Bray P, Bundy AC, Ryan MM, North KN, Everett A. Health-related quality of life in boys with Duchenne muscular dystrophy: agreement between parents and their sons. J Child Neurol. 2010;25:1188-94.

[154] McDouall RM, Dunn MJ, Dubowitz V. Nature of the mononuclear infiltrate and the mechanism of muscle damage in juvenile dermatomyositis and Duchenne muscular dystrophy. J Neurol Sci. 1990;99:199-217.

[155] Deconinck N, Dan B. Pathophysiology of duchenne muscular dystrophy: current hypotheses. Pediatric neurology. 2007;36:1-7.

[156] Wren TA, Bluml S, Tseng-Ong L, Gilsanz V. Three-point technique of fat quantification of muscle tissue as a marker of disease progression in Duchenne muscular dystrophy: preliminary study. AJR American journal of roentgenology. 2008;190:W8-12.

[157] Kinali M, Arechavala-Gomeza V, Cirak S, Glover A, Guglieri M, Feng L, et al. Muscle histology vs MRI in Duchenne muscular dystrophy. Neurology. 2011;76:346-53.

[158] van der Graaf M, Tack CJ, de Haan JH, Klomp DW, Heerschap A. Magnetic resonance spectroscopy shows an inverse correlation between intramyocellular lipid content in human calf muscle and local glycogen synthesis rate. NMR in biomedicine. 2010;23:133-41.

[159] Kent-Braun JA, Ng AV, Young K. Skeletal muscle contractile and noncontractile components in young and older women and men. J Appl Physiol. 2000;88:662-8.

[160] Gray C, MacGillivray TJ, Eeley C, Stephens NA, Beggs I, Fearon KC, et al. Magnetic resonance imaging with k-means clustering objectively measures whole muscle volume compartments in sarcopenia/cancer cachexia. Clin Nutr. 2011;30:106-11.

[161] Mercuri E, Pichiecchio A, Allsop J, Messina S, Pane M, Muntoni F. Muscle MRI in inherited neuromuscular disorders: past, present, and future. Journal of magnetic resonance imaging : JMRI. 2007;25:433-40.

[162] Wattjes MP, Kley RA, Fischer D. Neuromuscular imaging in inherited muscle diseases. Eur Radiol. 2010;20:2447-60.

[163] Manini TM, Clark BC, Nalls MA, Goodpaster BH, Ploutz-Snyder LL, Harris TB. Reduced physical activity increases intermuscular adipose tissue in healthy young adults. Am J Clin Nutr. 2007;85:377-84.

[164] Sled JG, Zijdenbos AP, Evans AC. A nonparametric method for automatic correction of intensity nonuniformity in MRI data. IEEE Trans Med Imaging. 1998;17:87-97.

[165] Arai Y, Osawa M, Fukuyama Y. Muscle CT scans in preclinical cases of Duchenne and Becker muscular dystrophy. Brain & development. 1995;17:95-103.

[166] Cros D, Harnden P, Pellissier JF, Serratrice G. Muscle hypertrophy in Duchenne muscular dystrophy. A pathological and morphometric study. J Neurol. 1989;236:43-7.

[167] van Deutekom JC, Janson AA, Ginjaar IB, Frankhuizen WS, Aartsma-Rus A, Bremmer-Bout M, et al. Local dystrophin restoration with antisense oligonucleotide PRO051. N Engl J Med. 2007;357:2677-86.

[168] Richards P, Saywell WR, Heywood P. Pseudohypertrophy of the temporalis muscle in Xp21 muscular dystrophy. Dev Med Child Neurol. 2000;42:786-7.

[169] Beenakker EA, de Vries J, Fock JM, van Tol M, Brouwer OF, Maurits NM, et al. Quantitative assessment of calf circumference in Duchenne muscular dystrophy patients. Neuromuscul Disord. 2002;12:639-42.

[170] Jones DA, Round JM, Edwards RH, Grindwood SR, Tofts PS. Size and composition of the calf and quadriceps muscles in Duchenne muscular dystrophy. A tomographic and histochemical study. J Neurol Sci. 1983;60:307-22.

[171] Lynch GS, Hinkle RT, Chamberlain JS, Brooks SV, Faulkner JA. Force and power output of fast and slow skeletal muscles from mdx mice 6-28 months old. J Physiol. 2001;535:591-600.

[172] Prior BM, Ploutz-Snyder LL, Cooper TG, Meyer RA. Fiber type and metabolic dependence of T2 increases in stimulated rat muscles. J Appl Physiol. 2001;90:615-23.

[173] Pastoret C, Sebille A. mdx mice show progressive weakness and muscle deterioration with age. J Neurol Sci. 1995;129:97-105.

[174] Carnwath JW, Shotton DM. Muscular dystrophy in the mdx mouse: histopathology of the soleus and extensor digitorum longus muscles. J Neurol Sci. 1987;80:39-54.

[175] Coulton GR, Morgan JE, Partridge TA, Sloper JC. The mdx mouse skeletal muscle myopathy: I. A histological, morphometric and biochemical investigation. Neuropathol Appl Neurobiol. 1988;14:53-70.

[176] McGeachie JK, Grounds MD, Partridge TA, Morgan JE. Age-related changes in replication of myogenic cells in mdx mice: quantitative autoradiographic studies. J Neurol Sci. 1993;119:169-79.

[177] Pastoret C, Sebille A. Time course study of the isometric contractile properties of mdx mouse striated muscles. J Muscle Res Cell Motil. 1993;14:423-31.

[178] DiMario JX, Uzman A, Strohman RC. Fiber regeneration is not persistent in dystrophic (MDX) mouse skeletal muscle. Dev Biol. 1991;148:314-21.

[179] Stedman HH, Sweeney HL, Shrager JB, Maguire HC, Panettieri RA, Petrof B, et al. The mdx mouse diaphragm reproduces the degenerative changes of Duchenne muscular dystrophy. Nature. 1991;352:536-9.

[180] Anderson JE, Ovalle WK, Bressler BH. Electron microscopic and autoradiographic characterization of hindlimb muscle regeneration in the mdx mouse. Anat Rec. 1987;219:243-57.

[181] Radley HG, Grounds MD. Cromolyn administration (to block mast cell degranulation) reduces necrosis of dystrophic muscle in mdx mice. Neurobiol Dis. 2006;23:387-97.

[182] Shavlakadze T, White J, Hoh JF, Rosenthal N, Grounds MD. Targeted expression of insulin-like growth factor-I reduces early myofiber necrosis in dystrophic mdx mice. Mol Ther. 2004;10:829-43.

[183] Passaquin AC, Renard M, Kay L, Challet C, Mokhtarian A, Wallimann T, et al. Creatine supplementation reduces skeletal muscle degeneration and enhances mitochondrial function in mdx mice. Neuromuscul Disord. 2002;12:174-82.

[184] Khurana TS, Watkins SC, Chafey P, Chelly J, Tome FM, Fardeau M, et al. Immunolocalization and developmental expression of dystrophin related protein in skeletal muscle. Neuromuscul Disord. 1991;1:185-94.

[185] McClure WC, Rabon RE, Ogawa H, Tseng BS. Upregulation of the creatine synthetic pathway in skeletal muscles of mature mdx mice. Neuromuscul Disord. 2007;17:639-50.

[186] Bertocchini F, Ovitt CE, Conti A, Barone V, Scholer HR, Bottinelli R, et al. Requirement for the ryanodine receptor type 3 for efficient contraction in neonatal skeletal muscles. EMBO J. 1997;16:6956-63.

[187] Schiaffino S, Reggiani C. Molecular diversity of myofibrillar proteins: gene regulation and functional significance. Physiol Rev. 1996;76:371-423.

[188] Landisch RM, Kosir AM, Nelson SA, Baltgalvis KA, Lowe DA. Adaptive and nonadaptive responses to voluntary wheel running by mdx mice. Muscle Nerve. 2008;38:1290-3.

[189] Lynch GS, Rafael JA, Chamberlain JS, Faulkner JA. Contraction-induced injury to single permeabilized muscle fibers from mdx, transgenic mdx, and control mice. Am J Physiol Cell Physiol. 2000;279:C1290-4.

[190] Lovering RM, De Deyne PG. Contractile function, sarcolemma integrity, and the loss of dystrophin after skeletal muscle eccentric contraction-induced injury. Am J Physiol Cell Physiol. 2004;286:C230-8.

[191] Lovering RM, Hakim M, Moorman CT, 3rd, De Deyne PG. The contribution of contractile pre-activation to loss of function after a single lengthening contraction. J Biomech. 2005;38:1501-7.

[192] Brussee V, Tardif F, Tremblay JP. Muscle fibers of mdx mice are more vulnerable to exercise than those of normal mice. Neuromuscular disorders : NMD. 1997;7:487-92.

[193] Vilquin JT, Brussee V, Asselin I, Kinoshita I, Gingras M, Tremblay JP. Evidence of mdx mouse skeletal muscle fragility in vivo by eccentric running exercise. Muscle Nerve. 1998;21:567-76.

[194] Spurney CF, Gordish-Dressman H, Guerron AD, Sali A, Pandey GS, Rawat R, et al. Preclinical drug trials in the mdx mouse: assessment of reliable and sensitive outcome measures. Muscle & nerve. 2009;39:591-602.

[195] Marqueste T, Giannesini B, Fur YL, Cozzone PJ, Bendahan D. Comparative MRI analysis of T2 changes associated with single and repeated bouts of downhill running leading to eccentric-induced muscle damage. J Appl Physiol. 2008;105:299-307.

[196] Bickel CS, Slade JM, Dudley GA. Long-term spinal cord injury increases susceptibility to isometric contraction-induced muscle injury. Eur J Appl Physiol. 2004;91:308-13.

[197] Larsen RG, Ringgaard S, Overgaard K. Localization and quantification of muscle damage by magnetic resonance imaging following step exercise in young women. Scand J Med Sci Sports. 2007;17:76-83.

[198] Meyer RA, Prior BM. Functional magnetic resonance imaging of muscle. Exerc Sport Sci Rev. 2000;28:89-92.

[199] Shah PK, Gregory CM, Stevens JE, Pathare NC, Jayaraman A, Behrman AL, et al. Non-invasive assessment of lower extremity muscle composition after incomplete spinal cord injury. Spinal cord. 2008;46:565-70.

[200] Ploutz-Snyder LL, Clark BC, Logan L, Turk M. Evaluation of spastic muscle in stroke survivors using magnetic resonance imaging and resistance to passive motion. Arch Phys Med Rehabil. 2006;87:1636-42.

[201] Maillard SM, Jones R, Owens C, Pilkington C, Woo P, Wedderburn LR, et al. Quantitative assessment of MRI T2 relaxation time of thigh muscles in juvenile dermatomyositis. Rheumatology (Oxford). 2004;43:603-8.

[202] McIntosh L, Granberg KE, Briere KM, Anderson JE. Nuclear magnetic resonance spectroscopy study of muscle growth, mdx dystrophy and glucocorticoid treatments: correlation with repair. NMR Biomed. 1998;11:1-10.

[203] Pacak CA, Walter GA, Gaidosh G, Bryant N, Lewis MA, Germain S, et al. Long-term skeletal muscle protection after gene transfer in a mouse model of LGMD-2D. Mol Ther. 2007;15:1775-81.

[204] Grounds MD, Radley HG, Lynch GS, Nagaraju K, De Luca A. Towards developing standard operating procedures for pre-clinical testing in the mdx mouse model of Duchenne muscular dystrophy. Neurobiol Dis. 2008;31:1-19.

[205] Yokota T, Lu QL, Partridge T, Kobayashi M, Nakamura A, Takeda S, et al. Efficacy of systemic morpholino exon-skipping in Duchenne dystrophy dogs. Ann Neurol. 2009;65:667-76.

[206] Kornegay JN, Li J, Bogan JR, Bogan DJ, Chen C, Zheng H, et al. Widespread muscle expression of an AAV9 human mini-dystrophin vector after intravenous injection in neonatal dystrophin-deficient dogs. Mol Ther. 2010;18:1501-8.

[207] Le Rumeur E, De Certaines J, Toulouse P, Rochcongar P. Water phases in rat striated muscles as determined by T2 proton NMR relaxation times. Magn Reson Imaging. 1987;5:267-72.

[208] Conley MS, Foley JM, Ploutz-Snyder LL, Meyer RA, Dudley GA. Effect of acute head-down tilt on skeletal muscle cross-sectional area and proton transverse relaxation time. J Appl Physiol. 1996;81:1572-7.

[209] Kinugasa R, Kawakami Y, Fukunaga T. Quantitative assessment of skeletal muscle activation using muscle functional MRI. Magn Reson Imaging. 2006;24:639-44.

[210] Lynch GS, Fary CJ, Williams DA. Quantitative measurement of resting skeletal muscle [Ca2+]i following acute and long-term downhill running exercise in mice. Cell calcium. 1997;22:373-83.

[211] Carter GT, Kikuchi N, Abresch RT, Walsh SA, Horasek SJ, Fowler WM, Jr. Effects of exhaustive concentric and eccentric exercise on murine skeletal muscle. Arch Phys Med Rehabil. 1994;75:555-9.

[212] Hamer PW, McGeachie JM, Davies MJ, Grounds MD. Evans Blue Dye as an in vivo marker of myofibre damage: optimising parameters for detecting initial myofibre membrane permeability. Journal of anatomy. 2002;200:69-79.

[213] Liu M, Bose P, Walter GA, Anderson DK, Thompson FJ, Vandenborne K. Changes in muscle T2 relaxation properties following spinal cord injury and locomotor training. European journal of applied physiology. 2006;97:355-61.

[214] Eston RG, Mickleborough J, Baltzopoulos V. Eccentric activation and muscle damage: biomechanical and physiological considerations during downhill running. British journal of sports medicine. 1995;29:89-94.

[215] Delp MD, Duan C. Composition and size of type I, IIA, IID/X, and IIB fibers and citrate synthase activity of rat muscle. J Appl Physiol. 1996;80:261-70.

[216] Prior BM, Foley JM, Jayaraman RC, Meyer RA. Pixel T2 distribution in functional magnetic resonance images of muscle. J Appl Physiol. 1999;87:2107-14.

[217] Handschin C, Kobayashi YM, Chin S, Seale P, Campbell KP, Spiegelman BM. PGC-1alpha regulates the neuromuscular junction program and ameliorates Duchenne muscular dystrophy. Genes Dev. 2007;21:770-83.

[218] Straub V, Campbell KP. Muscular dystrophies and the dystrophin-glycoprotein complex. Current opinion in neurology. 1997;10:168-75.

[219] Nigro G, Comi LI, Politano L, Bain RJ. The incidence and evolution of cardiomyopathy in Duchenne muscular dystrophy. Int J Cardiol. 1990;26:271-7.

[220] Sasaki K, Sakata K, Kachi E, Hirata S, Ishihara T, Ishikawa K. Sequential changes in cardiac structure and function in patients with Duchenne type muscular dystrophy: a two-dimensional echocardiographic study. Am Heart J. 1998;135:937-44.

[221] Perloff JK, de Leon AC, Jr., O'Doherty D. The cardiomyopathy of progressive muscular dystrophy. Circulation. 1966;33:625-48.

[222] Sicinski P, Geng Y, Ryder-Cook AS, Barnard EA, Darlison MG, Barnard PJ. The molecular basis of muscular dystrophy in the mdx mouse: a point mutation. Science. 1989;244:1578-80.

[223] Van Erp C, Loch D, Laws N, Trebbin A, Hoey AJ. Timeline of cardiac dystrophy in 3-18-month-old MDX mice. Muscle Nerve. 2010;42:504-13.

[224] Fayssoil A, Nardi O, Orlikowski D, Annane D. Cardiomyopathy in Duchenne muscular dystrophy: pathogenesis and therapeutics. Heart Fail Rev. 2010;15:103-7.

[225] Tinsley JM, Potter AC, Phelps SR, Fisher R, Trickett JI, Davies KE. Amelioration of the dystrophic phenotype of mdx mice using a truncated utrophin transgene. Nature. 1996;384:349-53.

[226] Alter J, Lou F, Rabinowitz A, Yin H, Rosenfeld J, Wilton SD, et al. Systemic delivery of morpholino oligonucleotide restores dystrophin expression bodywide and improves dystrophic pathology. Nat Med. 2006;12:175-7.

[227] Wu B, Moulton HM, Iversen PL, Jiang J, Li J, Li J, et al. Effective rescue of dystrophin improves cardiac function in dystrophin-deficient mice by a modified morpholino oligomer. Proc Natl Acad Sci U S A. 2008;105:14814-9.

[228] Song W, Dyer E, Stuckey D, Leung MC, Memo M, Mansfield C, et al. Investigation of a transgenic mouse model of familial dilated cardiomyopathy. J Mol Cell Cardiol. 2010;49:380-9.

[229] Stuckey DJ, Carr CA, Camelliti P, Tyler DJ, Davies KE, Clarke K. In vivo MRI characterization of progressive cardiac dysfunction in the mdx mouse model of muscular dystrophy. PLoS ONE. 2012;7:e28569.

[230] Jeneson JA, de Snoo MW, Verlinden NA, Joosten BJ, Doornenbal A, Schot A, et al. Treadmill but not wheel running improves fatigue resistance of isolated extensor digitorum longus muscle in mice. Acta Physiol (Oxf). 2007;190:151-61.

[231] Michele DE, Kabaeva Z, Davis SL, Weiss RM, Campbell KP. Dystroglycan matrix receptor function in cardiac myocytes is important for limiting activity-induced myocardial damage. Circ Res. 2009;105:984-93.

[232] Mavrogeni S, Tzelepis GE, Athanasopoulos G, Maounis T, Douskou M, Papavasiliou A, et al. Cardiac and sternocleidomastoid muscle involvement in Duchenne muscular dystrophy: an MRI study. Chest. 2005;127:143-8.

[233] Mavrogeni S, Papavasiliou A, Douskou M, Kolovou G, Papadopoulou E, Cokkinos DV. Effect of deflazacort on cardiac and sternocleidomastoid muscles in Duchenne muscular dystrophy: a magnetic resonance imaging study. Eur J Paediatr Neurol. 2009;13:34-40.

[234] Cury RC, Shash K, Nagurney JT, Rosito G, Shapiro MD, Nomura CH, et al. Cardiac magnetic resonance with T2-weighted imaging improves detection of patients with acute coronary syndrome in the emergency department. Circulation. 2008;118:837-44.

[235] Zagrosek A, Abdel-Aty H, Boye P, Wassmuth R, Messroghli D, Utz W, et al. Cardiac magnetic resonance monitors reversible and irreversible myocardial injury in myocarditis. JACC Cardiovasc Imaging. 2009;2:131-8.

[236] Shen CT, Jeng CM, Lin YM, Chieng PU. Intensification of relative myocardial T2-weighted magnetic resonance signals in patients with acute viral myocarditis: report of one case. Zhonghua Minguo xiao er ke yi xue hui za zhi [Journal] Zhonghua Minguo xiao er ke yi xue hui. 1993;34:405-11.

[237] Quinlan JG, Hahn HS, Wong BL, Lorenz JN, Wenisch AS, Levin LS. Evolution of the mdx mouse cardiomyopathy: physiological and morphological findings. Neuromuscul Disord. 2004;14:491-6.

[238] Doherty KR, McNally EM. Repairing the tears: dysferlin in muscle membrane repair. Trends Mol Med. 2003;9:327-30.

[239] McNeil PL, Kirchhausen T. An emergency response team for membrane repair. Nat Rev Mol Cell Biol. 2005;6:499-505.

BIOGRAPHICAL SKETCH

Ravneet Singh Vohra was born in Amritsar, India. He completed his high school and senior secondary education from St. Francis School, Amritsar and Khalsa College, Amritsar, respectively. He received his undergraduate degree in physical therapy from Guru Nanak Dev University, Amritsar. He joined the doctoral program in rehabilitation sciences at the University of Florida in fall of 2006. He received his PhD from the University of Florida in the fall of 2012.